Doctoral Dissertation

A Unified Computation Method for Seakeeping-Maneuvering of a Ship in Waves Using Slender-Ship Theory and MMG Model

Ardhana Wicaksono

July 2019

Dept. of Naval Architecture & Ocean Engineering
Division of Global Architecture
Graduate School of Engineering
Osaka University

Prophet Muhammad (peace be upon him) said,

"If God intends goodness for someone, He bestows upon him the knowledge."

Sahih al-Bukhari (Book of Knowledge:13)

Abstract

A unified seakeeping-maneuvering analysis is developed based on the weak-coupling approach of two-time scale method. At each time step, the second-order horizontal steady forces and yaw moment are estimated by the far-field method utilizing the Kochin function as a function of incident-wave frequency and amplitude, relative heading angle between incident wave and ship, and forward speed, and their magnitudes are added as the wave effect in the maneuvering motion equations.

The Kochin function representing ship-disturbance waves are evaluated by means of both enhanced unified theory (EUT) and new strip method (NSM) to see the difference due to bow wave diffraction, 3D and forward-speed effects in the final results of second-order steady forces and moment.

Accordingly, the maneuvering-motion simulation provides the instantaneous forward speed of a ship and the heading angle to the seakeeping analysis. In order to keep the accuracy of the simulation model, calm water hull derivatives are taken from the captive tests. Then, maneuvering simulations in waves are carried out by the coupling between slender-ship theory and modular maneuvering model in the framework of two-time scale method.

Validation of the seakeeping calculation method is made through comparison with the experiment conducted with bulk-carrier and container ship models advancing in regular oblique waves and motion-free condition. Good agreement between computed and measured results and also superiority of EUT to NSM are confirmed for all modes of ship motion and the steady forces and yaw moment in a wide range of wave frequency.

For the coupled seakeeping-maneuvering model, a comparison of simulated and measured turning motion in waves indicates the practical reliability of the mathematical model. Improvement in the estimation of wave-induced steady forces and yaw moment is crucial, particularly in short waves. Sensitivity study in this wave condition also implies that the steady sway force is the largest contributor to the phenomenon that the ship drifts to the direction of incident waves.

Acknowledgements

This work is carried out inside the International Program of Maritime and Urban Engineering of Osaka University, which is a 5-year Master-Doctor consecutive course supported by the Japanese Ministry of Education, Culture, Sports, Science and Technology (MEXT).

First and foremost, it is an honor to express my sincere gratitude to my supervisor, Professor Masashi Kashiwagi, whose expertise, perseverance and vision made the completion of this thesis possible. His exceptional ideas and continuous encouragement are invaluable for my study.

I would also like to thank Professor Munehiko Minoura as Associate Professor in our laboratory, who kindly gave constructive advice during laboratory meeting. I also appreciate Professor Takahito Iida as Assistant Professor, who has been a good friend since we were both Master students. His crazy passion for research inspired me a lot.

Moreover, to Professor Hironori Yasukawa as the Chairman of JASNAOE Strategy Research Committee on IMO Guideline of Minimum Engine Power and its members, who provided the oblique waves experimental report of JASNAOE-BC084. The validation of the steady forces theoretical formulations used in this thesis will be difficult without their support.

I am also in debt of gratitude to Emeritus Professor Eiichi Kobayashi and Professor Chen Chen of Kobe University. The development of calm water maneuvering model, as well as the practical coupling method in waves, would be troublesome without our lengthy discussions.

Cordially, my appreciation goes to Professor Pierre Ferrant as the *Directeur du* LHEEA, and Professor David Le Touzé as the *Responsable de l'équipe* H2i. It is a great pleasure to work with benevolent members of LHEEA and of Ecole Centrale de Nantes. Furthermore, the accompany of EMShip Class of 2018 in the *cours de français* of Julie Pourqier is appreciated. In addition, the exceptional PPI Nantes & Saint-Nazaire along with Indonesian families, you made Brétagne felt like home.

Special recognition is reserved to Yasushi Kitagawa, as researcher in the Marine Dynamics Research Group of the National Maritime Research Institute of Japan. Being the person-in-charge for my internship, his kindness and vast experience in his research field helped me to

realize crucial things in the simulation and tank experiment of the ship maneuvering problem. Kind help from Yoshiaki Tsukada is equally acknowledged.

By the completion of this dissertation, fruitful discussions with Professor Yonghwan Kim and Jae-Hoon Lee from Seoul National University improved our understanding on the complicated problem of seakeeping-maneuvering in waves, to which I am thankful.

Furthermore, I am blessed to belong to an incredible laboratory with fun and supporting members. I should say that this atmosphere is enviable to anyone, and is such a necessity in performing a graduate study. Besides, I should acknowledge my classmates and university colleagues for the lively friendship.

Of the utmost importance, I am always indebted to my dearest parents and family whose prayer has been the greatest support and reason for my life. Their unwavering love for the silly me is irreplaceable. Also to Musnindar, for the timeless memory and priceless affection. Then, to Atika Hanoum Rahasta, who made this meaningful journey even more precious at the end.

After all, I realize that it would take pages to acknowledge every single individual whose contribution is worth a mention. I profoundly thank everyone from the bottom of my heart.

Osaka, July 2019

Ardhana Wicaksono

Contents

List of Figures

List of Tables

Symbols

In **Chapter 2**

V	volume of fluid in concern / volume integral
ρ	density of fluid
u_i	i-th component of velocity vector
p	pressure
n_i	i-th component of the outward pointing vector
g	acceleration of gravity
δ_{i3}	Kronecker's delta
F_i	i-th component of a vector (or scalar) quantity
t	time
S	surface surrounding the fluid / surface integral
∇	gradient operator (or displacement volume)
ω	encountering frequency
Φ	velocity potential
p_0	constant pressure
p_a	atmospheric pressure
U	ship forward speed
$\Re$	real part
$e^{i\omega t}$	time-harmonic term
P_S	steady pressure
P_U	unsteady pressure
ζ	free surface elevation
ξ_j	j-th mode of ship motions

X_j	j-th mode of complex amplitude
μ	Rayleigh's artificial viscosity coefficient
E	total energy
E_k	kinetic energy
E_p	potential energy
ζ_a	incident wave amplitude
ω_0	circular wave frequency
k_0	wavenumber
χ	ship-wave encountering angle
P	field point
Q	integration point along the wetted hull
G	Green function
τ	Hanaoka's parameter
$H(k)$	Kochin function of wave amplitude
$\pm$	complex signs
$\delta(x)$	Dirac's delta function
$\mathcal{F}$	Fourier transform
M_i	momentum
S_H	hull wetted surface
S_F	still-water free surface
S_C	control surface
$*$	complex conjugate
$\Im$	imaginary part
$\overline{R}$	added resistance
$\overline{Y}$	steady sway force
$\overline{N}$	steady yaw moment
κ	3D wavenumber
$'$	derivative
$C(k)$	symmetric component of Kochin function
$S(k)$	antisymmetric component of Kochin function
Q_j	source strength

D_j	doublet strength
ϵ	slenderness parameter
B	ship breadth
L	ship length
d	ship draft
σ_j	2D Kochin function of the ith mode
C_H	contour of the transverse section
$f(x-\xi)$	kernel function
M_{ij}	mass matrix
A_{ij}	added mass matrix
B_{ij}	damping coefficient matrix
C_{ij}	restoring coefficient matrix
E_i	wave-exciting force
k_{yy}	pitch gyrational radius
A_w	waterplane area
x_w	center of A_w in x-axis
$\overline{GM}$	metacentric height
$\overline{GM_L}$	longitudinal metacentric height
LPP	length between perpendiculars
C_B	block coefficient
C_M	midship coefficient
C_{WP}	waterplane coefficient
OG	center of gravity
k_{xx}	roll gyrational radius
k_{zz}	yaw gyrational radius
Fn	Froude number
λ	wavelength

In **Chapter 3** and **4**

m	ship mass
$\dot{u}$	surge acceleration

$\dot{v}$	sway acceleration
$\dot{r}$	yaw acceleration
I_{zz}	yaw moment of inertia
u	surge velocity
v	sway velocity
r	yaw velocity
X	force in x-axis
Y	force in y-axis
N	moment about z-axis
Ψ	heading angle
β	drift angle
$_H$	hull force
$_R$	rudder force
$_P$	propeller force
m_x	surge added mass
m_y	sway added mass
J_z	yaw added moment of inertia
$'$	nondimensionalized quantity
M_A	zero-frequency added mass
D_M	zero-frequency damping coefficient
C_{D0}	ship drag coefficient at zero drift angle
x_P	distance between center of gravity and center of pressure
t_P	thrust deduction factor
T	thrust
n_P	propeller revolution per second
D_P	propeller diameter
K_T	thrust coefficient
J_P	advance ratio
k_0, k_1, k_2	open water constants
w_P	effective wake fraction
t_R	steering resistance deduction factor

a_H	rudder force increase factor
x_H	position of additional lateral force component
F_N	rudder normal force
δ	rudder angle
A_R	rudder area
Λ	rudder aspect ratio
U_R	effective inflow velocity
α_R	angle into rudder
TD	tactical diameter
Ad	advance distance
Rtd	rating of turning ability
$\alpha 10_1$	first overshoot angle in the 10/10 zig-zag test
$Rt\alpha_{10}$	rating for the first overshoot angle in the 10/10 zig-zag test

* Definition of symbol should be refered to the corresponding chapter or section when ambiguity is observed

Chapter 1

Introduction

1.1 Background

It is well known that the resistance of a ship will increase when the ship is advancing in waves at constant forward speed. This increment is called the added resistance, which is the longitudinal component of the wave-induced steady force of second order in the wave amplitude. Since the prediction of ship resistance is crucial for the economic operation in actual seas, many studies on the added resistance have been conducted so far. In actual seaways, owing to the nature of the ocean, ships must sail obliquely to the direction of wave propagation. In oblique waves, not only the added resistance, but also the same kind of steady sway force and yaw moment may be exerted. As an effect of these steady sway force and yaw moment, the check helm and drift angle of the ship may be exerted to attain equilibrium, which will induce another kind of resistance increase.

On the other hand, IMO (International Maritime Organization) requires that the maneuverability of a full scale ship is to be evaluated in a calm weather condition through the so-called sea trial. One of the tests is to measure the steady turning circle with the maximum design rudder angle until completing at least two turning circles. Then, the maneuverability is judged by the tactical diameter, advance, transfer, and other information. However, oceangoing ships are expected to

sail the real seas, with ocean current, wind, and wave. Compared to the ocean current, the wind and wave are known to be more complex in nature, especially the waves. In certain conditions, the steady forces can be significantly large to drift the ship from its course, or at least to impair the course stability. Therefore, it is unsafe to judge the ship maneuverability in waves based only on the trials performed in calm sea. Accurate prediction of wave-induced steady forces and moment becomes important in considering the maneuvering motion of a ship in waves.

Early development of the theoretical formulation for the added resistance was provided by Maruo [1] by means of the principles of momentum and energy conservation. In the calculation formula derived, the Kochin function, equivalent to the amplitude of ship-generated disturbance waves far from the ship, is required as the input. Newman [2] studied the wave-induced steady yaw moment on a floating body at zero speed, and derived a formula using the angular momentum conservation principle. Their analyses were based on the stationary-phase method, which is expedient for the zero-speed problem, but becomes messy for the case of forward speed. In fact, Lin and Reed [3] succeeded in obtaining a formula in this condition for the steady sway force using the stationary-phase method, but they found it difficult to derive a formula for the steady yaw moment.

Kashiwagi [4–6] proposed an analysis method utilizing the Fourier-transform theory to tackle the difficulty of stationary-phase method, and consequently derived the formulae for the steady forces and yaw moment at forward speed. Kashiwagi [5] computed further the Kochin function and then the added resistance, steady sway force, and steady yaw moment for the forward-speed but motion-fixed cases by means of the unified theory of Sclavounos [7]. Later Kashiwagi [8] proposed Enhanced Unified Theory (EUT) as an extension from the unified theory of Newman [9] and Sclavounos [7], and analyzed surge-related problems by retaining the x-component of the normal vector in the body boundary condition. The lateral motion modes were treated in the same fashion as that for heave and pitch, with 3D and forward-speed effects taken into account.

Compared to a large amount of work on the added resistance, few studies have been made on the steady sway force and yaw moment. Naito et al [10] measured the wave-induced steady forces

on a tanker model for motion-fixed cases. Iwashita et al [11] compared computed results by the 3D Green function method with measured results for the steady sway force and yaw moment only for the diffraction problem, but agreement was not good in shorter waves when the forward speed is present. Another measurement of wave-induced steady forces was conducted by Ueno et al [12] using a VLCC model at Froude number Fn = 0.069 in a very short wave. Utilizing a time-domain 3D higher order boundary element method, Joncquez [13] evaluated the second-order forces and moments for all motion modes at zero speed, but the ship was free to heave and pitch. When the forward speed is considered, evaluation of forces and moment was done only for head-wave case.

In the presence of waves, the maneuvering motion equations should be modified to incorporate these wave-induced steady drift forces into the horizontal motions of the ship. This necessity requires us to solve not only the maneuvering but also seakeeping problems simultaneously. Research work on this topic can be classified into two depending on the methods applied: hybrid method and two-time scale method.

The hybrid method integrates steering and wave-induced motions, then evaluates the convolution integral of Cummins [14] to account for the wave memory effects. Some of works in this method are those by Bailey et al [15], Lee [16], Fossen [17], Subramanian and Beck [18], etc. For instance, Subramanian and Beck [18] utilized the time-domain strip theory taking account the instantaneous wetted surface when computing Froude-Krylov force, diffracted wave force, radiated wave memory force and the exact hydrostatic force. The maneuvering forces (viscous hull derivatives, propeller and rudder forces) were however considered conventionally through typical model test and semi-empirical formulas. Since the low- and high-frequency problems are unified in one set of equations of motion, velocity-squared ($\nabla\phi \cdot \nabla\phi$) term was taken to estimate the steady wave drifts. Alike other similar works, this concept limits the sophistication of the second-order forces formulation, which are vital in understanding a ship maneuvering in waves.

In contrast, the two-time scale method evaluates the seakeeping and maneuvering problems

individually in a weak-coupling framework, with the exchange of information between them. This separation disposes the need to consider the fluid memory, allows the steady drift forces to be evaluated in a more precise way, and substantially cuts the computational cost. Some eminent works in this framework are those of Kobayashi and Wada [19], Yasukawa [20, 21], Skejic and Faltinsen [25], Seo and Kim [32] and Zhang et al [35, 37].

Yasukawa [20, 21] carried out free running model tests consisting of turning, zig-zag, and stopping motions in regular and irregular waves. SR108 container ship was taken as the subject ship. The wave effect (drift) to the maneuvering was included in the MMG equations of motion as additional force module. The values of horizontal wave drifts were computed and tabulated prior to the maneuvering simulation. The added resistance in forward speed condition was calculated using the Maruo [1] formula taking account the influence of reflection waves proposed by Fujii and Takahashi [22], with the ship motion being estimated by new strip method (NSM). In contrast, its value in zero forward speed was evaluated by source distribution method [23] based on the analyses of Maruo [24] and Newman [2]. Steady sway force and steady yaw moment were computed in the same fashion for all cases by assuming negligible forward speed effect.

Skejic and Faltinsen [25] presented the details of time-domain maneuvering simulation using two-time scale. STF strip theory [26] was chosen as the seakeeping module to estimate the zero-encounter-frequency hydrodynamic coefficients and the second order wave loads. The flow separation at the stern was taken into account in the linear maneuvering added masses and damping coefficients through the introduction of end terms. Then, the nonlinear viscous forces were estimated by the ITTC'57 frictional resistance (x) and cross flow principle (y and z) explained in Newman [27] and Faltinsen [28]. Through the turning simulations in regular waves, several formulation of second-order wave loads were extensively tested, such as those of: Loukakis and Sclavounos [29], Salvesen [30], as well as the direct pressure integration method and the short waves asymptotic formulation of Faltinsen et al. [31]. Authors ultimately emphasized the importance of second-order steady forces and moment to the maneuvering motion in waves.

Seo and Kim [32] employed the similar concept of two-time scale for a SR108 (or S175) container ship. Seakeeping problem was solved by the time-domain Rankine panel method, while the maneuvering problem was considered by MMG model altogether with the maneuvering derivatives obtained from model tests. The wave drift forces were accounted by near field method - direct pressure integration approach. Difficulty in estimating the mean yaw moment was observed in the validation against experimental data of Yasukawa and Adnan [33], and its accurate evaluation was mentioned as important future work. The extension of this research was presented recently for speed loss problem by Lee and Kim [34].

Zhang and Zou [35] addressed the problem in similar way with Seo and Kim [32] for SR108 container ship. The main difference lies in the treatment of double-body basis flow which was equipped with trailing vortex sheet. Governing Laplace equation was added with a $\Delta\Phi$ term representing the Kutta condition at the hull trailing edge [36]. This introduction was then tested through the numerical oblique towing and steady turning motions of Series 60, showing significant underestimation of hydrodynamic forces as drift angle increases. Then, with the experimentally-derived maneuvering derivatives, simulation was conducted to observe the time-domain wave-induced motions of a ship turning in regular waves. Their more detailed survey on the maneuverability in waves was presented in Zhang et al. [37], including their new experimental data.

Even though various numerical techniques had been presented by world's researchers, lack of published experimental data restricted comprehensive validation of the developed codes. However, since the research on this field has been strongly encouraged by research institutions all over the world, the amount of experimental works has been increasing recently. SHOPERA Project published some data on DTC container ship maneuvering in waves through Sprenger et al. [38], followed with its international benchmark study by Shigunov et al. [39]. Sanada et al. [40] disclosed an experimental study of maneuvering in waves using Office of Naval Research Tumblehome (ONRT) surface combatant, as a continuation of Sanada et al. [41]. The tests, which were performed at The University of Iowa IIHR wave basin, comprised of coursekeeping,

turning and zig-zag tests in calm water and in regular waves. Then, Korean Research Institute of Ships and Ocean Engineering (KRISO) [42] recently presented an experimental work of the turning motion of KVLCC2 model in regular waves. This data complements the measurements for the same ship turning in irregular waves of Yasukawa et al [43].

It is however noteworthy that not every experimental work could be directly used as the benchmark for theoretical study. The complete information regarding the model particulars, experimental settings, maneuvering derivatives and coefficients are fundamental for constructing a prudent numerical validation.

1.2 Objective

The research objective is to develop a practical seakeeping-maneuvering analysis tool by employing the philosophy of linearized marine hydrodynamics. In this dissertation, the numerical scheme with high efficiency and reasonable accuracy is proposed through the study of: slender-ship theory, far-field formulation of wave drift forces, modular mathematical model for calm water maneuvering and their coupling within two-time scale framework.

In **Chapter 2**, study is made on the wave-induced added resistance, steady sway force, and steady yaw moment using the calculation formulae derived by Kashiwagi [4] for the general forward-speed case. The Kochin functions for symmetric and antisymmetric components of ship-disturbance waves are important input in those calculation formulae, and they are computed by EUT and NSM. Special attention is paid on the precise integration method to remove square-root singularities at the limits of integration range and to ensure the convergence in semi-infinite integrals appearing in the calculation formulae not only for the added resistance, but also for the steady sway force and yaw moment. Therefore, the calculation method in this paper is markedly different from conventional ones based on the strip-theory methods in that the numerical integration is exactly implemented without introducing any artificial convergence factor and that the computation method for the Kochin function is exact in the framework of the linear

slender-ship theory and applicable to all frequencies. In the effort to validate this computation scheme, numerical computations are made for comparison with the experiment conducted by Yasukawa et al. [44] using a bulk carrier model advancing in regular oblique waves with forward speed and six degrees-of-freedom motion. Validation using a SR108 container ship is also performed in accordance to Yasukawa and Adnan [33].

In **Chapter 3**, modular mathematical model is constructed to define the ship steering motions in calm water, mainly based on the MMG standard method [45]. As previous researches have acknowledged, the calm water maneuvering model plays a vital role in the coupled analysis in waves. Therefore, the derivation of motion equations is presented, and associated external forces are explained. In order to maintain the accuracy, model test results are used to define the hull derivatives, as well as other maneuvering coefficients. Accordingly, propeller and rudder forces are estimated by semi-empirical formulas. Numerical simulation is then validated against tank measurement for SR108 container ship [20], and ship maneuverability is discussed based on IMO criteria.

In **Chapter 4**, a unified model is developed by the concept of two-time scale method. The seakeeping problem is solved by the slender-ship theory, while the second-order steady forces are analyzed by the far-field formulae as in **Chapter 2**. The calm water maneuvering model described in **Chapter 3** is extended to incorporate wave-induced steady forces and yaw moment, as functions of incident-wave amplitude and frequency (ζ_a, ω_0), ship-wave relative heading angle $(\chi - \Psi)$, and ship's forward speed (U). SR108 container ship is taken as the subject ship since the necessary derivatives and coefficients are comprehensively available, as well as the measured maneuvering motions in regular waves [20, 21]. Comparison is also made for the turning trajectories in regular waves of $\lambda/L = 0.5$ and 1.0. Sensitivity study in short waves is also conducted by utilizing the modular nature of external forces. The contribution of each wave drift is accordingly discussed based on the deviation from the original trajectory.

Chapter 2

Seakeeping Problem by Slender-Ship Theory and Far-Field Method

2.1 Introduction

As the first step in solving the coupled seakeeping and maneuvering problem, we are going to address the seakeeping of a ship by the assumption of ideal fluid. Enhanced unified theory (EUT) is chosen among the slender-ship theory to address the ship-wave interaction. The far-field formula of steady horizontal forces and moment are constructed by means of the principle of momentum and energy conservation. On this purpose, the fundamental relations that governs the linearized fluid domain is going to be described here as explained on Kashiwagi [46].

2.2 Fundamental Equations of Water Waves

In order to derive the governing equations, conservation of mass and momentum is assumed. Taking a fluid volume in concern as $V(t)$ and defining its density as ρ, the mass conservation can be expressed as

$$\frac{d}{dt}\iiint_{V(t)} \rho \, dV = 0 \tag{2.1}$$

Then, by omitting the viscous shear, and considering only the normal pressure and gravity forces, we can write following relation expressing the momentum conservation,

$$\frac{d}{dt}\iiint_{V(t)} \rho u_i \, dV = -\iint_{S(t)} p n_i \, dS + \iiint_{V(t)} \rho g \delta_{i3} \, dV \tag{2.2}$$

with the fluid volume surface S, pressure p acting on it with the i-th component (i=1,2,3) of the outward-pointing unit normal vector n_i, i-th component of the velocity vector u_i, gravity acceleration g and the Kronecker's delta δ_{i3}, equal to 1 if $i = 3$ and 0 otherwise.

Here, we may apply following transport theorem [27] to the left-hand sides of (2.1) and (2.2),

$$\frac{d}{dt}\iiint_{V(t)} F_i \, dV = \iiint_V \frac{\partial F_i}{\partial t} \, dV + \iint_S F_i u_n \, dS \quad \left(= \iiint_V \left[\frac{\partial F_i}{\partial t} + \frac{\partial}{\partial x_j}(F_i u_j) \right] dV \right) \tag{2.3}$$

with F_i the i-th component of a vector (or scalar) quantity.

The transformation of surface integral in (2.3) into volume integral can be performed by using Gauss' theorem,

$$\iiint_V \frac{\partial A_j}{\partial x_j} dV = \iint_S A_j n_j dS \tag{2.4}$$

together with $u_n = u_j n_j$, therefore (2.1) takes the form of

$$\frac{d}{dt}\iiint_V \rho \, dV = \iiint_V \left[\frac{\partial \rho}{\partial t} + \frac{\partial}{\partial x_j}(\rho u_j) \right] dV = 0 \tag{2.5}$$

The volume V can be composed of an arbitrary group of fluid particles; thus the integrand should be equal to zero throughout the fluid. Hence the right-hand side of (2.5) may be replaced by following partial differential equation,

$$\frac{\partial \rho}{\partial t} + \frac{\partial}{\partial x_j}(\rho u_j) = 0 \tag{2.6}$$

which often referred to as the **continuity** equation.

For an incompressible fluid having constant density, the continuity equation can be simplified to

$$\frac{\partial u_j}{\partial x_j} = 0 \text{ or } \nabla \cdot \boldsymbol{u} = 0 \tag{2.7}$$

In the same fashion, application of transport theorem (2.3) and Gauss' theorem (2.4) to the momentum conservation (2.2) gives us

$$\iiint_V \left[\frac{\partial}{\partial t}(\rho u_i) + \frac{\partial}{\partial x_j}(\rho u_i u_j) \right] dV = \iiint_V \left[-\frac{\partial \rho}{\partial x_i} + \rho g \delta_{i3} \right] dV \tag{2.8}$$

Again, since the volume in consideration is arbitrary, (2.8) should hold for the integrands alone:

$$\frac{\partial}{\partial t}(\rho u_i) + \frac{\partial}{\partial x_j}(\rho u_i u_j) = -\frac{\partial \rho}{\partial x_i} + \rho g \delta_{i3} \tag{2.9}$$

At last, by expanding the products' derivatives on the left-hand side of (2.9) by the chain rule, and imposing the continuity equation (2.7), we acquire the **Euler's equation** for an incompressible fluid in the form

$$\frac{\partial u_i}{\partial t} + u_j \frac{\partial u_i}{\partial x_j} = -\frac{1}{\rho}\frac{\partial p}{\partial x_i} + g \delta_{i3} \tag{2.10}$$

so that we have (2.7) and (2.10) as the governing equations for an ideal fluid.

2.3 Potential Flow and Velocity Potential

In linear water waves problem, it is common to assume that the motion of fluid is irrotational; $\boldsymbol{\omega} = \nabla \times \boldsymbol{u} = 0$, justifying zero vorticity throughout the fluid. Taking this assumption, the transformations of (2.7) and (2.10) are considered.

By understanding that an identity of $\nabla \times \nabla \Phi = 0$ holds for an arbitrary scalar function $\Phi(\boldsymbol{x}, t)$, velocity vector $\boldsymbol{u}$ can be described as $\boldsymbol{u} = \nabla \Phi$ in terms of a scalar function, the so-called velocity potential Φ. Thereupon, the flows which may be described with this function are identified as the

potential flows. This introduction provides an advantage in term of mathematics in which from a single scalar unknown of velocity potential, all three velocity components can be computed.

By the substitution of $\boldsymbol{u} = \nabla\Phi$ in the (2.7), we define the Laplace equation,

$$\frac{\partial^2 \Phi}{\partial x_j^2} = 0 \quad \text{or} \quad \nabla \cdot \nabla\Phi = \nabla^2\Phi = 0 \tag{2.11}$$

that expresses the mass conservation and stands as the governing equation for potential flow.

Next, in order to reconstruct the Euler's equation (2.10) for the potential flow ($\nabla \times \boldsymbol{u} = 0$), the advection term on its left-hand side can be transformed as

$$\begin{aligned} u_j \frac{\partial u_i}{\partial x_j} &\equiv u_j \partial_j u_i = u_j(\partial_j u_i - \partial_i u_j) + u_j \partial_i u_j \\ &= u_j \varepsilon_{kji} (\nabla \times \boldsymbol{u})_k + \frac{1}{2}\partial_i (u_j u_j) = \frac{1}{2}\nabla\left(\nabla\Phi \cdot \nabla\Phi\right) \end{aligned} \tag{2.12}$$

Adopting this relation and invoking $\boldsymbol{u} = \nabla\Phi$ in (2.10) gives

$$\frac{\partial}{\partial x_i}\left(\frac{\partial \Phi}{\partial t} + \frac{1}{2}\nabla\Phi \cdot \nabla\Phi + \frac{p}{\rho} - gz\right) = 0 \tag{2.13}$$

Then, the integration of (2.13) with respect to the space variables gives the **Bernoulli's pressure equation**:

$$p - p_0 = -\rho\left(\frac{\partial \Phi}{\partial t} + \frac{1}{2}\nabla\Phi \cdot \nabla\Phi - gz\right) \tag{2.14}$$

with a constant p_0 that can be taken equal to the atmospheric pressure p_a on the undisturbed water surface.

2.3.1 Boundary Conditions

In the venture of solving the Laplace equation, it is required to employ appropriate boundary conditions on the fluid boundaries. Accordingly, we may directly express the velocity potential

as

$$\Phi(\boldsymbol{x},t) = U[\Phi_D(\boldsymbol{x},t) + \phi_s(\boldsymbol{x})] + \Phi_U(\boldsymbol{x},t) \tag{2.15}$$

$$\Phi_U(\boldsymbol{x},t) = \Re\left[\phi(\boldsymbol{x})e^{i\omega t}\right] \tag{2.16}$$

with constant forward velocity in x-axis U, the double-body flow potential Φ_D and steady wave-making flow potential $\phi_s(\boldsymbol{x})$. The latter is taken as zero due to the ship slenderness assumption. The last term Φ_U is the unsteady velocity potential due to the ship disturbance in waves. This term is assumed to be time-harmonic with term $e^{i\omega t}$ and real part ($\Re$) to be taken as in (2.16). Based on these expressions, the Bernoulli's pressure equation (2.14) can be decomposed into

$$P(\boldsymbol{x},t) = \rho g z + P_S(\boldsymbol{x}) + P_U(\boldsymbol{x},t) \tag{2.17}$$

where

$$\begin{aligned} P_S &= \frac{1}{2}\rho U^2 (1 - \boldsymbol{V}\cdot\boldsymbol{V}) \\ &= \frac{1}{2}\rho U^2 (1 - \nabla\Phi_D\cdot\nabla\Phi_D - 2\nabla\Phi_D\cdot\nabla\phi_s) + O(\phi_s^2) \end{aligned} \tag{2.18}$$

$$\begin{aligned} P_U &= -\rho\left(\frac{\partial}{\partial t} + U\boldsymbol{V}\cdot\nabla\right)\Phi_U - \frac{1}{2}\nabla\Phi_U\cdot\nabla\Phi_U \\ &= -\rho\left(\frac{\partial}{\partial t} + U\nabla\Phi_D\cdot\nabla\right)\Phi_U + O(\phi_s\Phi_U, {\Phi_U}^2) \end{aligned} \tag{2.19}$$

and

$$\boldsymbol{V} = \nabla(\Phi_D + \phi_s) \tag{2.20}$$

with higher-order terms in ϕ_s and Φ_U are neglected on (2.18) and (2.19). By substituting the definition of (2.16) to (2.19), we may write the linearized unsteady pressure as

$$\left.\begin{aligned} P_U(\boldsymbol{x},t) &= \Re\left[p(\boldsymbol{x})e^{i\omega t}\right] \\ p &= -\rho(i\omega + U\nabla\Phi_D\cdot\nabla)\phi \end{aligned}\right\} \tag{2.21}$$

Free-Surface Boundary Conditions In order to derive the free-surface boundary condition, we need to consider the substantial derivative of the zero pressure on the free surface:

$$\left(\frac{\partial}{\partial t} + \nabla\Phi \cdot \nabla\right)[\rho g z + P_S(\boldsymbol{x}) + P_U(\boldsymbol{x}, t)] = 0 \ \text{ on } z = \zeta \tag{2.22}$$

with $z = \zeta(x, y, t)$ expresses the surface elevation.

Next step is to substitute the velocity potential Φ (2.15), steady pressure P_S (2.18), unsteady pressure P_U (2.21), and once again omitting the higher order terms of ϕ_s and ϕ. Hence, the linearized free-surface boundary conditions can be obtained as follows:

$$\begin{aligned}&\frac{U^2}{2}\nabla\Phi_D \cdot \nabla(\nabla\Phi_D \cdot \nabla\Phi_D) + U^2\nabla\Phi_D \cdot \nabla(\nabla\Phi_D \cdot \nabla\phi_s)\\ &+\frac{U^2}{2}\nabla(\nabla\Phi_D \cdot \nabla\Phi_D) \cdot \nabla\phi_s - g\frac{\partial\phi_s}{\partial z} \ \text{ on } z = 0\end{aligned} \tag{2.23}$$

$$\begin{aligned}&-\omega^2\phi + 2iU\omega\nabla\Phi_D \cdot \nabla\phi + U^2\nabla\Phi_D \cdot \nabla(\Phi_D \cdot \nabla\phi)\\ &+\frac{U^2}{2}\nabla(\nabla\Phi_D \cdot \nabla\Phi_D) \cdot \nabla\phi + U\nabla^2\Phi_D(i\omega + U\nabla\Phi_D \cdot \nabla)\phi - g\frac{\partial\phi}{\partial z} = 0 \ \text{ on } z = 0\end{aligned} \tag{2.24}$$

respectively for the steady and unsteady velocity potentials. Furthermore if the Neumann-Kelvin assumption is considered ($\Phi_D = -x$), it is then possible to approximate

$$\nabla\Phi_D = -\boldsymbol{e}_1 \tag{2.25}$$

with $\boldsymbol{e}_1$ the unit vector along the x-axis. Therefore, (2.23) and (2.24) take the consecutive forms

$$U^2\frac{\partial^2\phi_s}{\partial x^2} - g\frac{\partial\phi_s}{\partial z} = 0 \qquad \text{on } z = 0 \tag{2.26}$$

$$\left(i\omega - U\frac{\partial}{\partial x}\right)^2\phi - g\frac{\partial\phi}{\partial z} = 0 \ \text{ on } z = 0 \tag{2.27}$$

Body Boundary Conditions The boundary condition on the ship hull can also be obtained by taking the substantial derivative of the hull surface equal to zero.

In the body-fixed coordinate system $\overline{\boldsymbol{x}} = (\overline{x}, \overline{y}, \overline{z})$, it translates into the hull surface being defined as $F(\overline{\boldsymbol{x}}) = 0$. Subsequently, with respect to the space-fixed coordinate system $\boldsymbol{x} = (x, y, z)$, we obtain

$$\begin{aligned}\left(\frac{\partial}{\partial t} + \nabla\Phi(\boldsymbol{x}, t) \cdot \nabla\right) F(\overline{\boldsymbol{x}}) &= \nabla F \cdot \frac{\partial \boldsymbol{x}}{\partial t} + \nabla\Phi(\boldsymbol{x}, t)\left\{\left(\nabla F \cdot \frac{\partial \overline{\boldsymbol{x}}}{\partial x}\right)\boldsymbol{e}_1\right. \\ &\left. + \left(\nabla F \cdot \frac{\partial \overline{\boldsymbol{x}}}{\partial y}\right)\boldsymbol{e}_2 + \left(\nabla F \cdot \frac{\partial \overline{\boldsymbol{x}}}{\partial z}\right)\boldsymbol{e}_3\right\} = 0 \end{aligned} \tag{2.28}$$

Taking the linear theory justification of the small-amplitude ship motions, we may relate $\boldsymbol{x}$ and $\overline{\boldsymbol{x}}$ as

$$\boldsymbol{x} = \overline{\boldsymbol{x}} + \boldsymbol{\alpha}(t) \tag{2.29}$$

$$\boldsymbol{\alpha}(t) = \boldsymbol{\alpha}_T(t) + \boldsymbol{\alpha}_R(t) \times \overline{\boldsymbol{x}}, \quad \boldsymbol{\alpha}_T(t) = \sum_{j=1}^{3} \xi_j(t)\boldsymbol{e}_j, \quad \boldsymbol{\alpha}_R(t) = \sum_{j=1}^{3} \xi_{j+3}(t)\boldsymbol{e}_j \tag{2.30}$$

with the displacement in the j-th mode of ship motions $\xi_j(t)$ being defined as surge, sway, heave, roll, pitch, yaw for $j = 1 \sim 6$, respectively.

Taking the division of (2.28) by $|\overline{\nabla}F|$ and the normal vector definition $\overline{\boldsymbol{n}} = \overline{\nabla}F/|\overline{\nabla}F|$, we obtain

$$\nabla\Phi(\boldsymbol{x}, t) \cdot \overline{\boldsymbol{n}} = \dot{\boldsymbol{\alpha}}(t) \cdot \overline{\boldsymbol{n}} + [(\nabla\Phi(\boldsymbol{x}, t) \cdot \nabla)\boldsymbol{\alpha}(t)] \cdot \overline{\boldsymbol{n}} \tag{2.31}$$

from (2.28) and (2.29). In order to account for the difference between $\boldsymbol{x}$ and $\overline{\boldsymbol{x}}$, we apply the Taylor-series expansion to $\nabla\Phi(\boldsymbol{x}, t)$ that gives following result:

$$\begin{aligned}\nabla\Phi(\boldsymbol{x}, t) &= \boldsymbol{UV}(\boldsymbol{x}) + \nabla\Phi_U(\boldsymbol{x}, t) \\ &= \boldsymbol{UV}(\overline{\boldsymbol{x}}) + \nabla\Phi_U(\overline{\boldsymbol{x}}, t) \\ &\quad + (\boldsymbol{\alpha}(t) \cdot \nabla)\left[\boldsymbol{UV}(\overline{\boldsymbol{x}}) + \nabla\Phi_U(\overline{\boldsymbol{x}}, t)\right] + O(\boldsymbol{\alpha}^2)\end{aligned} \tag{2.32}$$

By the substitution of (2.32) in (2.31), we may define the linearized body-boundary conditions to be

$$\boldsymbol{V}\cdot\boldsymbol{n} = \frac{\partial \Phi_D}{\partial n} + \frac{\partial \phi_s}{\partial n} = 0 \quad \text{on } S_H \tag{2.33}$$

$$\nabla\Phi_U\cdot\boldsymbol{n} = \frac{\partial \Phi_U}{\partial n} = \dot{\boldsymbol{\alpha}}(t)\cdot\boldsymbol{n} + U\left[(\boldsymbol{V}\cdot\nabla)\boldsymbol{\alpha}(t) - (\boldsymbol{\alpha}(t)\cdot\nabla)\boldsymbol{V}\right]\cdot\boldsymbol{n} \quad \text{on } S_H \tag{2.34}$$

for steady and unsteady parts, respectively, with S_H representing the hull wetted surface. The $\overline{\boldsymbol{x}}$ and $\overline{\boldsymbol{n}}$ have been replaced with $\boldsymbol{x}$ and $\boldsymbol{n}$ since their difference is considered as negligible higher-order term.

Through the time-harmonic assumption, the unsteady displacement in the j-th mode of motion can be written in the form of

$$\xi_j(t) = \Re\left[X_j e^{i\omega t}\right] \tag{2.35}$$

with the complex amplitude X_j. Therefore (2.34) can be transformed into

$$\frac{\partial \phi}{\partial n} = i\omega \sum_{j=1}^{6} X_j \left(n_j + \frac{U}{i\omega} m_j\right) \tag{2.36}$$

with

$$\left.\begin{aligned} (n_1, n_2, n_3) &= \boldsymbol{n}, \quad (n_4, n_5, n_6) = \boldsymbol{x}\times\boldsymbol{n} \\ (m_1, m_2, m_3) &= -(\boldsymbol{n}\cdot\nabla)\boldsymbol{V} \equiv \boldsymbol{m} \\ (m_4, m_5, m_6) &= -(\boldsymbol{n}\cdot\nabla)(\boldsymbol{x}\times\boldsymbol{V}) = \boldsymbol{V}\times\boldsymbol{n} + \boldsymbol{x}\times\boldsymbol{m} \end{aligned}\right\} \tag{2.37}$$

often referred to as the n and m-terms. Moreover, if the uniform flow approximation is taken ($\Phi_D = -x$), we obtain $\boldsymbol{V} = (-1, 0, 0)$ so that (2.33) and (2.37) can be simplified into

$$\frac{\partial \phi_s}{\partial n} = n_1 \quad \text{on } S_H \tag{2.38}$$

$$\left.\begin{aligned} (m_1, m_2, m_3) &= (0, 0, 0) \\ (m_4, m_5, m_6) &= (0, n_3, -n_2) \end{aligned}\right\} \tag{2.39}$$

Note on Radiation Condition At a distance from the ship, we should also impose the radiation condition. Mathematically, one of the known approach is the introduction of the Rayleigh's artificial viscosity coefficient (μ) into the free-surface boundary conditions. For the uniform-flow type of free-surface conditions, (2.26) and (2.27) should be rewritten as follows:

$$U^2\frac{\partial^2\phi_s}{\partial x^2} - g\frac{\partial\phi_s}{\partial z} - \mu U\frac{\partial\phi_s}{\partial x} = 0 \qquad \text{on } z = 0 \tag{2.40}$$

$$\left(i\omega - U\frac{\partial}{\partial x}\right)^2\phi - g\frac{\partial\phi}{\partial z} + \mu\left(i\omega - U\frac{\partial}{\partial x}\right)\phi = 0 \qquad \text{on } z = 0 \tag{2.41}$$

with μ supposed to be very small. This coefficient may be set equal to zero once a solution satisfying the radiation condition is realized.

2.3.2 Principle of Energy Conservation

The conservation of energy is an important principle in deriving the formula of steady forces and moment. In the study of mechanics, the total energy is described as the sum of kinetic energy and potential energy, which can be expressed as

$$E = E_k + E_p \tag{2.42}$$

Within a prescribed volume of V, we may write by a volume integral:

$$E = \rho\iiint_V\left(\frac{1}{2}\boldsymbol{u}^2 - gz\right)dV = \rho\iiint_V\left(\frac{1}{2}\nabla\Phi\cdot\nabla\Phi - gz\right)dV \tag{2.43}$$

with z is positive downward. Using the transport theorem (2.3), the rate-of-change of energy in function of time can be explained as

$$\frac{dE}{dt} = \rho\iiint_V\frac{\partial}{\partial t}\left(\frac{1}{2}\nabla\Phi\cdot\nabla\Phi - gz\right)dV + \rho\iint_S\left(\frac{1}{2}\nabla\Phi\cdot\nabla\Phi - gz\right)u_n\,dS \tag{2.44}$$

First of all, let us take a look on the integrand of (2.43). Kinetic energy provides the only contribution to this integral with the form of:

$$\frac{\partial}{\partial t}\left(\frac{1}{2}\nabla\Phi\cdot\nabla\Phi\right)=\nabla\Phi\cdot\nabla\frac{\partial\Phi}{\partial t}=\nabla\cdot\left(\frac{\partial\Phi}{\partial t}\nabla\Phi\right) \tag{2.45}$$

Meanwhile for the surface integral of (2.44), we may use Bernoulli's equation (2.14) to define the integrand as

$$\frac{1}{2}\nabla\Phi\cdot\nabla\Phi-gz=-\left(\frac{p-p_a}{\rho}+\frac{\partial\Phi}{\partial t}\right) \tag{2.46}$$

Finally, taking these forms into (2.44) and utilizing the transport theorem, we obtain

$$\frac{dE}{dt}=\rho\iint_S\left[\frac{\partial\Phi}{\partial t}\frac{\partial\Phi}{\partial n}-\left(\frac{p-p_a}{\rho}+\frac{\partial\Phi}{\partial t}\right)u_n\right]dS \tag{2.47}$$

The reader should refer to Newman [9] and Kashiwagi [8] for further details on the water waves problem.

2.4 Formulation of Steady Forces and Moment

The velocity potential and associated steady forces and moment will be explained based on the approach of Kashiwagi [4]. Mathematical complication of the stationary-phase analysis used in Maruo formula [1] is resolved by the new analysis method employing the Parseval theorem (Fourier transform). The derived formulas will allow us to estimate the drift forces and moment acting on the horizontal plane of a ship: added resistance (x-translation), steady lateral/sway force (y-translation) and steady yaw moment (z-rotation).

2.4.1 Asymptotic Form of Velocity Potential in the Far Field

In order to obtain the formula to approximate wave drift forces, we need to introduce the disturbance velocity potential afar from the ship. Firstly, the coordinate system is considered as

shown in Fig. 2.1. It is assumed that the ship scatters the incident waves while translating at a constant velocity U to the positive x-axis, and simultaneously having oscillations in six degrees-of-freedom (DOF). The incident wave amplitude is denoted as ζ_a, circular frequency ω_0 and wavenumber k_0 ($= \omega_0^2/g$, with the gravitational acceleration g) at infinitely deep water. The ship-wave encountering angle is defined to be the following waves for $\chi = 0^\circ$, therefore $\chi = 180^\circ$ for the head-waves condition. In this case, the encountering frequency is given by $\omega = \omega_0 - k_0 U \cos\chi$. Therefore by linear justification that amplitude of incident waves and ship oscillations are small, in the inviscid and irrotational fluid, the total velocity potential is rewritten from (2.15) and (2.16) to be

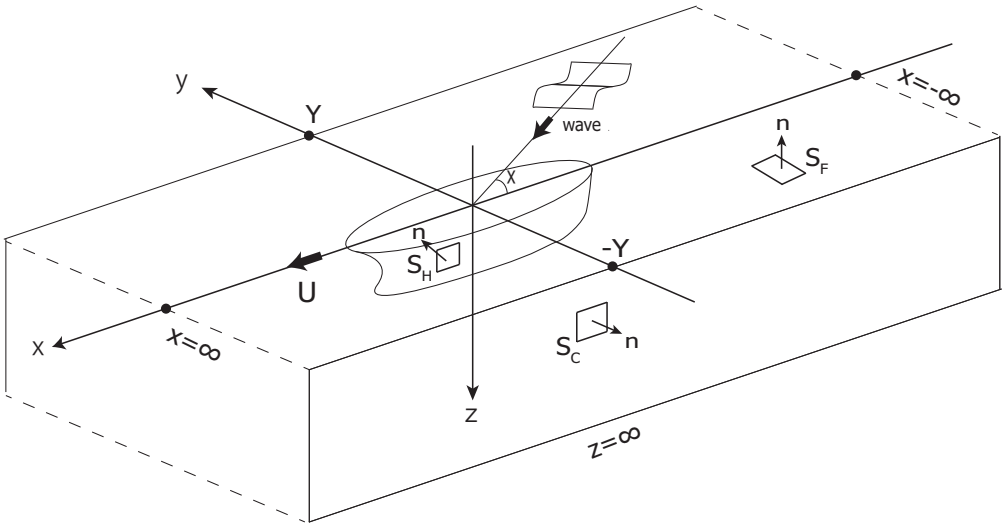

FIGURE 2.1: Coordinate system and notations

$$\Phi(x,y,z,t) = U[\Phi_D(x,y,z,t) + \phi_s(x,y,z)] + \Phi_U(x,y,z,t) \tag{2.48}$$

$$\Phi_U(x,y,z,t) = \Re[\phi(x,y,z)e^{i\omega t}] \tag{2.49}$$

with notations corresponding to (2.15) and (2.16): Φ_D the double-body flow potential, ϕ_s the steady disturbance potential due to the steady translation in calm water and Φ_U the unsteady potential due to wave-induced ship motions. The latter component takes the contributions from

the diffraction and radiation potentials as follows:

$$\phi(x, y, z) = \frac{gA}{i\omega_0}(\varphi_0 + \varphi) \tag{2.50}$$

with

$$\varphi_0 = e^{-k_0 z - ik_0(x\cos\chi + y\sin\chi)} \tag{2.51}$$

$$\varphi = \varphi_7 - \frac{\omega\omega_0}{g}\sum_{j=1}^{6}\frac{X_j}{A}\varphi_j \tag{2.52}$$

expressing the incident-wave potential and the ship-disturbed velocity potential, respectively. The φ_7 stands for the diffraction-wave potential, while φ_j denotes the radiation-wave potential due to the j-th mode of ship oscillation ($j = 1 \sim 6$) with complex amplitude X_j. These potentials must comply with following boundary conditions:

$$[L] \qquad \nabla^2\phi = 0 \tag{2.53}$$

$$[F] \qquad \left(i\omega - U\frac{\partial}{\partial x}\right)^2\phi - g\frac{\partial\phi}{\partial z} = 0, \quad \text{on } z = 0 \tag{2.54}$$

$$[B] \qquad \frac{\partial\phi}{\partial z} = 0, \quad \text{at } z \to \infty \tag{2.55}$$

$$[H] \qquad \frac{\partial\phi}{\partial n} = i\omega\sum_{j=1}^{6} X_j\left(n_j + \frac{U}{i\omega}m_j\right), \quad \text{on } S_H \tag{2.56}$$

with n_j and m_j have been explained previously in (2.37).

By means of Green's theorem, the disturbance velocity potential that satisfies (2.53) to (2.56) as well as the radiation condition can be signified as

$$\varphi(P) = \iint_{S_H}\left(\frac{\partial\varphi(Q)}{\partial n_Q} - \varphi(Q)\frac{\partial}{\partial n_Q}\right)G(P;Q)\,dS(Q) \tag{2.57}$$

with the field point $P = (x, y, z)$ and the integration point along the hull wetted surface $Q =$

(ξ, η, ζ). The Green function G suitable for the existing problem can be expressed by Fourier transform as follows

$$\begin{aligned} G(P,Q) &= -\frac{1}{4\pi}\left(\frac{1}{r}-\frac{1}{r'}\right) \\ &\quad -\frac{1}{2\pi}\int_{-\infty}^{\infty} e^{-ik(x-\xi)}\,dk \cdot \mathrm{Re}\int_0^{\infty} \frac{e^{-in(z+\zeta)-|y-\eta|\sqrt{n^2+k^2}}}{(n+i\kappa)\sqrt{n^2+k^2}} n\,dn \\ &\quad -\frac{1}{2\pi}\left[\int_{k_1}^{k_2}+\int_{k_3}^{k_4}\right]\frac{\kappa}{\sqrt{k^2-\kappa^2}} e^{-\kappa(z+\zeta)-|y-\eta|\sqrt{k^2-\kappa^2}-ik(x-\xi)}\,dk \\ &\quad +\frac{i}{2\pi}\left[-\int_{-\infty}^{k_1}+\int_{k_2}^{k_3}+\int_{k_4}^{\infty}\right]\frac{\kappa}{\sqrt{\kappa^2-k^2}} \\ &\qquad\qquad \times e^{-\kappa(z+\zeta)-i\varepsilon_k|y-\eta|\sqrt{\kappa^2-k^2}-ik(x-\xi)}\,dk \end{aligned} \tag{2.58}$$

with

$$\left.\begin{matrix} r \\ r' \end{matrix}\right\} = \sqrt{(x-\xi)^2+(y-\eta)^2+(z\mp\zeta)^2} \tag{2.59}$$

$$\kappa = \frac{1}{g}(\omega+kU)^2 = K+2k\tau+\frac{k^2}{K_0} \tag{2.60}$$

$$K = \frac{\omega^2}{g},\ \tau = \frac{U\omega}{g},\ K_0 = \frac{g}{U^2} \tag{2.61}$$

$$\left.\begin{matrix} k_1 \\ k_2 \end{matrix}\right\} = -\frac{K_0}{2}\left[1+2\tau \pm \sqrt{1+4\tau}\,\right] \tag{2.62}$$

$$\left.\begin{matrix} k_3 \\ k_4 \end{matrix}\right\} = \frac{K_0}{2}\left[1-2\tau \mp \sqrt{1-4\tau}\,\right] \tag{2.63}$$

$$\varepsilon_k = \mathrm{sgn}(\omega+kU) = \begin{cases} -1 & \text{for } -\infty < k < k_1 \\ 1 & \text{for } k_2 < k < \infty \end{cases} \tag{2.64}$$

It is understood that wavenumbers k_3 and k_4 in (2.63) are not real when $\tau > 1/4$, hence the integration limits of (2.58) must be modified to $k_3 = k_4$. Moreover, it is noteworthy that we have discarded the line integral term in (2.57) for the sake of simplicity, which is rational in

accordance with the slenderness assumption.

Next, we consider the asymptotic approximation of the Green function to formulate the far-field disturbance potential. When large transverse distance $|y|$ is concerned, only the last term of (2.58) remains since the other terms represent the local disturbance adjacent to x-axis. Hence, the substitution of this remaining term into (2.57) provides the expression of the velocity potential valid at large transverse distance from the x-axis:

$$\varphi(x,y,z) \sim \frac{i}{2\pi}\left[-\int_{-\infty}^{k_1} + \int_{k_2}^{k_3} + \int_{k_4}^{\infty}\right] H^{\pm}(k)\frac{\kappa}{\sqrt{\kappa^2-k^2}} e^{-\kappa z \mp i\varepsilon_k y\sqrt{\kappa^2-k^2}-ikx}\,dk \tag{2.65}$$

with a function representing the complex amplitude of the far-field disturbance wave:

$$H^{\pm}(k) = \iint_{S_H}\left(\frac{\partial\varphi}{\partial n} - \varphi\frac{\partial}{\partial n}\right) e^{-\kappa\zeta \pm i\varepsilon_k\eta\sqrt{\kappa^2-k^2}+ik\xi}\,dS \tag{2.66}$$

the so-called **Kochin function**. The complex signs ($\pm$) in previous equations are according to the sign of y (positive or negative). Understanding that the Kochin function is equal to zero outside the integration range of (2.65), we may reform the (2.65) into:

$$\varphi(x,y,z) \sim \frac{1}{2\pi}\int_{-\infty}^{\infty} i\varepsilon_k H^{\pm}(k)\frac{\kappa}{\sqrt{\kappa^2-k^2}} e^{-\kappa z \mp i\varepsilon_k y\sqrt{\kappa^2-k^2}} e^{-ikx}\,dk \tag{2.67}$$

From here onwards, it is beneficial to define the Fourier transform and the property of Dirac's delta function $\delta(x)$ correspondingly, as follows:

$$\left.\begin{aligned} \mathcal{F}[f(x)](k) &\equiv \int_{\infty}^{\infty} f(x)e^{ikx}\,dx = F(k) \\ \mathcal{F}^{-1}[F(k)](x) &\equiv \frac{1}{2\pi}\int_{\infty}^{\infty} F(k)e^{-ikx}\,dk = f(x) \end{aligned}\right\} \tag{2.68}$$

$$\int_{\infty}^{\infty} f(x)\delta(x-x_0)\,dx = f(x_0) \tag{2.69}$$

By the attribute of the Fourier transform, we may recast the far-field disturbance potential as

$$\begin{aligned}\mathcal{F}[\varphi(x,y,z)] &= \int_{-\infty}^{\infty} \varphi(x,y,z)e^{ikx}\,dx \\ &= i\varepsilon_k H^{\pm}(k)\frac{\kappa}{\sqrt{\kappa^2-k^2}}e^{-\kappa z \mp i\varepsilon_k y\sqrt{\kappa^2-k^2}}\end{aligned} \tag{2.70}$$

The same transformation may be performed for the incident wave potential to obtain:

$$\begin{aligned}\mathcal{F}[\varphi_0(x,y,z)] &= \int_{-\infty}^{\infty} \varphi_0(x,y,z)e^{ikx}\,dx \\ &= \mathcal{F}[e^{-i(k_0\cos\chi)x}]e^{-k_0 z - ik_0 y\sin\chi}\end{aligned} \tag{2.71}$$

Thus employing the property of (2.69) provides us with the following relation:

$$\left.\begin{aligned}\frac{1}{2\pi}\int_{\infty}^{\infty}\delta(k-k_0)e^{-ikx}\,dk = \frac{1}{2\pi}e^{-ik_0x} \\ \mathcal{F}^{-1}[\delta(k-k_0)] = \frac{1}{2\pi}e^{-ik_0x} \\ 2\pi\delta(k-k_0) = \mathcal{F}[e^{-ik_0x}]\end{aligned}\right\} \tag{2.72}$$

Ultimately, by applying (2.72), the incident wave potential may given as

$$\begin{aligned}\mathcal{F}[\varphi_0(x,y,z)] &= 2\pi\delta(k-k_0\cos\chi)e^{-k_0z-ik_0y\sin\chi} \\ \varphi_0(x,y,z) &= \mathcal{F}^{-1}[2\pi\delta(k-k_0\cos\chi)e^{-k_0z-ik_0y\sin\chi}]\end{aligned} \tag{2.73}$$

2.4.2 Derivation of Added Resistance Formula

The formula of added resistance in waves will be derived by considering the linear momentum conservation. Transforming the left-hand side of (2.2) by the transport theorem (2.3) gives us following relation,

$$\frac{dM_i}{dt} \equiv \frac{d}{dt}\iiint_V \rho v_i\,dV = \rho\left(\iiint_V \frac{\partial v_i}{\partial t}\,dV + \iint_S v_i u_n\,dS\right) \tag{2.74}$$

Taking the substantial derivative, we may write the $\frac{\partial v_i}{\partial t}$ on the right-hand side of (2.74) as

$$\frac{\partial v_i}{\partial t} = -\frac{\partial}{\partial x_i}\left(\frac{p}{\rho} - gz\right) - v_j \partial_j v_i \tag{2.75}$$

with the value of atmospheric pressure p_a is taken for pressure p. The term $v_j \partial_j v_i$ of (2.75) can be given as

$$v_j \partial_j v_i = \partial_j (v_j v_i) - v_i \partial_j v_j \tag{2.76}$$

with the continuity equation (2.7) defines its last term $\partial_j v_j = \nabla \cdot \boldsymbol{v}$, while the last term can be modified as $\partial_j (v_j v_i) = \partial (v_j v_i)/\partial x_j$. Subsequently, the substitution of this term into (2.75) and (2.74), followed by invoking the divergence theorem, gives the momentum conservation relation in the form of

$$\frac{dM_i}{dt} = -\rho \iint_S \left[\left(\frac{p}{\rho} - gz\right) n_i + v_i (v_n - u_n)\right] dS \tag{2.77}$$

with the surface integral (S) encloses the hull wetted surface (S_H), the still-water free surface (S_F) and the control surface (S_C) afar from the body, as elucidated in Fig. 2.1. Therefore by considering zero flux across S_H and S_F and zero value of pressure on S_F,

$$\left.\begin{aligned} v_n &= u_n \quad \text{on } S_H \text{ and } S_F \\ u_n &= 0 \quad \text{on } S_C^{\pm} \\ p &= 0 \quad \text{on } S_F \end{aligned}\right\} \tag{2.78}$$

we may write following equation

$$\frac{dM_i}{dt} = -\iint_{S_H} [(pn_i - \rho g z n_i)]\, dS - \iint_{S_C^{\pm}} [(pn_i - \rho g z n_i) + \rho v_i v_n]\, dS \tag{2.79}$$

Then, by defining $v_i = \nabla \Phi_T$ and $v_n = v_i \cdot n_i = \nabla \Phi_T \cdot \boldsymbol{n}$ and accounting only the forces in the transverse plane ($g z n_i = 0$), we obtain the linear momentum conservation as

$$\frac{d\boldsymbol{M}}{dt} = -\iint_{S_H} p\boldsymbol{n}\, dS - \iint_{S_C^{\pm}} [p\boldsymbol{n} + \rho \nabla \Phi_T (\nabla \Phi_T \cdot \boldsymbol{n})]\, dS \tag{2.80}$$

Next, we will obtain the force acting on the ship from (2.80). By the substitution of (2.48) into the linear momentum conservation, considering only the x longitudinal component, then omitting the steady disturbance potential, we may express the force as follows:

$$F_x \equiv \iint_{S_H} pn_x \, dS = -\frac{dM_x}{dt} - \iint_{S_C^{\pm}} \left[pn_x + \rho \left(\frac{\partial \Phi}{\partial x} - U \right) \left(\frac{\partial \Phi}{\partial n} - Un_x \right) \right] dS \tag{2.81}$$

Since the time average will eliminate the dM_x/dt due to the periodicity of fluid motions, there should be no net increase of momentum in the fluid volume throughout the cycles. Regarding the resistance as a force pushing back to the negative x-axis, it may be calculated as

$$\overline{R} = \iint_{S_C^{\pm}} \overline{\left[pn_x + \rho \left(\frac{\partial \Phi}{\partial x} - U \right) \left(\frac{\partial \Phi}{\partial n} - Un_x \right) \right]} \, dS \tag{2.82}$$

In Maruo [1] the control surface (S_C) was considered as a circular cylinder extending from the free-surface all the way to the infinitely-deep seabed. However, in this analysis, (S_C) will be considered as two flat plates located at $y = \pm Y$ which extend from $x = -\infty$ to $x = \infty$, as well as from free surface down to $z = +\infty$. Considering $n_x = 0$ on $S_C^{\pm}$, we can express the added resistance as follows:

$$\overline{R} = \iint_{S_C} \overline{\left[\frac{\partial \Phi}{\partial x} \frac{\partial \Phi}{\partial y} \right]_{-Y}^{Y}} \, dS \tag{2.83}$$

with $[\ \ ]_{-Y}^{Y}$ means taking the difference between the quantity in brackets at $y = Y$ and $y = -Y$.

The local wave at the ship vicinity can be neglected due to the large Y assumption. This also means that the local waves will be zero at $x = \pm\infty$ in the 3D case, while the disturbance waves radiating away from the x-axis are taken into account. By this control surface, and denoting the free surface elevation as $z = \zeta_F$, the surface integral (2.83) can be modified as

$$\begin{aligned} \iint_{S_C} dS &= \int_{\zeta_F}^{\infty} dz \int_{-\infty}^{\infty} dx \\ &= \left[\int_{\zeta_F}^{0} + \int_{0}^{\infty} \right] dz \int_{-\infty}^{\infty} dx \end{aligned} \tag{2.84}$$

Here, the order of $(\zeta_F, 0)$ contribution is higher than $O(\Phi^3)$ since integrand itself is on the $O(\Phi^2)$, thus can be neglected. Accordingly, we should recast the (2.84) to be

$$\iint_{S_C} dS = \int_0^\infty dz \int_{-\infty}^\infty dx \tag{2.85}$$

By means of this equation, the surface integral in (2.83) can be obtained in the form of

$$\overline{R} = \rho \int_0^\infty dz \int_{-\infty}^\infty \overline{\left[\frac{\partial \Phi}{\partial x}\frac{\partial \Phi}{\partial y}\right]_{-Y}^{Y}} dx \tag{2.86}$$

Then we substitute Φ in (2.49) into (2.86) as

$$\overline{R} = \rho \int_0^\infty dz \int_{-\infty}^\infty \overline{\Re\left[\left(\frac{\partial \phi}{\partial x}e^{i\omega t}\right)\left(\frac{\partial \phi}{\partial y}e^{i\omega t}\right)\right]_{-Y}^{Y}} dx \tag{2.87}$$

Considering time-average approximation of

$$\overline{\Re[Ae^{i\omega t}]\Re[Be^{i\omega t}]} = \frac{1}{2}\Re[AB^*] \tag{2.88}$$

with the asterisk (*) denotes the complex conjugate, the (2.87) can therefore be obtained as follows:

$$\overline{R} = \frac{1}{2}\rho\,\Re \int_0^\infty dz \int_{-\infty}^\infty \left[\frac{\partial \phi}{\partial x}\frac{\partial \phi^*}{\partial y}\right]_{-Y}^{Y} dx \tag{2.89}$$

Next we introduce the definition of velocity potential in (2.49) into (2.89) that gives

$$\overline{R} = \frac{1}{2}\rho\left(\frac{gA}{\omega_0}\right)^2 \Re \int_0^\infty dz \int_{-\infty}^\infty \left[\left(\frac{\partial \varphi_0}{\partial x} + \frac{\partial \varphi}{\partial x}\right)\left(\frac{\partial \varphi_0^*}{\partial y} + \frac{\partial \varphi^*}{\partial y}\right)\right]_{-Y}^{Y} dx \tag{2.90}$$

By the previously explained assumptions of infinite water depth ($k_0 = \omega_0^2/g$) and zero contribution of φ_0 due to undisturbed incident wave system, the added resistance can be reformed

into

$$\begin{aligned}\overline{R} &= \frac{\rho g A^2}{k_0}\frac{1}{2}\Re\int_0^\infty dz\int_{-\infty}^{\infty}\left[\frac{\partial\varphi}{\partial x}\frac{\partial\varphi^*}{\partial y}+\frac{\partial\varphi_0}{\partial x}\frac{\partial\varphi^*}{\partial y}+\frac{\partial\varphi}{\partial x}\frac{\partial\varphi_0^*}{\partial y}\right]_{-Y}^{Y}dx\\ &= \frac{\rho g A^2}{k_0}\left[\overline{R_1}+\overline{R_2}\right]\end{aligned} \tag{2.91}$$

where

$$\overline{R_1} = \frac{1}{2}\Re\int_0^\infty dz\int_{-\infty}^{\infty}\left[\frac{\partial\varphi}{\partial x}\frac{\partial\varphi^*}{\partial y}\right]_{-Y}^{Y}dx \tag{2.92}$$

$$\overline{R_2} = \frac{1}{2}\Re\int_0^\infty dz\int_{-\infty}^{\infty}\left[\frac{\partial\varphi_0}{\partial x}\frac{\partial\varphi^*}{\partial y}+\frac{\partial\varphi}{\partial x}\frac{\partial\varphi_0^*}{\partial y}\right]_{-Y}^{Y}dx \tag{2.93}$$

Then, as derived in Tasrief [47], we are required to: 1) apply the Parseval's theorem with respect to the x-integration, 2) differentiate φ and φ_0 with respect to x and y, 3) solving the integral equations and 4) invoking the theory of hyperfunction to the sinusoidal terms.

After the lengthy process, we obtain following components:

$$\begin{aligned}\overline{R_1} &= \frac{1}{8\pi}\int_{-\infty}^{\infty}\varepsilon_k(|H^+(k)|^2+|H^-(k)|^2)\frac{\kappa}{\sqrt{\kappa^2-k^2}}k\,dk\\ &= \frac{1}{8\pi}\left[-\int_{-\infty}^{k_1}+\int_{k_2}^{k_3}+\int_{k_4}^{\infty}\right](|H^+(k)|^2+|H^-(k)|^2)\frac{\kappa}{\sqrt{\kappa^2-k^2}}k\,dk\end{aligned} \tag{2.94}$$

$$\begin{aligned}\overline{R_2} &= -\frac{k_0\cos\chi}{4}\left[\Im\left[\mp H(k_0,\chi)^*+H(k_0,\chi)\right]_{-Y}^{Y}\right]\\ &= -\frac{k_0\cos\chi}{4}\Im\left[-H\left(k_0,\chi\right)^*+H\left(k_0,\chi\right)-\left\{H\left(k_0,\chi\right)^*+H\left(k_0,\chi\right)\right\}\right]\\ &= \frac{k_0\cos\chi}{2}\Im\left[H\left(k_0,\chi\right)^*\right]\\ &= -\frac{k_0\cos\chi}{2}\Im\left[H(k_0,\chi)\right]\end{aligned} \tag{2.95}$$

with $k_3 = k_4$ in case of $\tau > 1/4$ for (2.94), and symbol $\Im$ denotes the imaginary part.

Hence, the total added resistance can be recast by substituting $\overline{R_1}$ and $\overline{R_2}$ into (2.91) to be:

$$\begin{aligned}\frac{\overline{R}}{\rho g\zeta_a^2} &= \frac{1}{8\pi k_0}\left[-\int_{-\infty}^{k_1}+\int_{k_2}^{k_3}+\int_{k_4}^{\infty}\right]\left\{\left|H^+(k)\right|^2+\left|H^-(k)\right|^2\right\}\frac{\kappa}{\sqrt{\kappa^2-k^2}}kdk \\ &\quad -\frac{1}{2}\cos\chi\,\Im\left[H\left(k_0,\chi\right)\right]\end{aligned} \tag{2.96}$$

After completing the analysis based on the principle of momentum conservation, we have to consider the principle of energy conservation (2.47) to derive the expected formula of added resistance as explained in [1].

Taking account the boundary conditions of control surfaces in (2.78), we can write (2.47) in the form

$$\frac{dE}{dt} = -\iint_{S_H}(p-p_a)v_n\,dS+\iint_{S_C}\frac{\partial\Phi}{\partial t}\frac{\partial\Phi}{\partial n}\,dS \tag{2.97}$$

Considering the time average of (2.47), the rate $\overline{dE/dt}$ should be zero due to the periodicity of fluid motions. Therefore, there is no dissipation energy by the ship because there is no external force aside the constant towing force and gravity force keeping the equilibrium position of the ship in space.

Then, by treating the surface integrals, employing the time average relation and once again applying the Fourier transform, we may retransform the added resistance as

$$\frac{\overline{R}}{\rho g\zeta_a^2} = \frac{1}{8\pi k_0}\left[-\int_{-\infty}^{k_1}+\int_{k_2}^{k_3}+\int_{k_4}^{\infty}\right]\left\{\left|H^+(k)\right|^2+\left|H^-(k)\right|^2\right\}\frac{\kappa\left(k-k_0\cos\chi\right)}{\sqrt{\kappa^2-k^2}}dk \tag{2.98}$$

where the symmetric and antisymmetric Kochin functions with respect to the ship $y=0$ plane being defined as

$$H^{\pm}(k) = C(k)\pm i\varepsilon_k S(k) \tag{2.99}$$

with

$$\begin{aligned} C(k) &= \frac{1}{2}\left\{H^{\pm}(k;\eta=\eta)+H^{\pm}(k;\eta=-\eta)\right\} \\ &= \frac{1}{2}\iint_{S_H}\left(\frac{\partial\varphi}{\partial n}-\varphi\frac{\partial}{\partial n}\right)e^{-\kappa\zeta}e^{ik\xi}\left(e^{\pm i\varepsilon_k\eta\sqrt{\kappa^2-k^2}}+e^{\mp i\varepsilon_k\eta\sqrt{\kappa^2-k^2}}\right)dS \\ &= \iint_{S_H}\left(\frac{\partial\varphi}{\partial n}-\varphi\frac{\partial}{\partial n}\right)e^{-\kappa\zeta}e^{ik\xi}\cos\left(\varepsilon_k\eta\sqrt{\kappa^2-k^2}\right)dS \\ &= \iint_{S_H}\left(\frac{\partial\varphi}{\partial n}-\varphi\frac{\partial}{\partial n}\right)e^{-\kappa\zeta+ik\xi}\cos\left(\eta\sqrt{\kappa^2-k^2}\right)dS \end{aligned} \tag{2.100}$$

and

$$\begin{aligned} \pm i\varepsilon_k S(k) &= \frac{1}{2}\left\{H^{\pm}(k;\eta=\eta)-H^{\pm}(k;\eta=-\eta)\right\} \\ &= \frac{1}{2}\iint_{S_H}\left(\frac{\partial\varphi}{\partial n}-\varphi\frac{\partial}{\partial n}\right)e^{-\kappa\zeta}e^{ik\xi}\left(e^{\pm i\varepsilon_k\eta\sqrt{\kappa^2-k^2}}-e^{\mp i\varepsilon_k\eta\sqrt{\kappa^2-k^2}}\right)dS \\ &= \iint_{S_H}\left(\frac{\partial\varphi}{\partial n}-\varphi\frac{\partial}{\partial n}\right)e^{-\kappa\zeta}e^{ik\xi}\left\{\pm i\sin\left(\varepsilon_k\eta\sqrt{\kappa^2-k^2}\right)\right\}dS \\ &= \pm i\varepsilon_k\iint_{S_H}\left(\frac{\partial\varphi}{\partial n}-\varphi\frac{\partial}{\partial n}\right)e^{-\kappa\zeta+ik\xi}\sin\left(\eta\sqrt{\kappa^2-k^2}\right)dS \end{aligned} \tag{2.101}$$

At the end, the added resistance in (2.98) can be given in the form

$$\frac{\overline{R}}{\rho g\zeta_a^2}=\frac{1}{4\pi k_0}\left[-\int_{-\infty}^{k_1}+\int_{k_2}^{k_3}+\int_{k_4}^{\infty}\right]\left\{|C(k)|^2+|S(k)|^2\right\}\frac{\kappa(k-k_0\cos\chi)}{\sqrt{\kappa^2-k^2}}dk \tag{2.102}$$

It is clear that there is no contribution from the interaction between $C(k)$ and $S(k)$ to the added resistance, where they give only independent contributions. For more detail on the derivation, reader may refer to Kashiwagi [4] and Tasrief [47].

2.4.3 Derivation of Steady Sway Force Formula

Based on the (2.80) obtained by the use of Gauss' theorem and taking account the momentum conservation, the formula for the sway force as the y-component of (2.82) is

$$\overline{Y} = -\iint_{S_C^{\pm}} \overline{\left[pn_y + \rho\left(\frac{\partial \Phi}{\partial y} - U\right)\left(\frac{\partial \Phi}{\partial n} - Un_x\right)\right]} \, dS \tag{2.103}$$

Moreover, by evaluating (2.103) on the control surface shown in Fig. 2.1 and substituting the pressure p, the formula can be reduced to

$$\begin{aligned} \overline{Y} &= \frac{\rho}{2}\int_0^{\infty} dz \int_{-\infty}^{\infty} \overline{\left[\left(\frac{\partial \Phi}{\partial x}\right) + \left(\frac{\partial \Phi}{\partial z}\right) - \left(\frac{\partial \Phi}{\partial y}\right)\right]_{-Y}^{Y}} \, dx \\ &\quad + \frac{1}{2}\rho g \int_{-\infty}^{\infty} \overline{\left[\zeta_w^2\right]_{-Y}^{Y}} \, dx + O\left(\Phi^3\right) \end{aligned} \tag{2.104}$$

where the unsteady wave elevation of the free surface is given by

$$\zeta_w = \frac{1}{g}\left(\frac{\partial \Phi}{\partial t} - U\frac{\partial \Phi}{\partial x}\right)_{z=0} + O\left(\Phi^2\right) \tag{2.105}$$

After that, in the same manner with added resistance derivation, we calculate time average in (2.104) and also substitute velocity potential, so that (2.104) can be written in decomposed form:

$$\overline{Y} = \frac{\rho g A^2}{k_0}\left(\overline{Y_1} + \overline{Y_2}\right) \tag{2.106}$$

$$\begin{aligned} \overline{Y_1} &= \frac{1}{4}\int_0^{\infty} dz \int_{-\infty}^{\infty} \left[\left|\frac{\partial \varphi}{\partial x}\right|^2 + \left|\frac{\partial \varphi}{\partial z}\right|^2 - \left|\frac{\partial \varphi}{\partial y}\right|^2\right]_{-Y}^{Y} dx \\ &\quad + \frac{1}{4}\Re \int_{-\infty}^{\infty} \left[\left(K|\varphi|^2 + \frac{1}{K_o}\left|\frac{\partial \varphi}{\partial x}\right|^2 + i2\tau\varphi^* \frac{\partial \varphi}{\partial x}\right)_{z=0}\right]_{-Y}^{Y} dx \end{aligned} \tag{2.107}$$

$$\begin{aligned}\overline{Y_2} &= \frac{1}{2}\int_0^\infty dz \int_{-\infty}^{\infty}\left[\frac{\partial\varphi}{\partial x}\frac{\partial\varphi_0^*}{\partial x}+\frac{\partial\varphi}{\partial z}\frac{\partial\varphi_0^*}{\partial z}-\frac{\partial\varphi}{\partial y}\frac{\partial\varphi_0^*}{\partial y}\right]_{-Y}^{Y} dx \\ &\quad +\frac{1}{2}\Re\int_{-\infty}^{\infty}\left[\left(K\varphi\varphi_0^*+\frac{1}{K_o}\frac{\partial\varphi}{\partial x}\frac{\partial\varphi_0^*}{\partial x}+i\tau\left(\varphi_0^*\frac{\partial\varphi}{\partial x}-\varphi\frac{\partial\varphi_0^*}{\partial x}\right)\right)_{z=0}\right]_{-Y}^{Y} dx\end{aligned} \tag{2.108}$$

Note that $\overline{Y_1}$ stands for the contribution from ship-generated disturbance waves and $\overline{Y_2}$ the contribution from the interaction between incident waves and ship-generated waves.

For the purpose of applying the Parseval's theorem to the x-integrations in (2.107) and (2.108), we need to obtain the Fourier transform of φ and φ_0 which given by

$$F\{\varphi(x,y,z)\} = i\epsilon_k H^{\pm}(k)\frac{\kappa}{\sqrt{\kappa^2-k^2}}e^{-\kappa z\mp i\epsilon_k y\sqrt{\kappa^2-k^2}} \tag{2.109}$$

$$F\{\varphi_0(x,y,z)\} = 2\pi\delta(k-k_0\cos x)\,e^{-k_0 z-ik_0 y\sin\chi} \tag{2.110}$$

On the other hand, the z-integration can be performed with

$$\int_0^\infty e^{-2\kappa z}dz = \frac{1}{2\kappa} \tag{2.111}$$

Specifically for the second term $\overline{Y_2}$, it is sufficient to concentrate on the case of $k = k_0\cos\chi$; $k_0\sin\chi = \pm\epsilon_k\sqrt{\kappa^2-k^2}$; and thus $\kappa = k_0$. As in the added resistance formula, the $\overline{Y_2}$ can be transformed further by applying the principle of energy conservation. Hence, (2.107) and (2.108) can be written in the form

$$\overline{Y_1} = \frac{1}{4\pi}\left[-\int_{-\infty}^{k_1}+\int_{k_2}^{k_3}+\int_{k_4}^{\infty}\right]\Im\{2C(k)S^*(k)\}\kappa dk \tag{2.112}$$

$$\overline{Y_2} = \frac{1}{4\pi}k_0\sin\chi\left[-\int_{-\infty}^{k_1}+\int_{k_2}^{k_3}+\int_{k_4}^{\infty}\right]\{|C(k)|^2+|S(k)|^2\}\frac{\kappa}{\kappa^2-k^2}dk \tag{2.113}$$

Furthermore, substitution of (2.112) and (2.113) into (2.106) gives the expression for the second-order steady sway force,

$$\begin{aligned}\frac{\overline{Y}}{\rho g\zeta_a^2} &= -\frac{1}{4\pi k_0}\left[-\int_{-\infty}^{k_1}+\int_{k_2}^{k_3}+\int_{k_4}^{\infty}\right]\Im\{2C(k)S^*(k)\}\kappa dk \\ &\quad +\frac{\sin\chi}{4\pi}\left[-\int_{-\infty}^{k_1}+\int_{k_2}^{k_3}+\int_{k_4}^{\infty}\right]\{|C(k)|^2+|S(k)|^2\}\frac{\kappa}{\kappa^2-k^2}dk \end{aligned} \tag{2.114}$$

From this result, it is clear that the first term $\overline{Y_1}$ comes from the interaction between symmetric and antisymmetric waves, and the second term $\overline{Y_2}$ is multiplied by $\sin\chi$. Thus, the steady sway force becomes zero in head and following waves for a ship with transverse symmetry.

2.4.4 Derivation of Steady Yaw Moment Formula

In order to relate the steady yaw moment to the far-field velocity potential, we consider the expression for the rate of change of the vertical component of angular momentum given by Newman [2]. By taking time average and considering the periodic nature of the fluid motion, the steady yaw moment expression can be written as

$$\overline{N} = -\iint_{S_C^{\pm}}\overline{\left[p\,(\mathbf{r}\times\mathbf{n})_z+\rho\,(\mathbf{r}\times\nabla\phi)_z\,(\mathbf{n}\bullet\nabla\phi)\right]\,dS} \tag{2.115}$$

where $\mathbf{r}$ is the position vector, and it follows from the velocity potential that

$$\begin{aligned}(\mathbf{r}\times\mathbf{n})_z &= xn_y-yn_x \\ (\mathbf{r}\times\nabla\phi)_z &= x\frac{\partial\varphi}{\partial y}-y\left(\frac{\partial\varphi}{\partial x}-U\right) \\ (\mathbf{n}\bullet\nabla\phi) &= n_x\left(\frac{\partial\varphi}{\partial x}-U\right)+n_y\frac{\partial\varphi}{\partial y}\end{aligned} \tag{2.116}$$

Evaluating above equations on the control surface, (2.115) can be reduced to

$$\begin{aligned}\overline{N} &= \frac{\rho}{2}\int_0^\infty dz \int_{-\infty}^{\infty} \overline{\left[x\left\{\left(\frac{\partial\Phi}{\partial x}\right)^2+\left(\frac{\partial\Phi}{\partial z}\right)^2-\left(\frac{\partial\Phi}{\partial y}\right)^2\right\}\right]_{-Y}^{Y}} dx \\ &+\frac{1}{2}\rho g\int_{-\infty}^{\infty}\overline{\left[x\zeta_w^2\right]_{-Y}^{Y}}dx+\rho\int_0^\infty dz\int_{-\infty}^{\infty}\overline{\left[y\frac{\partial\Phi}{\partial x}\frac{\partial\Phi}{\partial y}\right]_{-Y}^{Y}}dx \\ &+\rho U\int_{-\infty}^{\infty}\overline{\left[y\zeta_w\frac{\partial\Phi}{\partial y}\right]_{-Y}^{Y}}dx \end{aligned} \tag{2.117}$$

where ζ_w is given by (2.105).

Then, performing time-average calculation and substituting the velocity potential gives the decomposed form of yaw moment formula:

$$\overline{N}=\frac{\rho g A^2}{k_0}\left(\overline{N_1}+\overline{N_2}\right) \tag{2.118}$$

where

$$\begin{aligned}\overline{N_1} &= \frac{1}{4}\Re\int_0^\infty dz\int_{-\infty}^{\infty}\left[x\left(\left|\frac{\partial\varphi}{\partial x}\right|^2+\left|\frac{\partial\varphi}{\partial z}\right|^2-\left|\frac{\partial\varphi}{\partial y}\right|^2\right)+2y\frac{\partial\varphi}{\partial x}\frac{\partial\varphi^*}{\partial y}\right]_{-Y}^{Y}dx \\ &-\frac{1}{4}\Re\int_{-\infty}^{\infty}\left[x\left(K|\varphi|^2+\frac{1}{K_o}\left|\frac{\partial\varphi}{\partial x}\right|^2+i2\tau\varphi^*\frac{\partial\varphi}{\partial x}\right)_{z=0}\right]_{-Y}^{Y}dx \\ &-\frac{1}{4}\Re\int_{-\infty}^{\infty}\left[2y\left(\left\{i\tau\varphi^*+\frac{1}{K_0}\frac{\partial\varphi}{\partial x}\right\}\frac{\partial\varphi}{\partial y}\right)_{z=0}\right]_{-Y}^{Y}dx \end{aligned} \tag{2.119}$$

$$\begin{aligned}\overline{N_2} &= \frac{1}{2}\Re\int_0^\infty dz\int_{-\infty}^{\infty}\left[x\left(\frac{\partial\varphi}{\partial x}\frac{\partial\varphi_0^*}{\partial x}+\frac{\partial\varphi}{\partial z}\frac{\partial\varphi_0^*}{\partial z}-\frac{\partial\varphi}{\partial y}\frac{\partial\varphi_0^*}{\partial y}\right)+y\left(\frac{\partial\varphi}{\partial x}\frac{\partial\varphi_0^*}{\partial y}+\frac{\partial\varphi_0^*}{\partial x}\frac{\partial\varphi}{\partial y}\right)\right]_{-Y}^{Y}dx \\ &-\frac{1}{2}\Re\int_{-\infty}^{\infty}\left[x\left(K\varphi\varphi_0^*+\frac{1}{K_o}\frac{\partial\varphi}{\partial x}\frac{\partial\varphi_0^*}{\partial x}+i\tau\left(\varphi_0^*\frac{\partial\varphi}{\partial x}-\varphi\frac{\partial\varphi_0^*}{\partial x}\right)\right)_{z=0}\right]_{-Y}^{Y}dx \\ &-\frac{1}{2}\Re\int_{-\infty}^{\infty}\left[y\left\{i\tau\left(\varphi_0^*\frac{\partial\varphi}{\partial y}-\varphi\frac{\partial\varphi_0^*}{\partial y}\right)+\frac{1}{K_0}\left(\frac{\partial\varphi}{\partial x}\frac{\partial\varphi_0^*}{\partial y}+\frac{\partial\varphi_0^*}{\partial x}\frac{\partial\varphi}{\partial y}\right)\right\}_{z=0}\right]_{-Y}^{Y}dx \end{aligned} \tag{2.120}$$

In applying the Parseval's theorem to the x-integration in (2.119) and (2.120), the Fourier transform of the derivatives of φ times the coordinate x must be obtained beforehand. Taking

$x(\partial\varphi/\partial x)$ as an example, the Fourier transform can be found as

$$\begin{aligned} F\{x\frac{\partial\varphi}{\partial x}\} \quad = \quad & -i\frac{d}{dk}\{H^{\pm}(k)\}\frac{\epsilon_k\kappa k}{\sqrt{\kappa^2-k^2}}e^{-\kappa z\mp i\epsilon_k y\sqrt{\kappa^2-k^2}} \\ & -iH^{\pm}(k)\frac{d}{dk}\left\{\frac{\epsilon_k\kappa k}{\sqrt{\kappa^2-k^2}}e^{-\kappa z}\right\}e^{\mp i\epsilon_k y\sqrt{\kappa^2-k^2}} \\ & \mp H^{\pm}(k)\frac{\kappa k\,(\kappa\kappa'-k)}{\sqrt{\kappa^2-k^2}}e^{-\kappa z}ye^{\mp i\epsilon_k y\sqrt{\kappa^2-k^2}} \end{aligned} \tag{2.121}$$

where

$$\kappa' = \frac{d\kappa}{dk} = 2\left(\tau + \frac{k}{K_0}\right) \tag{2.122}$$

Regarding the Fourier transform of $\partial\varphi^*/\partial x$, we also get

$$F\{\frac{\partial\varphi^*}{\partial x}\} = [H^{\pm}(k)]^*\frac{\epsilon_k\kappa k}{\sqrt{\kappa^2-k^2}}e^{-\kappa z\pm i\epsilon_k y\sqrt{\kappa^2-k^2}} \tag{2.123}$$

In the same way, we can obtain another Fourier transforms which are necessary in performing the x-integration in (2.119). Based on Parseval's theorem, we should consider the integration of products appearing in (2.119) with respect to k, including (2.121) and (2.123). In carrying out these integrations, it is noteworthy that the integrand originating from the second term on the right-hand side of (2.121) is pure imaginary, in which it does not contribute to the final result. Moreover, it can be confirmed that the summation of all the terms linearly proportional to y, including the contribution from the last term in (2.121), is exactly zero. In addition, the z-integration in (2.119) can be carried out by using (2.111).

By summarizing above reductions and substituting the Kochin function, following expression can be derived,

$$\overline{N_1} = \frac{1}{4\pi}\left[-\int_{-\infty}^{k_1} + \int_{k_2}^{k_3} + \int_{k_4}^{\infty}\right]\Re\{C'(k)S^*(k) - C^*(k)S'(k)\}\kappa dk \tag{2.124}$$

where $C'(k)$ and $S'(k)$ are the derivatives of $C(k)$ and $S(k)$ with respect to k, respectively. Here, we can see that only the interaction between symmetric and antisymmetric waves contributes to

the $\overline{N_1}$ term, which is identical to the first term of steady sway force.

The next step is considering the $\overline{N_2}$ which develops from the interaction between the incident waves and ship-generated waves. Following the preceding procedure, the Parseval's theorem is applied by using the Fourier transforms of (2.109) and (2.121). Then, we can put $k = k_0 \cos\chi$ due to the property of Dirac's delta function in (2.109), and $k_0 \sin\chi = \pm\epsilon_k \sqrt{\kappa^2 - k^2}$; so that $\kappa = k_0$. The z-integration in (2.120) can be solved by using (2.110) and following equation

$$\int_0^\infty z e^{-2\kappa z} dz = \left(\frac{1}{2\kappa}\right)^2 \tag{2.125}$$

The result will consist of three parts, which are similar to (2.121): the first ($\overline{N_{21}}$) includes the derivative of the Kochin function, the second ($\overline{N_{22}}$) constitutes terms which linearly proportional to y. and the third ($\overline{N_{23}}$) is the remainder. These three parts are as follows:

$$\overline{N_{21}} = -\frac{1}{2}\sin\chi \Re\left\{k_0 \frac{d}{dk}\left[H^{\pm}(k)\right]\right\} \tag{2.126}$$

$$\overline{N_{22}} = 0 \tag{2.127}$$

$$\overline{N_{23}} = -\frac{1}{2}\sin\chi \Re\left\{\left(\tau + \frac{k_0\cos\chi}{K_0}\right) H(k_0,\chi)\right\} \tag{2.128}$$

One should note that $H^{\pm}(k)$ in (2.126) must be evaluated at $k = k_0\cos\chi$ and $k_0\sin\chi = \pm\epsilon_k\sqrt{\kappa^2 - k^2}$. Accordingly, by using the relation $k_0 = \kappa = (\omega + kU)^2/g$ and substituting the Kochin function, the final result of $\overline{N_2}$ can be written in the form

$$\begin{aligned}\overline{N_2} &= \overline{N_{21}} + \overline{N_{22}} + \overline{N_{23}} \\ &= -\frac{1}{2}\sin\chi \Re\left[k_0\left\{C'(k_0,\chi) + iS'(k_0,\chi)\right\} + \left(\tau + \frac{k_0\cos\chi}{K_0}\right) H(k_0,\chi)\right]\end{aligned} \tag{2.129}$$

where $C'(k_0,\chi) + iS'(k_0,\chi)$ is to be defined as

$$\left[\frac{d}{dk}\left\{C(k) + iS(k)\right\}\right]_{k=k_0\sin\chi;\ \sqrt{\kappa^2-k^2}=k_0\sin\chi} \tag{2.130}$$

Finally, by substituting (2.124) and (2.129) into (2.118), the formula for the steady yaw moment in waves can be expressed as

$$\frac{\overline{N}}{\rho g \zeta_a^2} = \frac{1}{4\pi k_0}\Big[-\int_{-\infty}^{k_1} + \int_{k_2}^{k_3} + \int_{k_4}^{\infty} \Big] \Re\{C'(k)S^*(k) - C^*(k)S'(k)\}\kappa dk$$
$$- \frac{1}{2}\sin\chi \Re\Big[C'(k_0,\chi) + iS'(k_0,\chi) + \frac{1}{k_0}\Big(\tau + \frac{k_0\cos\chi}{K_0}\Big)H(k_0,\chi)\Big] \tag{2.131}$$

In order to correctly solve the integral in this equation, as well as in (2.102) and (2.114), one should consider numerical issues of square-root singularity and semi-infinite integral. Exact solutions to address these problems are presented comprehensively in the Appendices A, B and C.

2.4.5 Kochin Function

Based on the derivations on previous subsections, the final expressions of added resistance, steady sway force, and steady yaw moment have been obtained in (2.102), (2.114) and (2.131), respectively.

Kochin function of wave amplitude states that $H(k) = C(k) + iS(k)$, with $C(k)$ stands for symmetric component with respect to the center-plane of a ship symmetrical about $y = 0$, and $S(k)$ stands for the antisymmetric ones, that can be expressed by the followings

$$\left.\begin{aligned} C(k) &= C_7(k) - \frac{\omega\omega_0}{g}\sum_{j=1,3,5}\frac{X_j}{A}C_j(k) \\ S(k) &= S_7(k) - \frac{\omega\omega_0}{g}\sum_{j=2,4,6}\frac{X_j}{A}S_j(k) \end{aligned}\right\} \tag{2.132}$$

where the $j = 1 \sim 6$ suffix denotes the radiation wave of j-mode, $j = 7$ denotes the incident waves scattered/diffracted by the ship hull. X_j/A of each j-mode denotes the nondimensionalized ship motion in waves.

Then, radiation Kochin function $C_j(k)$ and $S_j(k)$ can be computed by

$$\left.\begin{aligned} C_j(k) &= \int_L Q_j(x) e^{ikx} dx \\ S_j(k) &= \frac{\sqrt{\kappa^2 - k^2}}{\kappa} \int_L D_j(x) e^{ikx} dx = \sqrt{1 - k^2/\kappa^2}\,\widehat{S}_j(k) \end{aligned}\right\} \tag{2.133}$$

Here, the x-integration range is from the ship's stern to bow, where the $Q_j(x)$ and $D_j(x)$, based on the slender-ship theory, represents the x-axis linear source strength ($z = 0$ on the free surface) and doublet strength, respectively.

2.5 Enhanced Unified Theory

Prior to the estimation of the second-order steady force and moment, the unsteady velocity potential given in (2.16) must be solved by satisfying the governing equations and boundary conditions. In the framework of slender-ship theory, these equations may be reduced into a simpler form by introducing the slenderness parameter ϵ.

At a distance far away from the ship ($\epsilon \to 0$), the ship hull will shrink into a line along the x-axis, therefore the body boundary condition cannot be imposed; the so-called "**outer problem**". By the transformation of $y = \epsilon Y$ and $z = \epsilon Z$, the y and z axes may be zoomed into the body surface. Hence, we obtain the body-boundary condition to be solved in the magnified $Y - Z$ plane. On the other side, the ship-generated waves at the far field cannot be understood in the vicinity of the ship, and thus the radiation condition cannot be imposed; the so-called "**inner problem**".

With this definition, we will consider symmetric and antisymmetric modes in the radiation problem ($j = 1 \sim 6$) and in the diffraction problem ($j = 7, 8$) with respect to the vertical $X - Z$ plane.

2.5.1 Radiation Problem

In the inner region, due to the small y-perturbation justified by the slenderness assumption, the flow velocity gradient along the x-axis is small compared to that in transverse sections; then

the radiation condition may not be imposed. Therefore the unsteady velocity potential for the radiation waves must satisfy the following boundary conditions:

$$\frac{\partial^2 \phi_j}{\partial y^2} + \frac{\partial^2 \phi_j}{\partial z^2} = 0 \qquad \text{for } z \geq 0 \tag{2.134}$$

$$\frac{\partial \phi_j}{\partial z} + K\phi_j = 0 \qquad \text{on } z \geq 0 \tag{2.135}$$

$$\frac{\partial \phi_j}{\partial n} = n_j + \frac{U}{i\omega} m_j \qquad \text{on } C_H(x) \tag{2.136}$$

with n and m terms previously explained in (2.37). These are considered on the contour $C_H(x)$ of the transverse section at position x over the ship length.

Since we are lacking of the radiation condition, a homogeneous solution may be used to construct the general inner solution satisfying the boundary conditions in the following form:

$$\phi_j(x; y, z) = \phi_j^P(y, z) + C_j(x)\phi^H(y, z) \tag{2.137}$$

$$\phi_j^P(y, z) = \varphi_j(y, z) + \frac{U}{i\omega}\widehat{\varphi}_j(y, z) \tag{2.138}$$

$$\phi_j^H(y, z) = \left\{\varphi_3(y, z) - \varphi_3^*(y, z)\right\} \tag{2.139}$$

Here, ϕ_j^P the particular solutions with φ_j and $\widehat{\varphi}_j$ correspond to the solutions of the first and second terms on the right-hand side of (2.139) respectively. ϕ_j^H is a homogeneous solution with the unknown coefficient $C_j(x)$, while the asterisk denotes the complex conjugate.

In the outer region far away from the ship, the body boundary condition cannot be imposed. Thus the outer solution can be formulated by a line distribution of the 3D source along the x-axis and expressed in the form

$$\phi_j(x, y, z) = \int_L Q_j(\xi) G(x - \xi, y, z) d\xi \tag{2.140}$$

where G is the 3D Green function given by (2.58) for the translating and oscillating problems, and Q_j is the unknown strength. By the matching between the outer expansion of the inner solution and the inner expansion of the outer solution in an overlapping (middle) region, the

unknown $C_j(x)$ in (2.130) and $Q_j(x)$ in (2.140) can be obtained and given as follows:

$$\phi_j(x) + \frac{i}{2\pi}\left(1 - \frac{\sigma_3}{\sigma_3^*}\right) = \int_L Q_j(\xi) f(x-\xi) d\xi = \sigma_j + \frac{U}{i\omega}\widehat{\sigma}_j \tag{2.141}$$

$$C_j(x)\left\{\sigma_3 - \sigma_3^*\right\} = Q_j - \left\{\sigma_j + \frac{U}{i\omega}\widehat{\sigma}_j\right\} \tag{2.142}$$

with $f(x-\xi)$ the kernel function containing the 3D and forward-speed effects. The explicit expression of this function is given in the original unified theory [48]. σ_j and $\widehat{\sigma}_j$ denote the 2D Kochin function to be computed from φ_j and $\widehat{\varphi}_j$, respectively.

2.5.2 Diffraction Problem

By assuming that the rapidly-varying component of the scattering potential along the ship length is of the same form as the incident wave, the scattering potential may be taken in the form

$$\phi_7(x;y,z) = \psi_7(x;,y,z)e^{ilx}; \quad l = -k_0\cos\chi \tag{2.143}$$

with ψ_7 the slowly-varying term of the inner solution that satisfies following boundary conditions:

$$\frac{\partial^2\psi_7}{\partial y^2} + \frac{\partial^2\psi_7}{\partial z^2} - l^2\psi_7 = 0 \quad \text{on } z \geq 0 \tag{2.144}$$

$$\frac{\partial\psi_7}{\partial z} + k_0\psi_7 = 0 \quad \text{on } z = 0 \tag{2.145}$$

$$\frac{\partial\psi_7}{\partial n} = k_0 e^{-k_0 z}\{(n_3 + in_1\cos\chi)\cos(k_0 y\sin\chi) + n_2\sin\chi\sin(k_0 y\sin\chi)\} \quad \text{on } C_H(x) \tag{2.146}$$

Therefore, the general inner solution can be expressed as follows:

$$\psi_7(x;y,z) = \psi_7^P(y,z) + C_7(x)\psi_7^H(y,z) \tag{2.147}$$

$$\psi_7^P(y,z) = -e^{-k_0 z}\cos(k_0 y \sin\chi) \tag{2.148}$$

$$\psi_7^H(y,z) = \left\{\psi_{2D}(x;y,z) + e^{-k_0 z}\cos(k_0 y \sin\chi)\right\} \tag{2.149}$$

with ψ_{2D} the numerical solution taking account the body-boundary condition which includes the n_1 contribution in (2.146). Using the same procedure in the radiation problem, the unknown $C_7(x)$ can also be obtained by the inner-outer matching procedure. Then by solving an integral of the source strength in the outer solution, the $C_7(x)$ can be calculated from

$$Q_7(x) + \frac{1}{\pi}\sigma_7\left\{Q_7(x)h_1(\chi) - \int_L Q_7(\xi)f(x-\xi)d\xi\right\} = \sigma_7 e^{ilx} \tag{2.150}$$

$$C_7(x)\sigma_7 e^{ilx} = Q_7(x) \tag{2.151}$$

with

$$h_1(x) = \csc\chi\cosh^{-1}(|\sec\chi|) - ln(2|\sec\chi|) \tag{2.152}$$

Moreover, details of radiation and diffraction problems on enhanced unified theory are explained in Kashiwagi [4, 8].

2.6 Wave-Induced Ship Motions

The motion equations for all modes of motion can be computed by the following equation

$$\sum_{j=1\sim6}[-\omega^2(M_{ij}+A_{ij}) + i\omega B_{ij} + C_{ij}]X_j = E_i \quad (i = 1 \sim 6) \tag{2.153}$$

with M_{ij} is the generalized mass matrix and C_{ij} the restoring force matrix. The resulting nonzero terms from these matrices are

$$\left.\begin{aligned} M_{11} &= M_{33}, \quad M_{55} = I_{55} = \rho\nabla\kappa_{yy}^2 \\ C_{33} &= \rho g A_w, \quad C_{35} = C_{53} = -\rho g A_w x_w \\ C_{55} &= \rho g\nabla\overline{GM_L}, \quad C_{44} = mg\overline{GM} \end{aligned}\right\} \tag{2.154}$$

with the displacement volume ∇ and the gyrational radius in pitch κ_{yy}. A_w is the waterplane area with x_w as its center in x-axis and $\overline{GM_L}$ is longitudinal metacentric height. Here, the viscous damping formulation of Himeno [49] is used to account for nonlinear damping.

2.7 Experiment

2.7.1 JASNAOE-BC084 (Bulk Carrier)

The computed ship in concern is a bulk carrier named JASNAOE-BC084. Comes with bulbous bow, the 3D projection of its body plan is illustrated on Fig. 2.2. Her principal particulars are shown in Table 2.1.

Table 2.1: Principal particulars of JASNAOE-BC084

Item	Value	Unit
Length between perpendiculars (L_{PP})	320.00	m
Breadth (B)	58.00	m
Draft (d)	20.80	m
Block coefficient (C_B)	0.84	-
Midship coefficient (C_M)	0.99	-
Waterplane coefficient (C_{WP})	0.93	-
Center of gravity (OG)	9.80	m
Roll gyrational radius (K_{xx}/B)	0.35	-
Pitch gyrational radius (K_{yy}/L)	0.25	-
Yaw gyrational radius (K_{zz}/L)	0.25	-

Experiment was done in the tank of Mitsubishi Heavy Industries for the JASNAOE Strategy Research Committee on IMO Guideline of Minimum Engine Power. In the experiment, motions

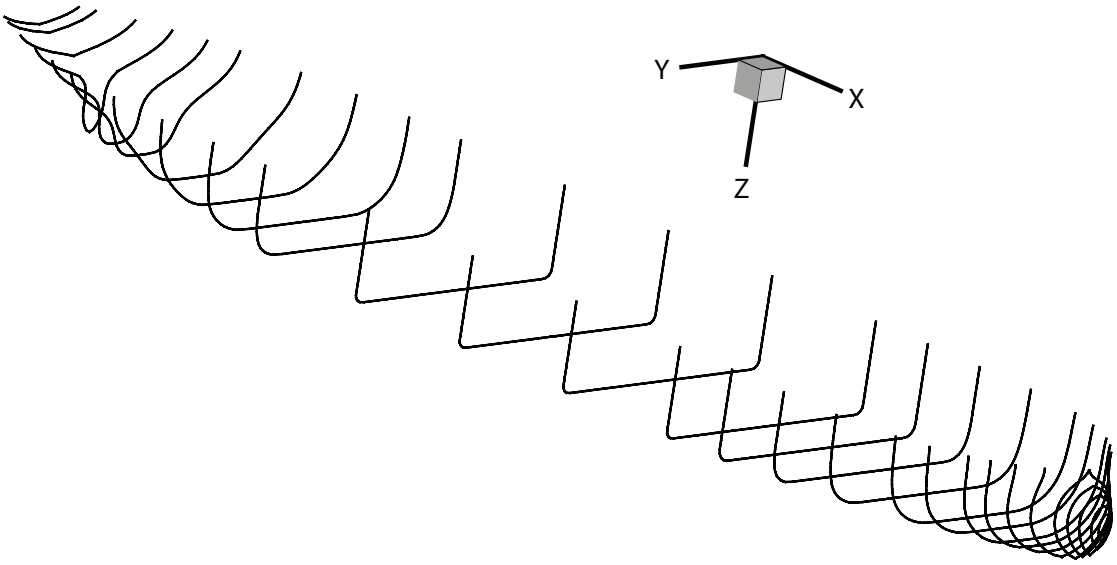

FIGURE 2.2: Body plan of JASNAOE-BC084

and steady forces were measured in four conditions of forward speed (Fn): 0.000, 0.037, 0.074, 0.124. At every Froude number except 0.124, measurements were done in four ship-waves encountering angles as shown in Fig. 2.3: $30^\circ, 90^\circ, 150^\circ, 180^\circ$, where 180° signifies the head waves as the sole heading condition at $Fn = 0.124$. The wavelengths in measurements were $\lambda/L = 0.4 \sim 1.5$.

On each experimental quantity, there are two measured values representing different mechanisms in capturing the incident wave amplitude, which resulted from encountering and stationary wave probes. The encountering wave probe is installed on the ship's carriage, thus runs together along the ship while measuring the wave amplitude. In contrast, the stationary wave probe is located close to the side wall of towing tank, and measures the wave amplitude at a distance from the ship.

By this understanding of technical problem in the experiment, it is rational in physics to judge that the incident wave amplitude recorded by the stationary wave probe will be less disturbed by the near-field ship-scattered waves than the distance-wise prone encountering wave probe. Accordingly, the measured data nondimensionalized by far-field incident wave amplitude are taken to validate the numerical computation.

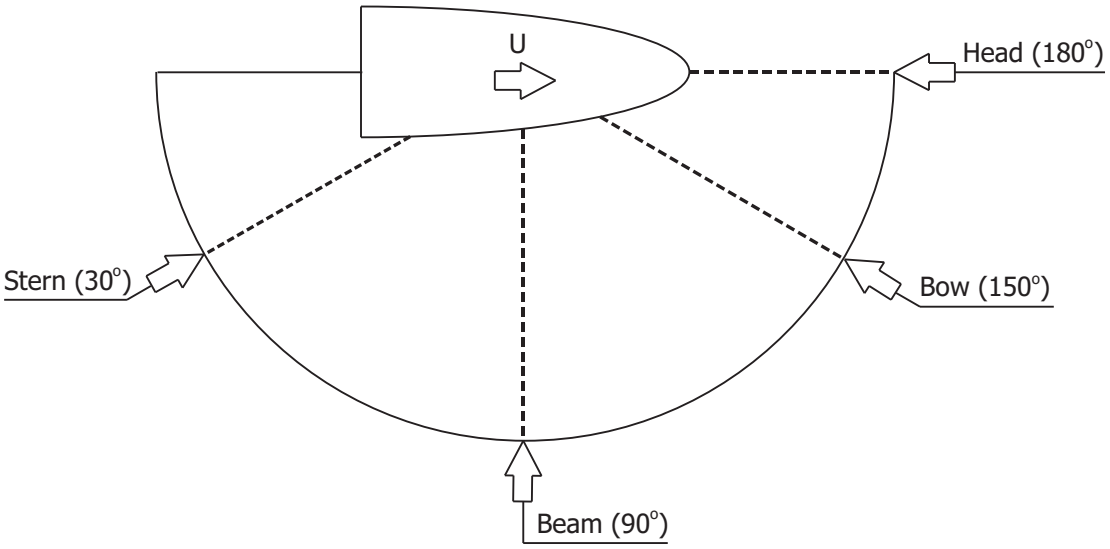

FIGURE 2.3: Ship-waves encountering angles

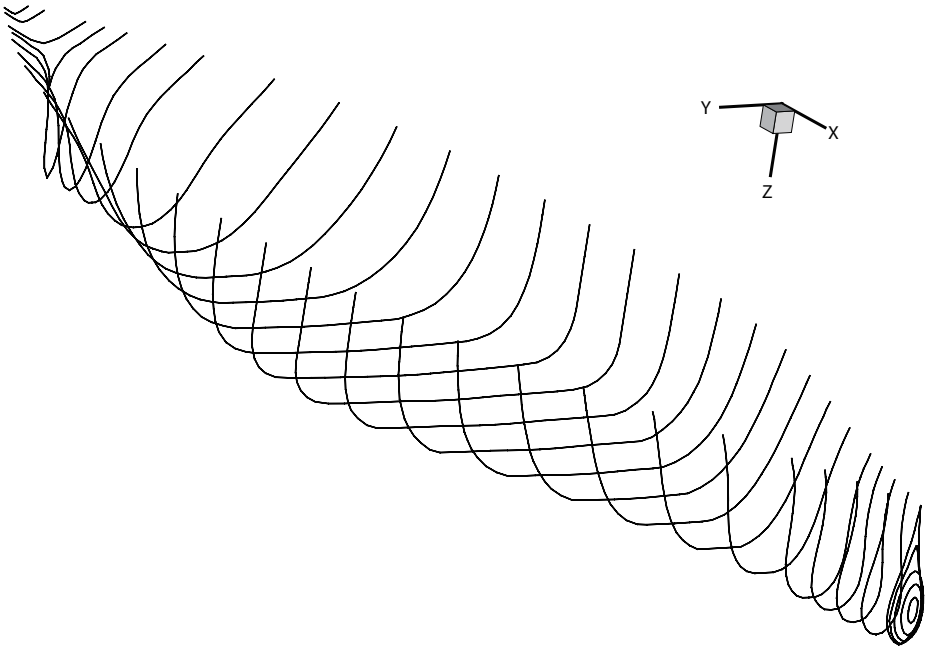

FIGURE 2.4: Body plan of SR108 container ship

2.7.2 SR108 (Container Ship)

The body plan and principal particulars of SR108 container ship model are presented in Fig. 2.4 and Table 2.2, respectively. In the experiment of Yasukawa [20], the added resistance, steady sway force , and steady yaw moment of SR108 container ship were measured at $Fn = 0.15$ with incident waves of $\chi = 90°, 180°$ (beam and head waves).

TABLE 2.2: Principal particulars of SR108 container ship model

Item	Value	Unit
Length: (L_{pp})	3.500	m
Breadth: (B)	0.508	m
Draft: (d)	0.190	m
Block coefficient (C_B)	0.572	-
Displacement: (∇)	1897.0	N
Metacentric height ($\overline{GM}$)	20.1	mm
Roll gyrational radius (κ_{xx}/B)	0.350	-
Pitch gyrational radius (κ_{yy}/L)	0.269	-
Yaw gyrational radius (κ_{zz}/L)	0.269	-

2.8 Computation Results and Discussion

2.8.1 JASNAOE-BC084 (Bulk Carrier)

Motion Based on aforesaid conditions, computed ship motions are depictured on Figs. 2.5 ~ 2.10. As representatives, only oblique waves cases are compared for the discussion. Several findings are described in the followings.

At zero forward speed, comparable motion quantities can be seen on bow and stern waves (30° and 150°). Slight variation is generated due to the dinstinct hull shapes at both ship ends. When forward speed is exist, the computed values also correspond with the measured ones. Slight difference is visible on the resonant frequency of roll motion, which has been corrected by Himeno's formulation [49].

The influence of the forward speed can be seen from the visible Doppler effect (shifting of peak) as the ship speed heightens. In addition, since x-component of normal vector is not retained in the NSM formulation of body boundary condition, surge motion is virtually predicted as zero for all frequencies. In few cases of short waves, the computed motions by EUT show minor spikes due to the slow convergence of unified-theory integral equation. Therefore, this should be understood as purely numerical issue. Regardless of certain extent of discrepancy, the overall agreement between computations and measurement is practically exceptional.

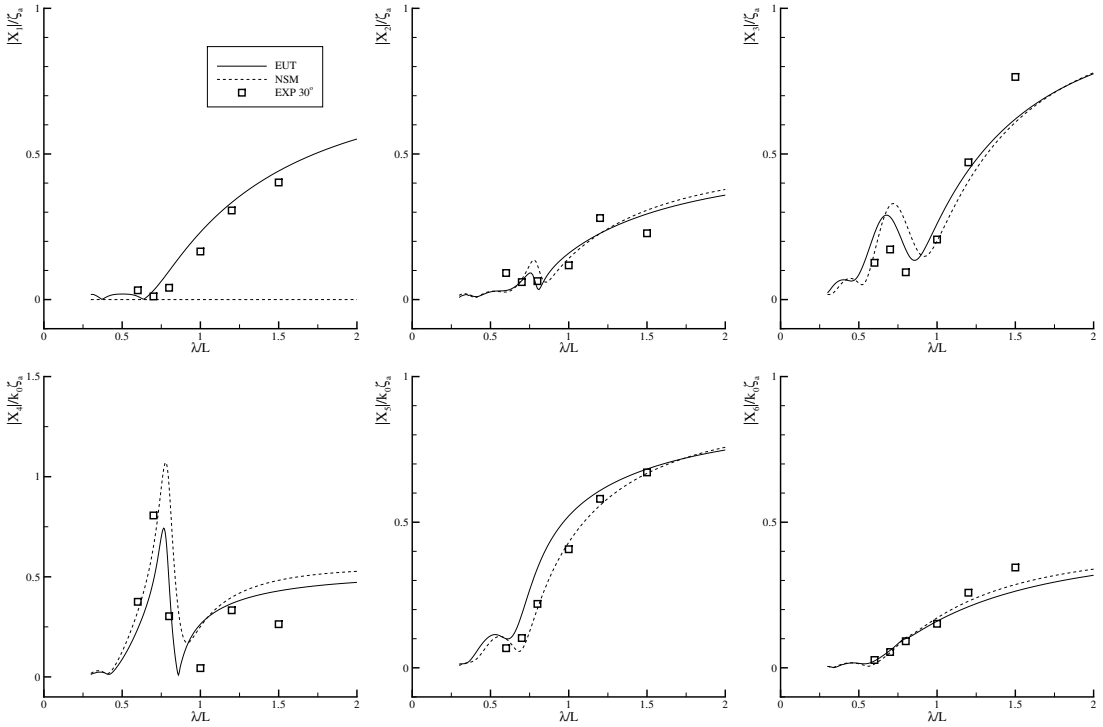

FIGURE 2.5: Motions of JASNAOE-BC084 ($\chi = 30°$, $U = 0$ knot $\propto Fn = 0.0$)

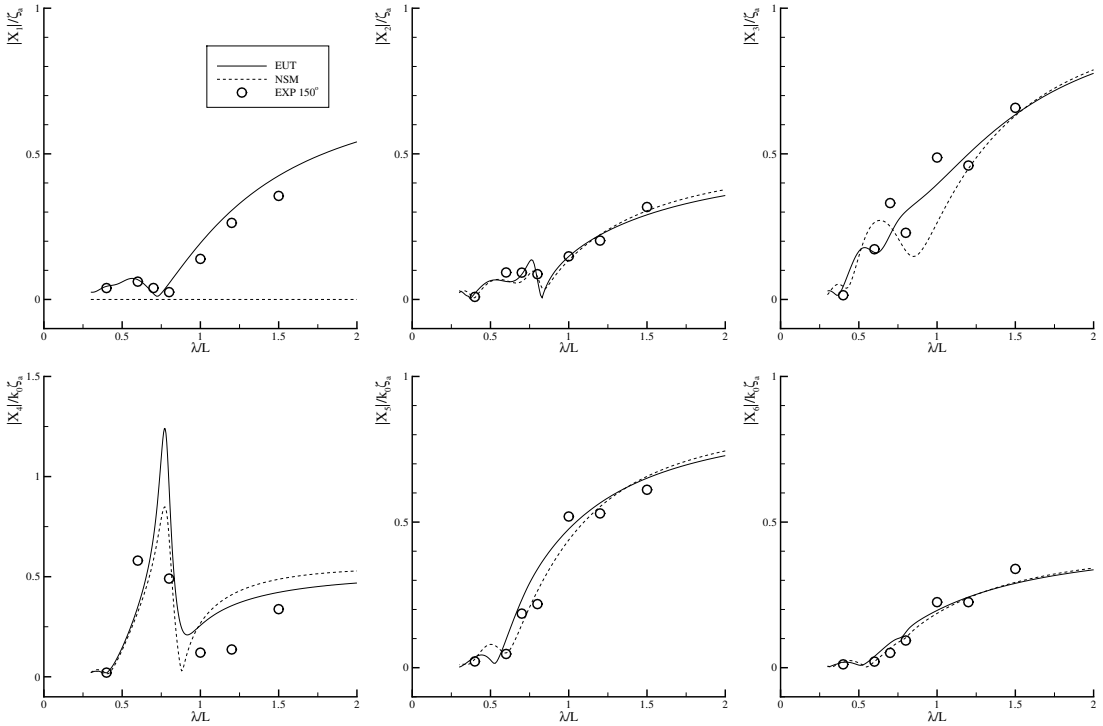

FIGURE 2.6: Motions of JASNAOE-BC084 ($\chi = 150°$, $U = 0$ knot $\propto Fn = 0.0$)

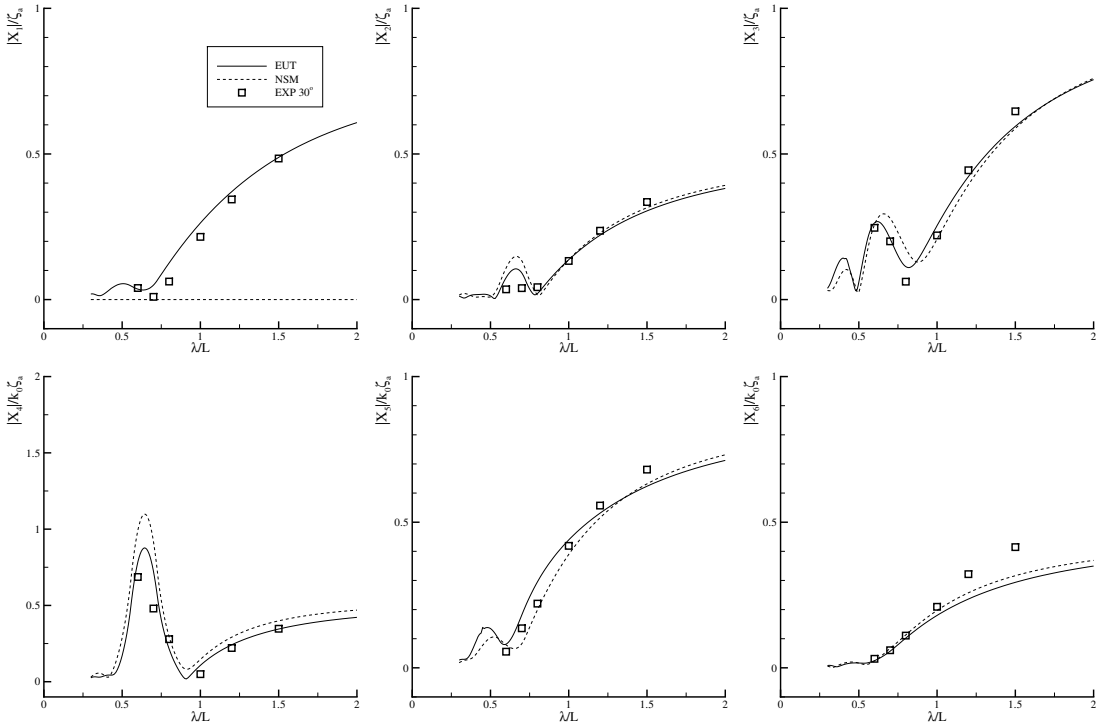

FIGURE 2.7: Motions of JASNAOE-BC084 ($\chi = 30°$, $U = 4$ knot $\propto Fn = 0.037$)

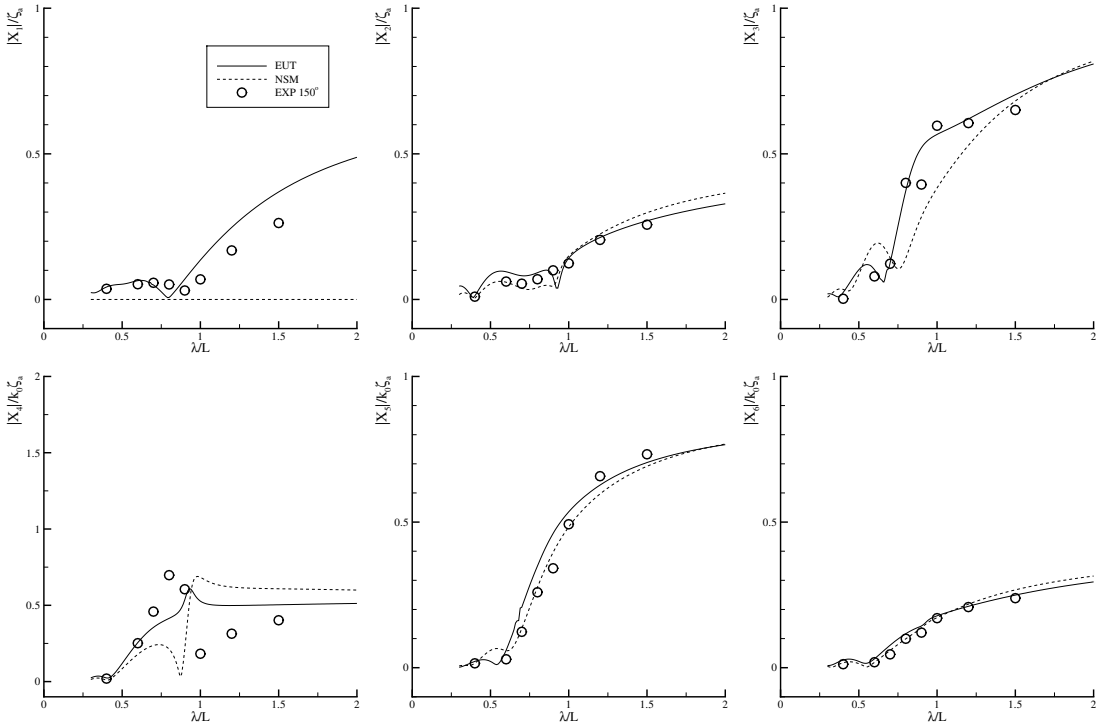

FIGURE 2.8: Motions of JASNAOE-BC084 ($\chi = 150°$, $U = 4$ knot $\propto Fn = 0.037$)

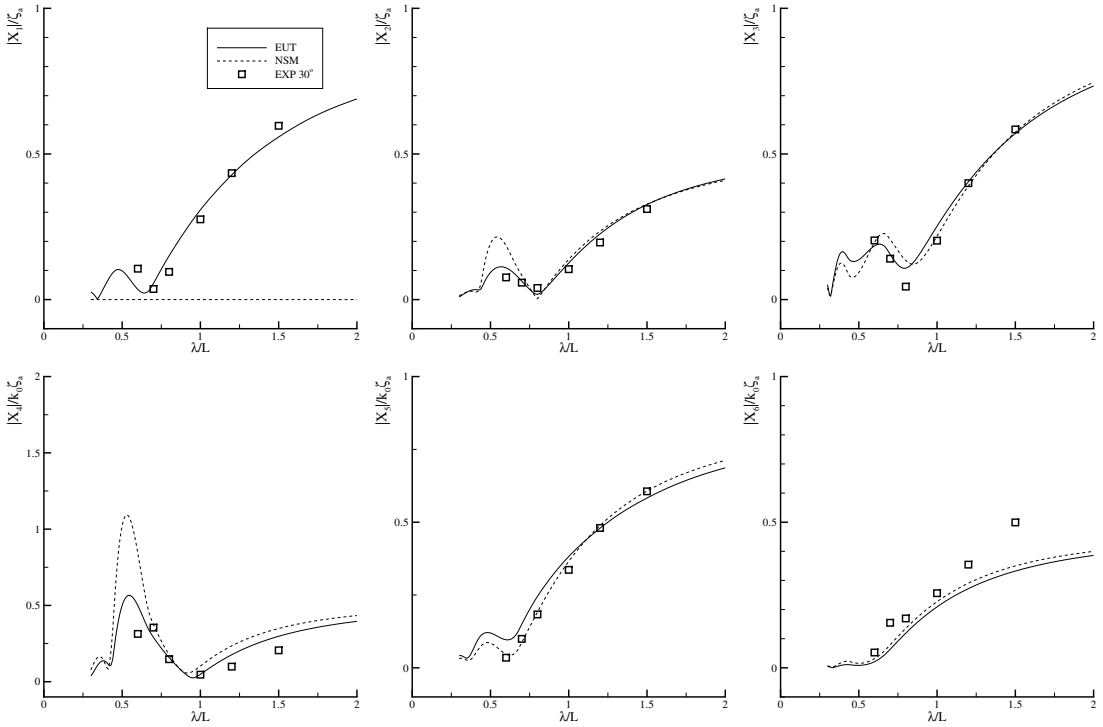

FIGURE 2.9: Motions of JASNAOE-BC084 ($\chi = 30°$, $U = 8$ knot $\propto Fn = 0.074$)

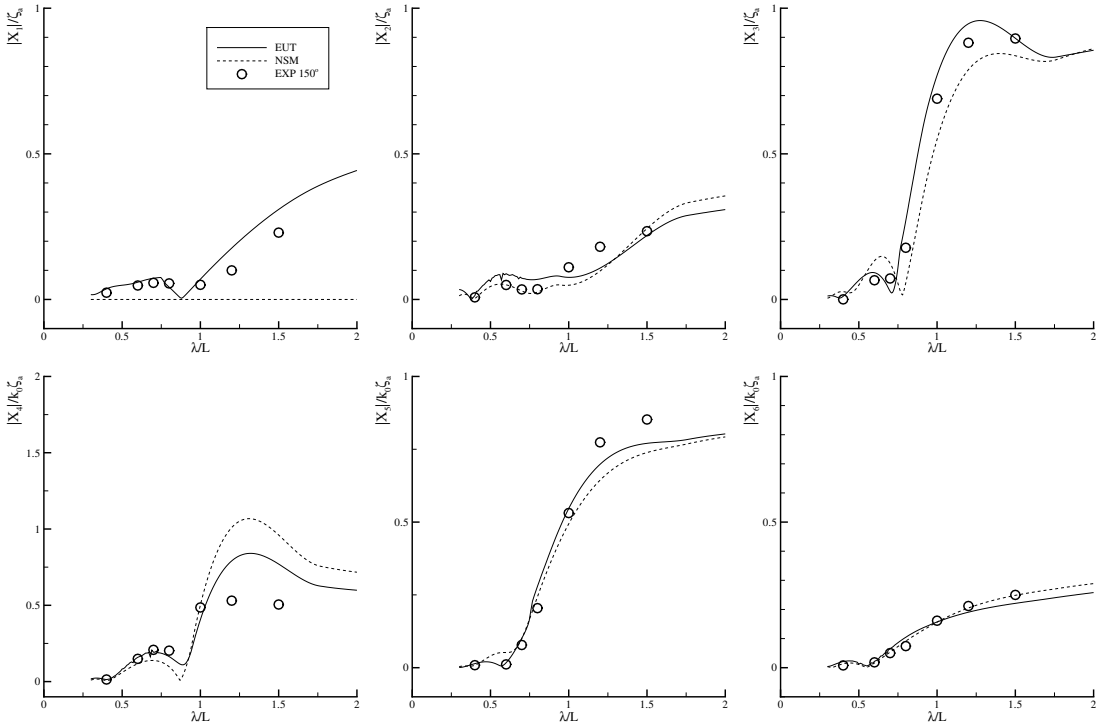

FIGURE 2.10: Motions of JASNAOE-BC084 ($\chi = 150°$, $U = 8$ knot $\propto Fn = 0.074$)

Second-Order Steady Forces and Moment Based on experimental conditions explained on Fig. 2.3, computations were done by enhanced unified theory (EUT) and new strip method (NSM). The antisymmetric motion resonant peaks are practically corrected by employing non-linear viscous damping forces [49] on pure roll and its couplings. The forces behavior and issues illustrated in Figs. 2.11 ~ 2.41 are presented below.

At zero speed, characteristic of the forces can be observed. Since they are functions of their corresponding motions, resembling mirrored results can be seen on both conditions, particularly on longer waves. In short waves, the values differ due to the distinctive bow-stern geometry since the diffraction wave is sensitive to the shape. Calculations by NSM mostly underestimated the forces magnitude in shorter waves region.

At $Fn = 0.037$, steady forces behavior is well predicted on wide range of frequency, and the agreement is remarkable. It is also investigated that the measured values in bow and stern waves give different trends due to the existence of forward speed. In shorter waves, the underestimation of NSM in computing the steady forces and moment are intensified, in contrast to the accurate observation by EUT.

At $Fn = 0.074$, the results fluctuate slightly in shorter waves. At this Froude number, the Hanaoka's parameter (τ) in each ship heading angle needs to be considered since it is exist inside the range of computed λ/L. This exact point may give drastic changes or bumps in relation to the quarter of τ. Besides, this might also be contributed by the sensitivity of diffraction component to the ship ends' shapes, which indicates the necessity in improving the ship geometry interpolation, more especially at the spots where the sectional contours vary rapidly.

Other factor is the integration method of outer source strength in the unified-theory integral equation. For zero or very low forward speed, linear interpolation is suitable for this integration, where Chebyshev polynomial is favorable for moderate or higher speeds. The transition between these two methods has been confirmed and is located around $Fn \approx 0.08$. Therefore, the case of $Fn = 0.074$ falls exactly in this transition zone.

Finally, at the highest velocity of $Fn = 0.1239$, EUT estimated the added resistance accurately, while the NSM predicted around 50% of the measured values at the peak frequency. The steady sway force and steady yaw moment on the head waves are virtually zero, with some noise shown in the experiment data.

Hence, computed wave-induced steady forces and moment by both means are showing good agreement with the measured quantities in experiment, where in general, EUT is more favorable.

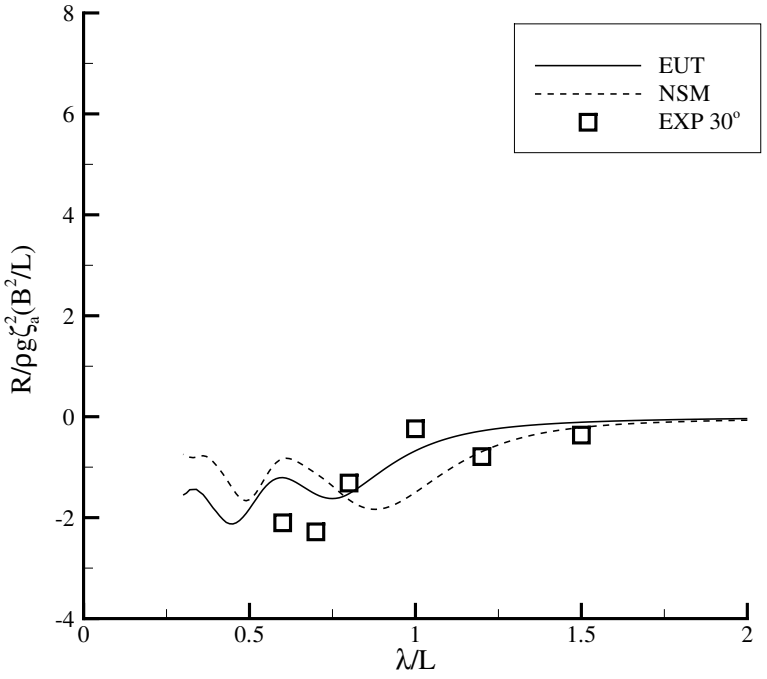

FIGURE 2.11: Longitudinal drift force of JASNAOE-BC084 ($\chi = 30°$, $Fn = 0.0$)

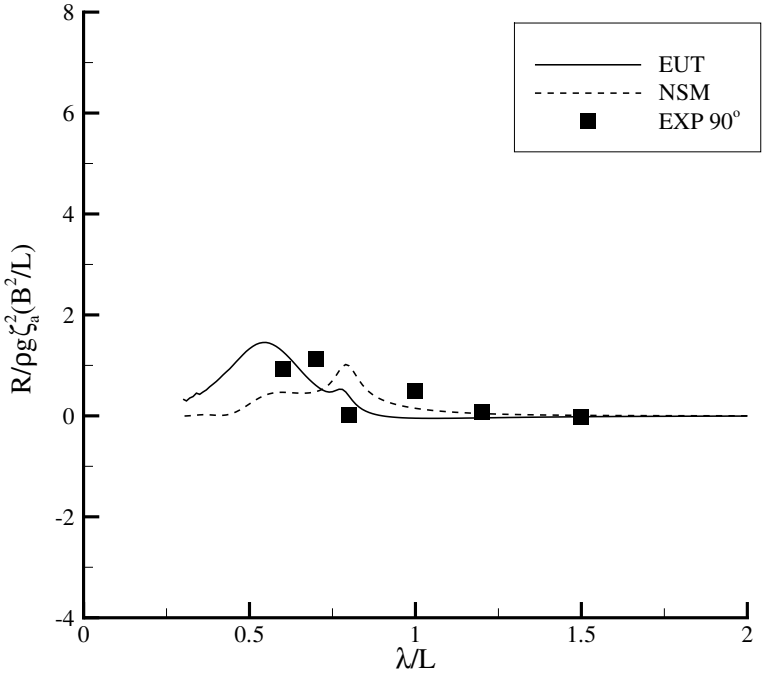

FIGURE 2.12: Longitudinal drift force of JASNAOE-BC084 ($\chi = 90°$, $Fn = 0.0$)

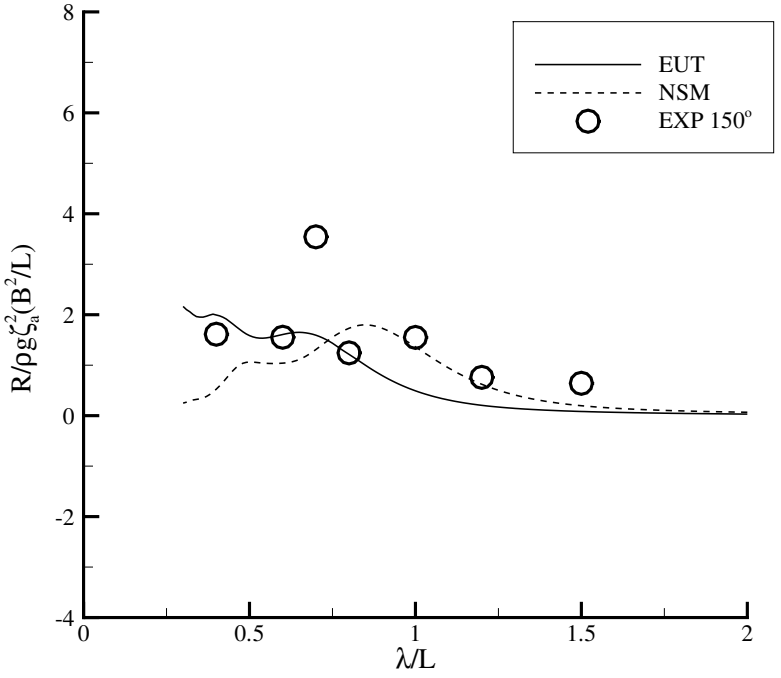

FIGURE 2.13: Longitudinal drift force of JASNAOE-BC084 ($\chi = 150°$, $Fn = 0.0$)

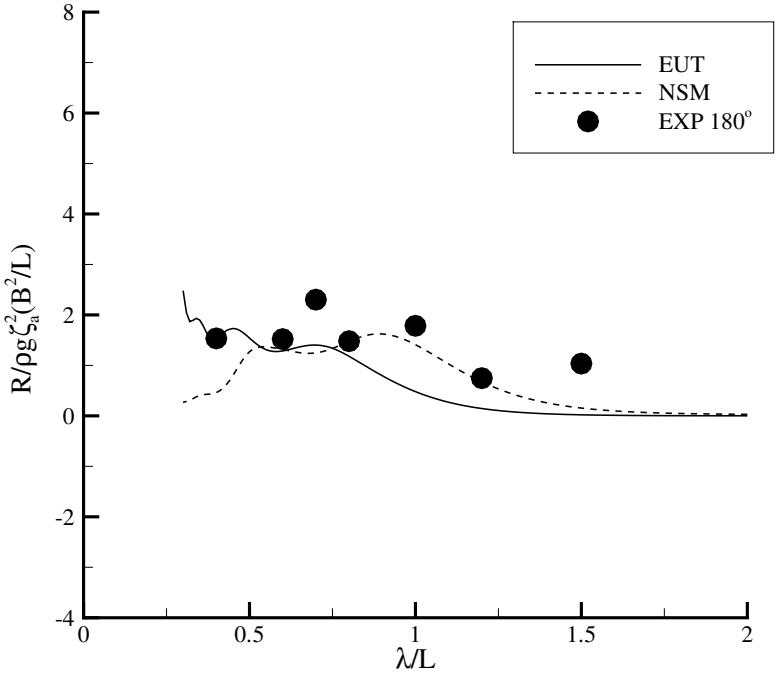

FIGURE 2.14: Longitudinal drift force of JASNAOE-BC084 (χ = 180°, Fn = 0.0)

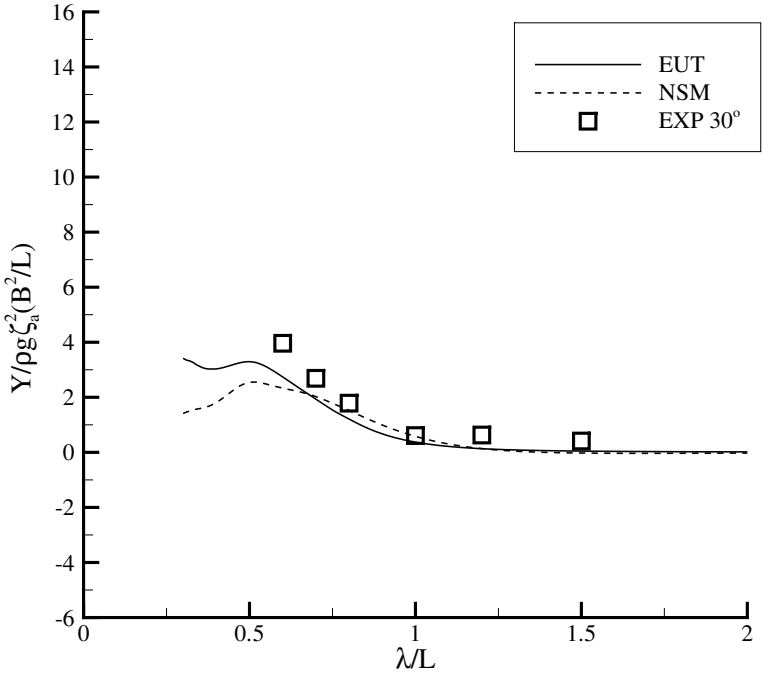

FIGURE 2.15: Sway drift force of JASNAOE-BC084 (χ = 30°, Fn = 0.0)

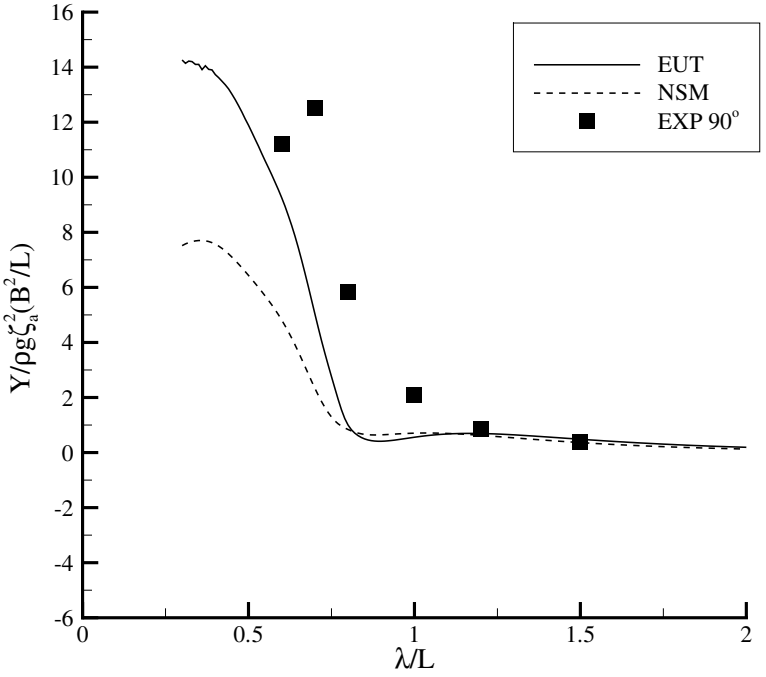

FIGURE 2.16: Sway drift force of JASNAOE-BC084 (χ = 90°, Fn = 0.0)

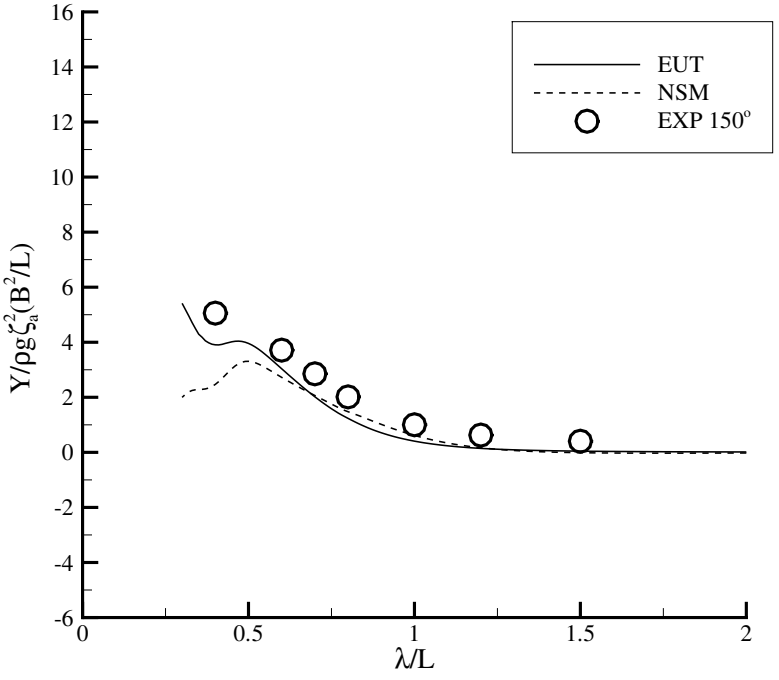

FIGURE 2.17: Sway drift force of JASNAOE-BC084 (χ = 150°, Fn = 0.0)

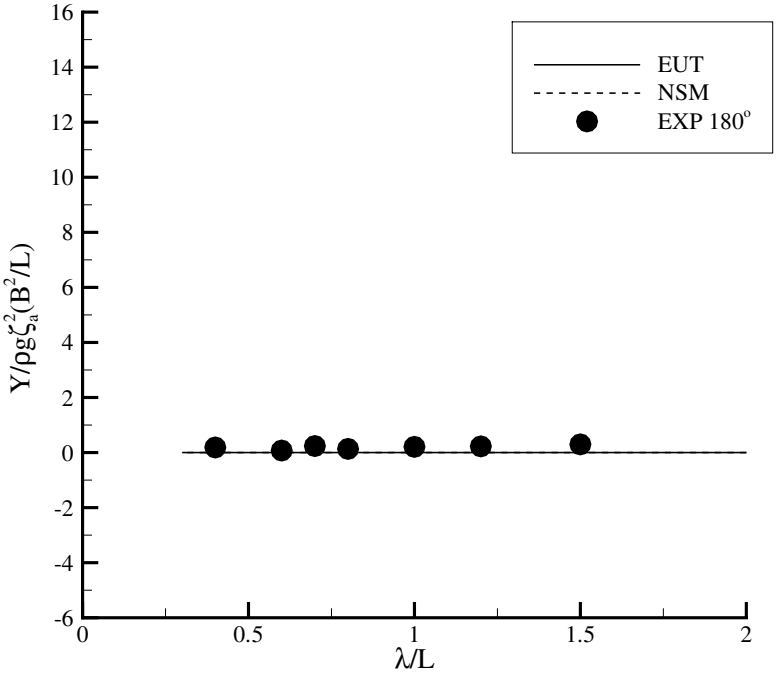

FIGURE 2.18: Sway drift force of JASNAOE-BC084 (χ = 180°, Fn = 0.0)

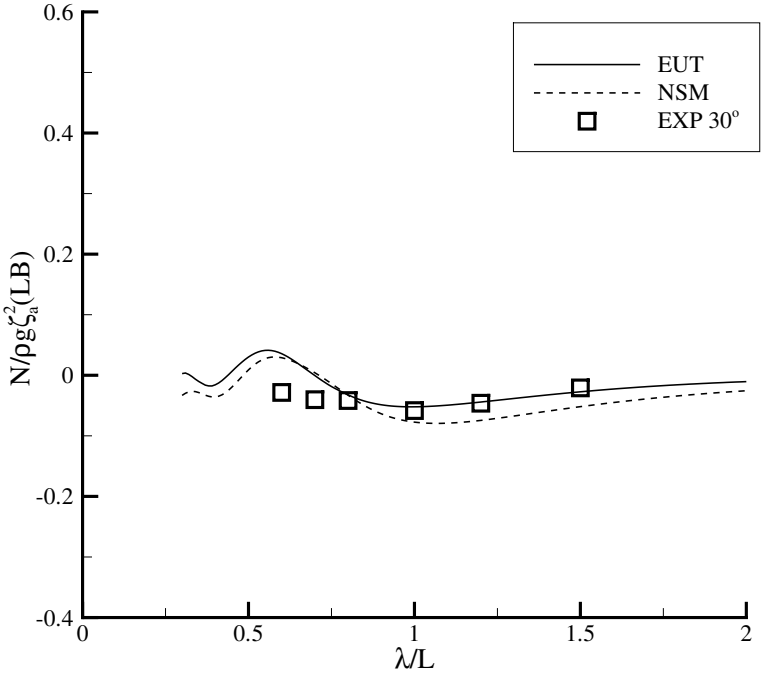

FIGURE 2.19: Yaw drift moment of JASNAOE-BC084 (χ = 30°, Fn = 0.0)

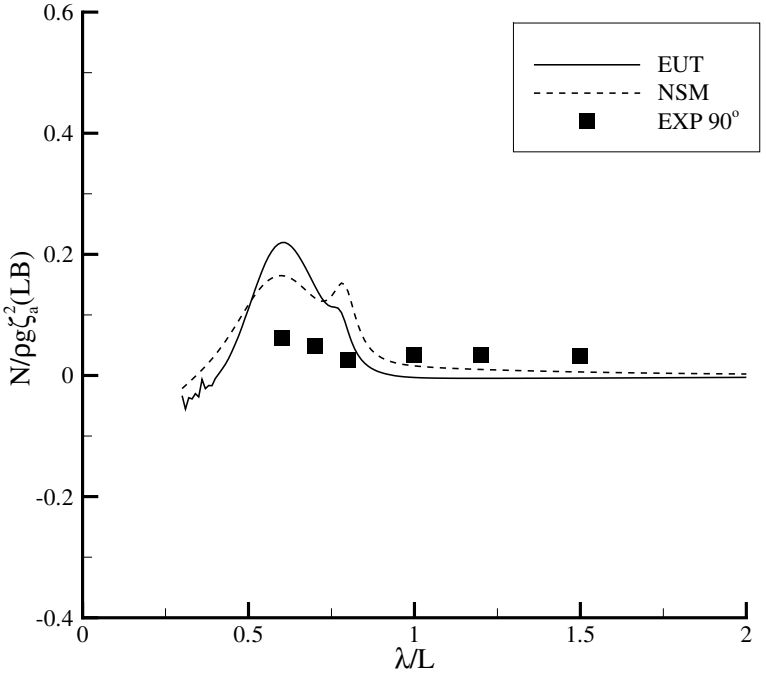

FIGURE 2.20: Yaw drift moment of JASNAOE-BC084 (χ = 90°, Fn = 0.0)

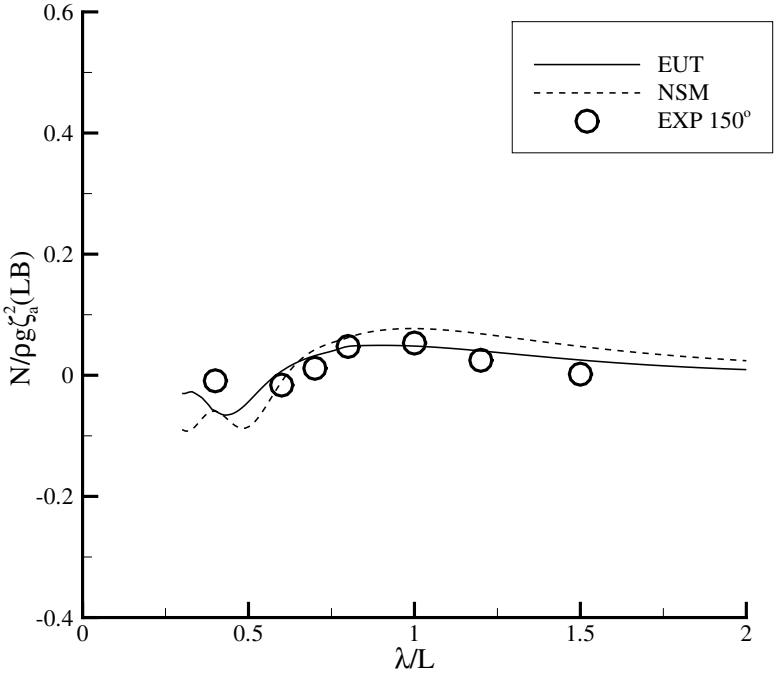

FIGURE 2.21: Yaw drift moment of JASNAOE-BC084 (χ = 150°, Fn = 0.0)

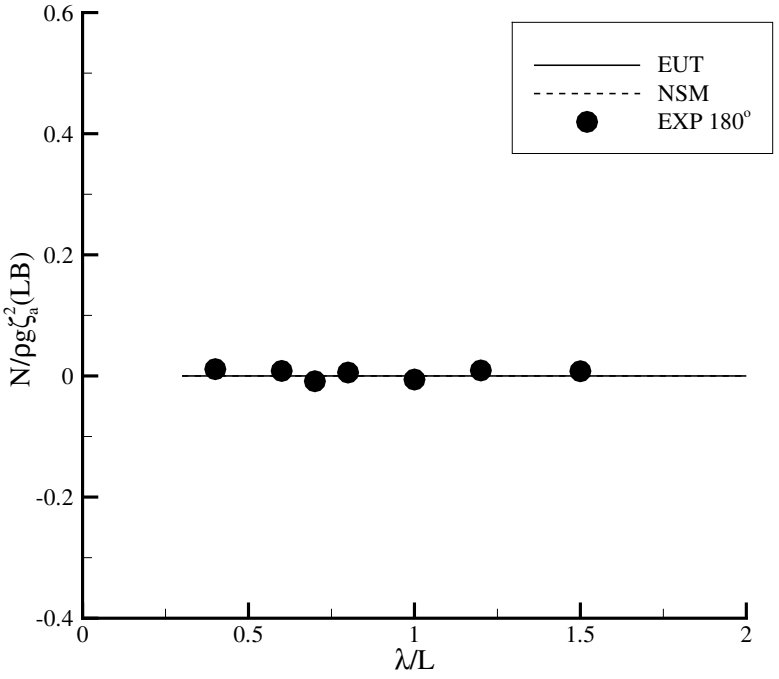

FIGURE 2.22: Yaw drift moment of JASNAOE-BC084 (χ = 180°, Fn = 0.0)

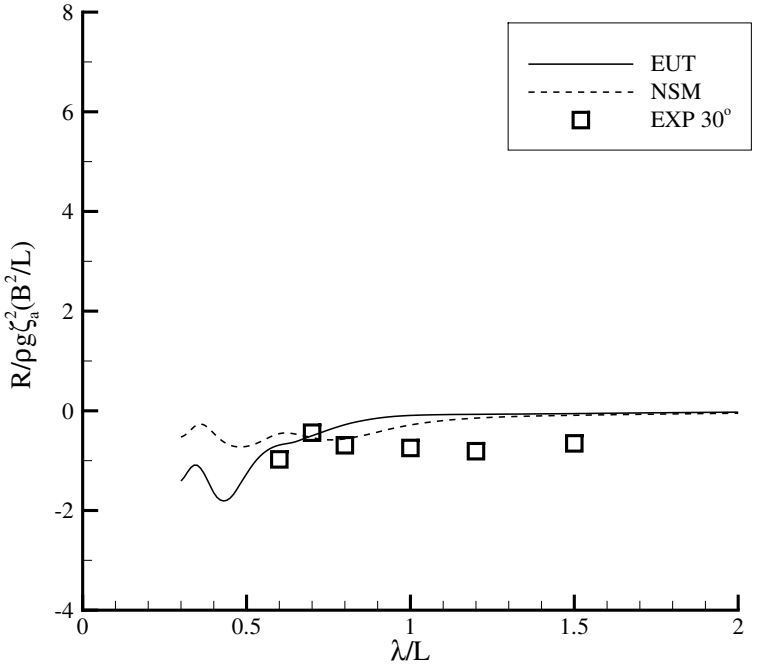

FIGURE 2.23: Added resistance of JASNAOE-BC084 (χ = 30°, Fn = 0.037)

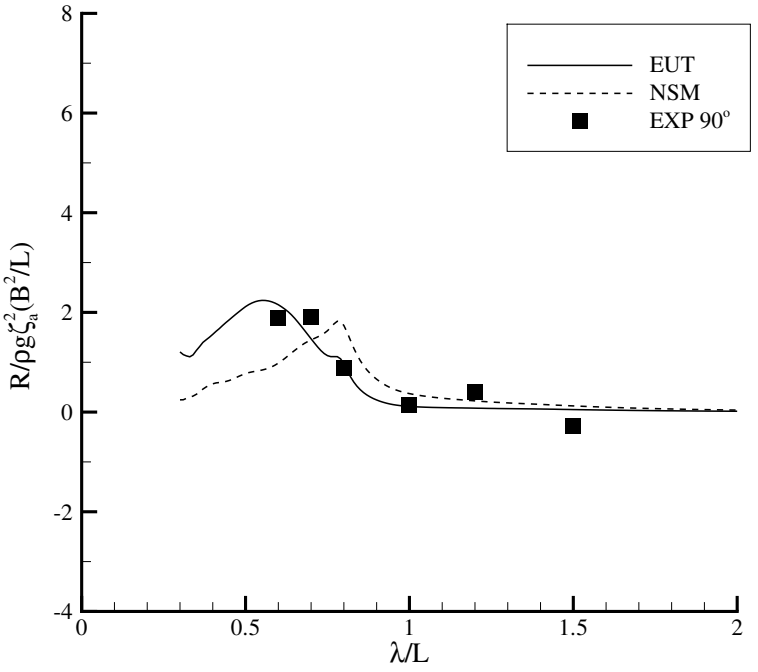

FIGURE 2.24: Added resistance of JASNAOE-BC084 (χ = 90°, Fn = 0.037)

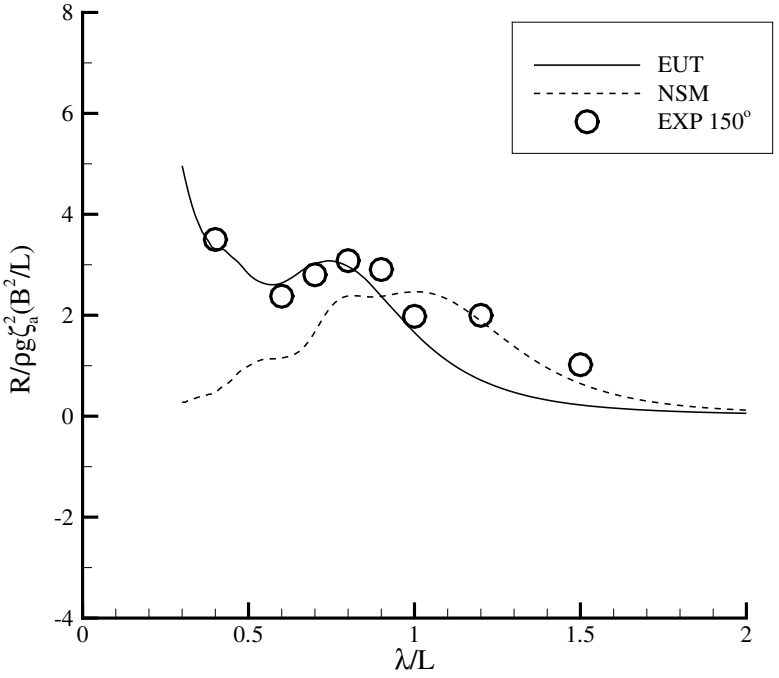

FIGURE 2.25: Added resistance of JASNAOE-BC084 (χ = 150°, Fn = 0.037)

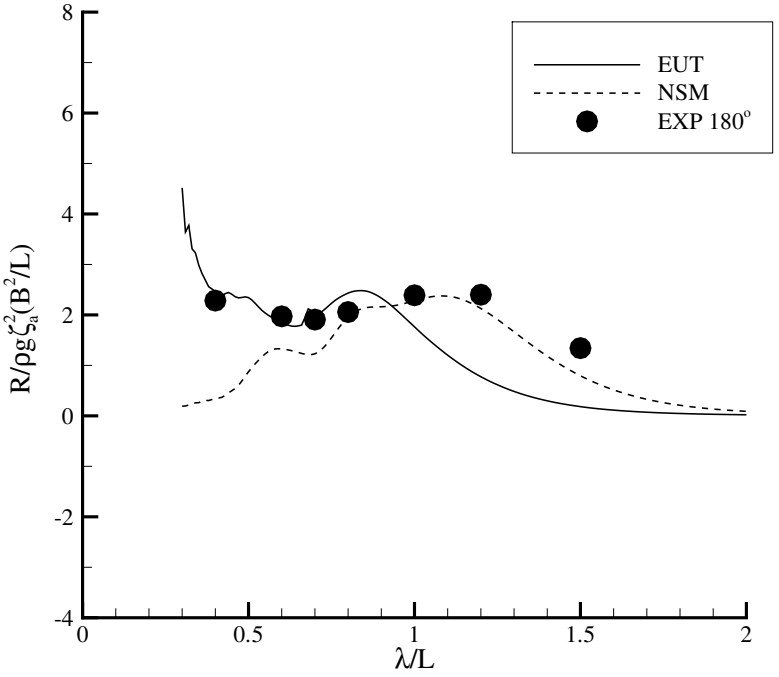

FIGURE 2.26: Added resistance of JASNAOE-BC084 ($\chi = 180°$, $Fn = 0.037$)

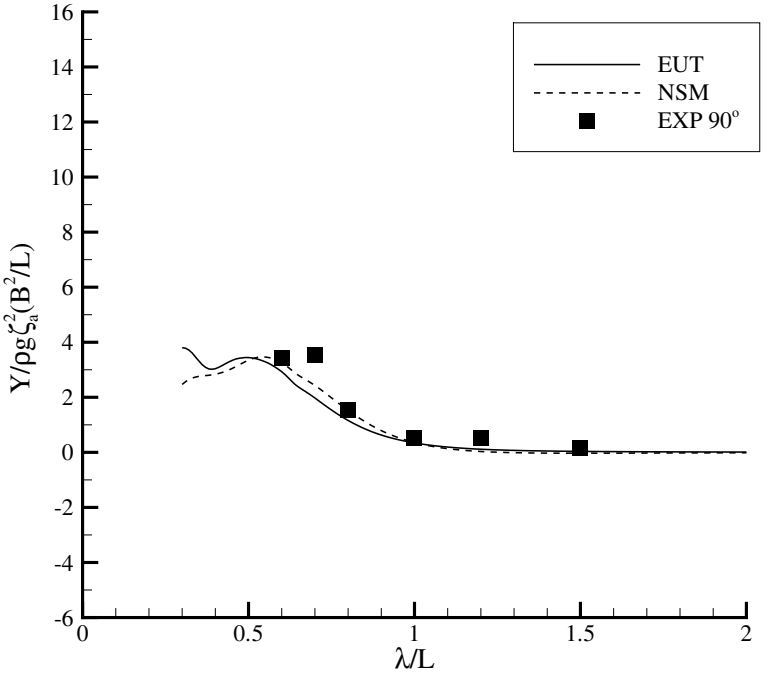

FIGURE 2.27: Steady sway force of JASNAOE-BC084 ($\chi = 30°$, $Fn = 0.037$)

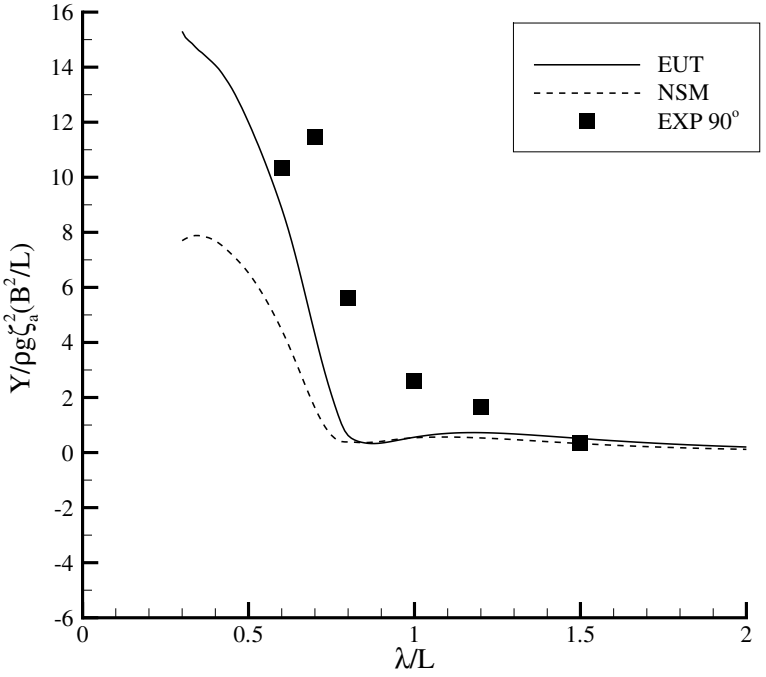

FIGURE 2.28: Steady sway force of JASNAOE-BC084 (χ = 90°, Fn = 0.037)

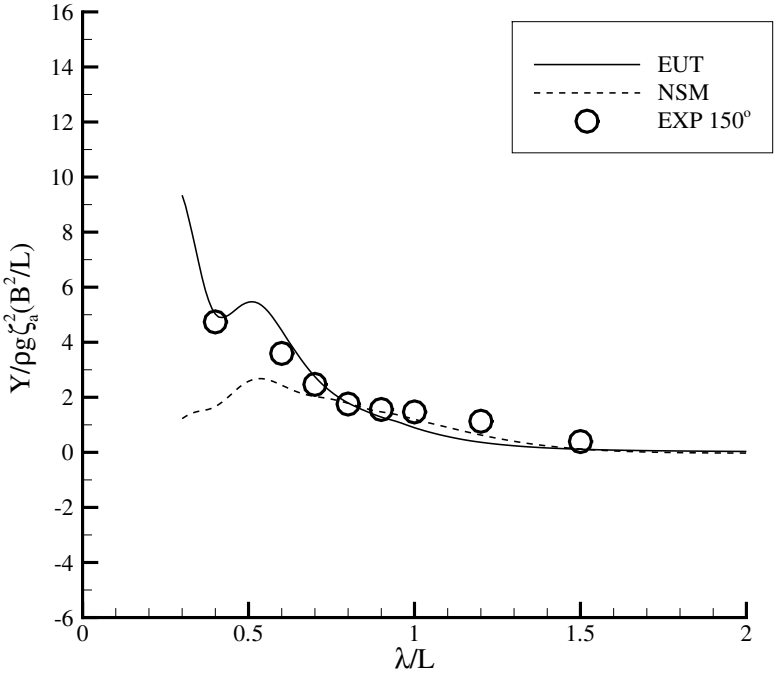

FIGURE 2.29: Steady sway force of JASNAOE-BC084 (χ = 150°, Fn = 0.037)

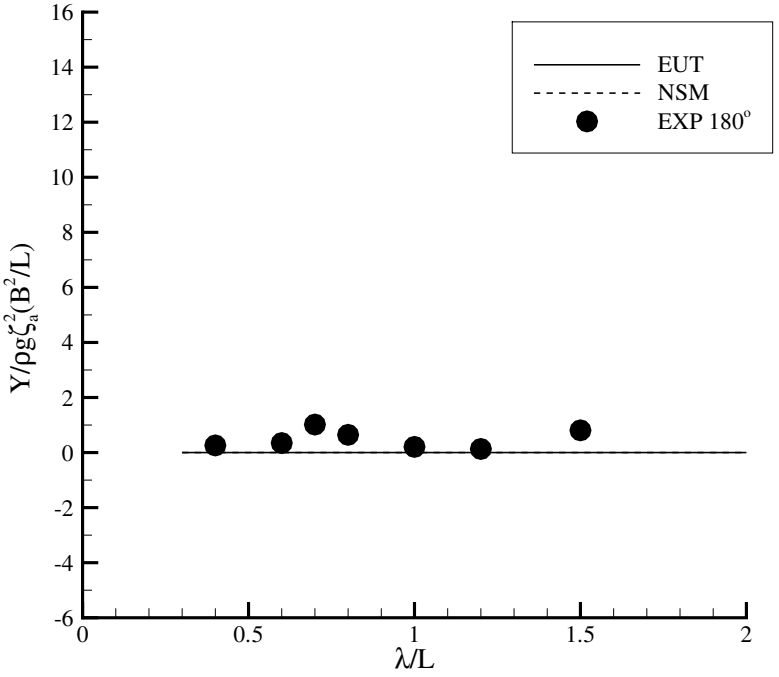

FIGURE 2.30: Steady sway force of JASNAOE-BC084 (χ = 180°, Fn = 0.037)

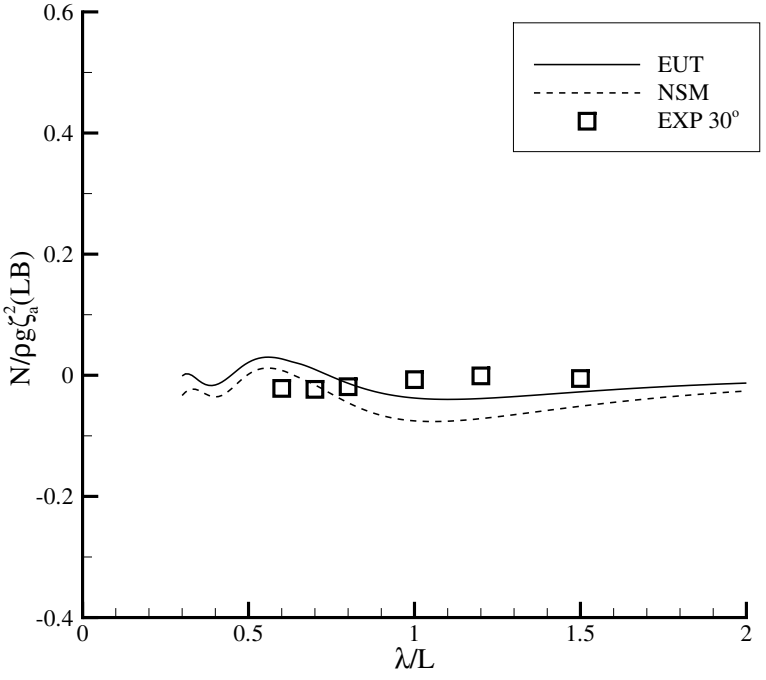

FIGURE 2.31: Steady yaw moment of JASNAOE-BC084 (χ = 30°, Fn = 0.037)

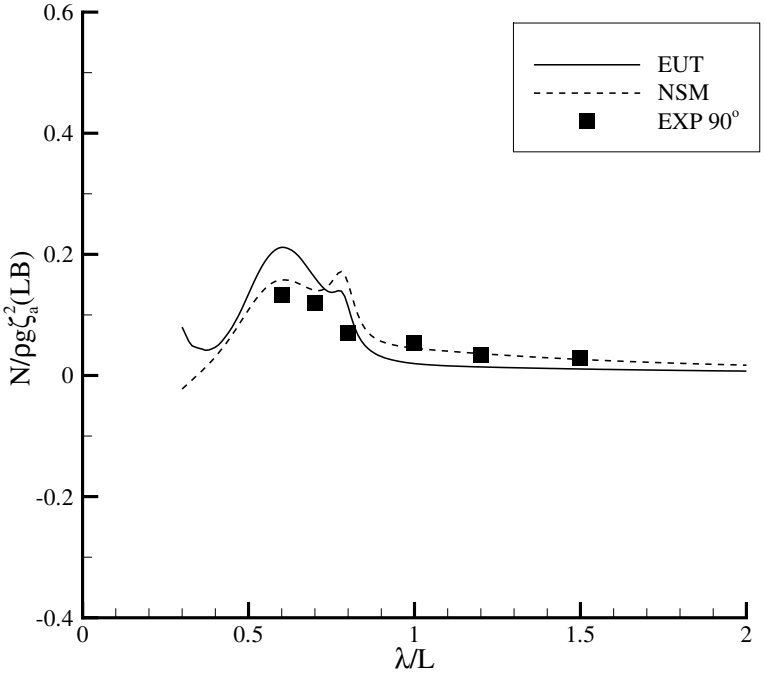

FIGURE 2.32: Steady yaw moment of JASNAOE-BC084 (χ = 90°, Fn = 0.037)

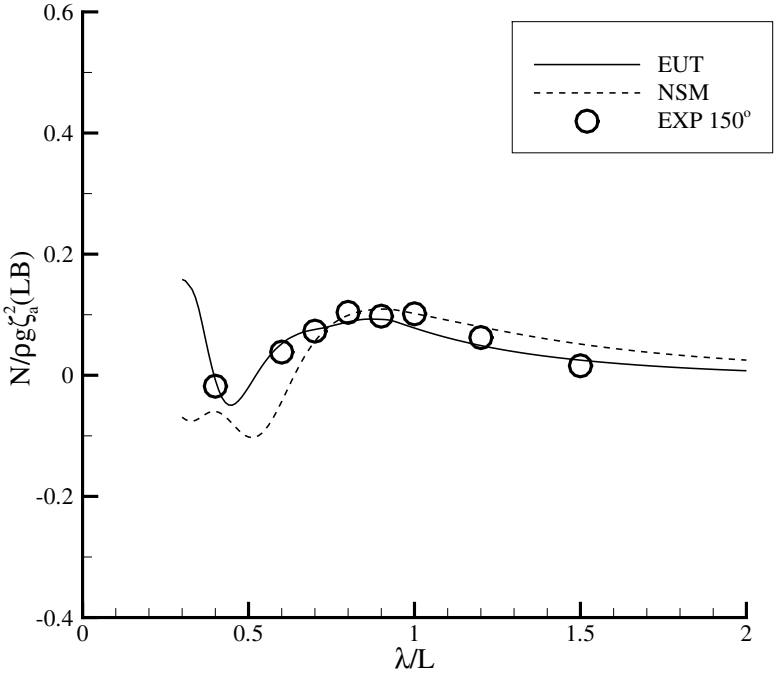

FIGURE 2.33: Steady yaw moment of JASNAOE-BC084 (χ = 150°, Fn = 0.037)

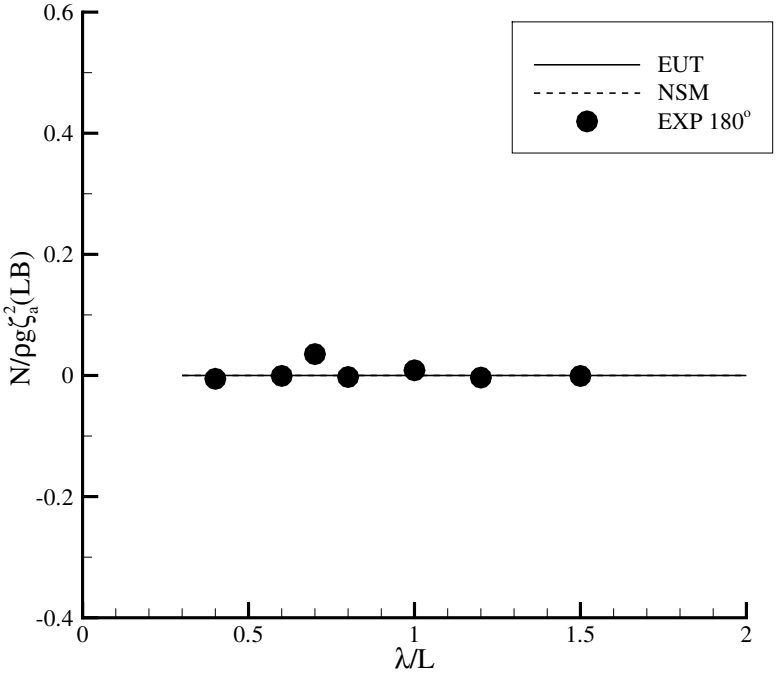

FIGURE 2.34: Steady yaw moment of JASNAOE-BC084 (χ = 180°, Fn = 0.037)

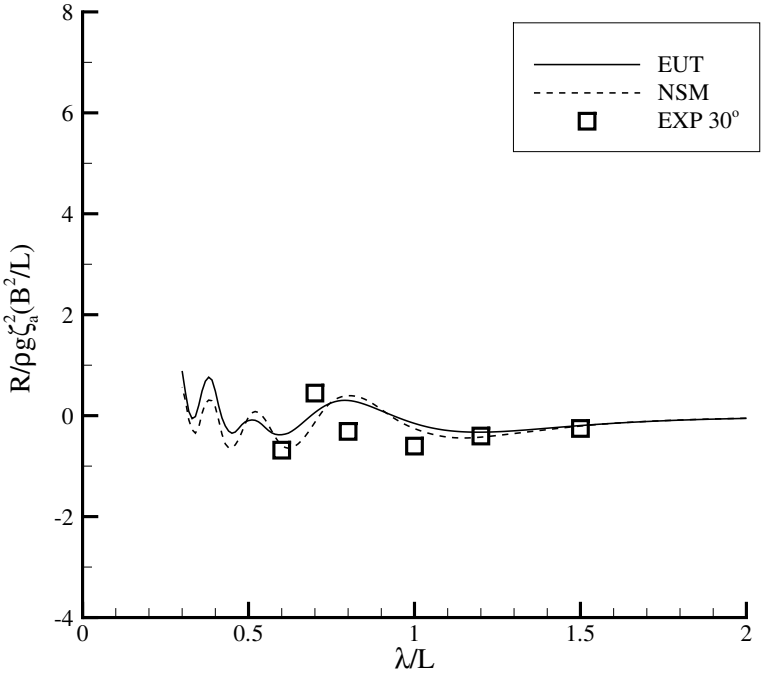

FIGURE 2.35: Added resistance of JASNAOE-BC084 (χ = 30°, Fn = 0.074)

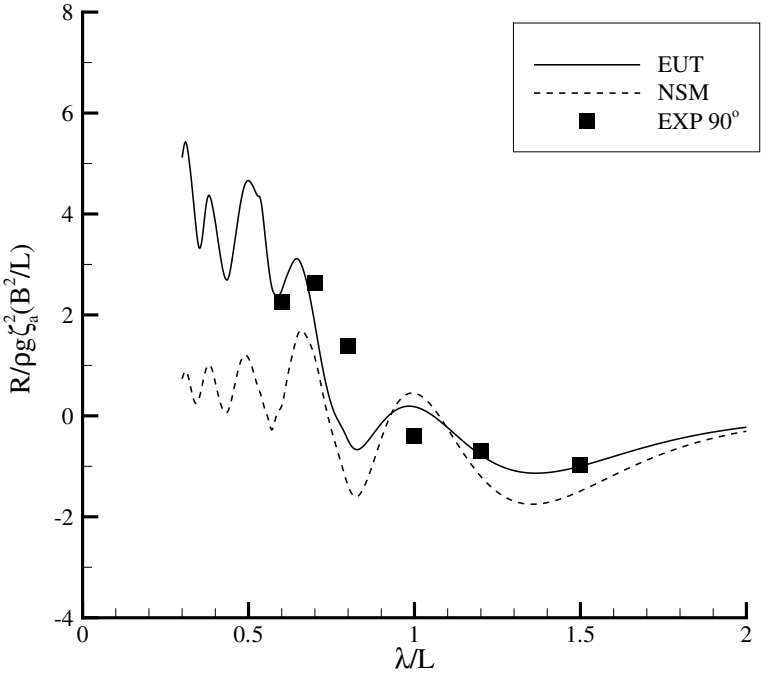

FIGURE 2.36: Added resistance of JASNAOE-BC084 (χ = 90°, Fn = 0.074)

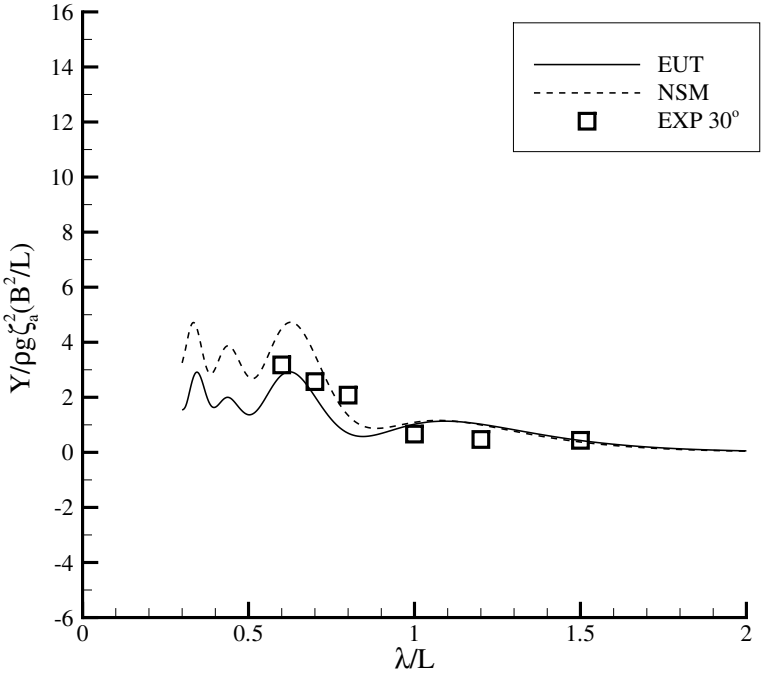

FIGURE 2.37: Steady sway force of JASNAOE-BC084 (χ = 30°, Fn = 0.074)

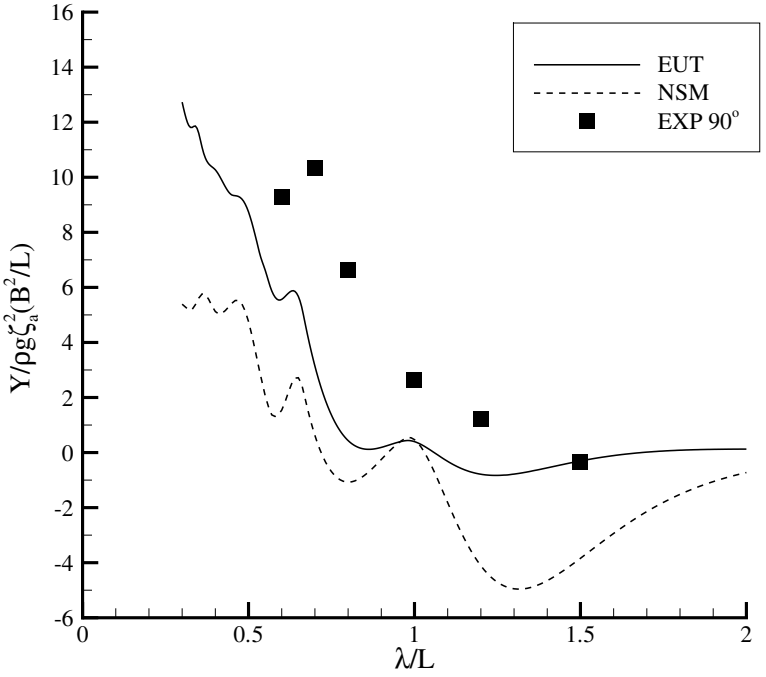

FIGURE 2.38: Steady sway force of JASNAOE-BC084 ($\chi = 90°$, $Fn = 0.074$)

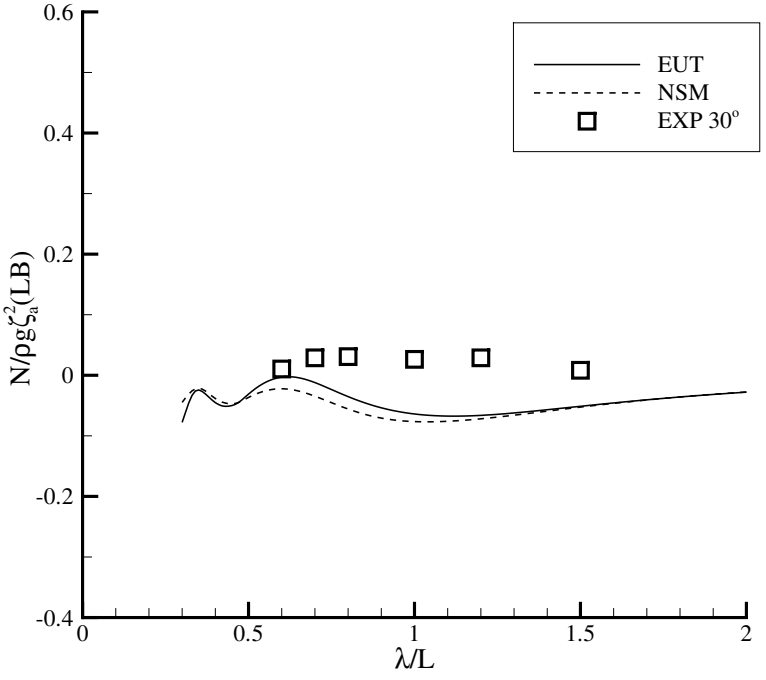

FIGURE 2.39: Steady yaw moment of JASNAOE-BC084 ($\chi = 30°$, $Fn = 0.074$)

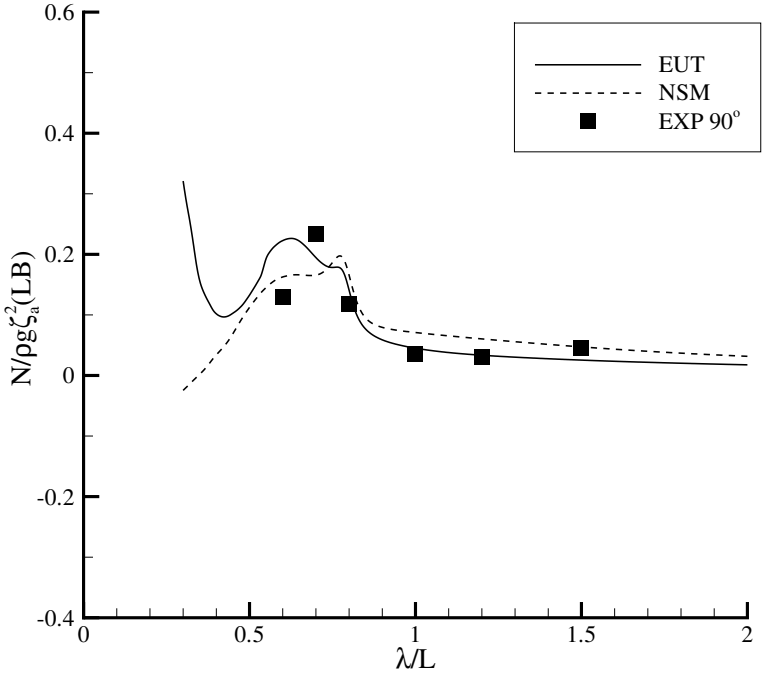

FIGURE 2.40: Steady yaw moment of JASNAOE-BC084 (χ = 90°, Fn = 0.074)

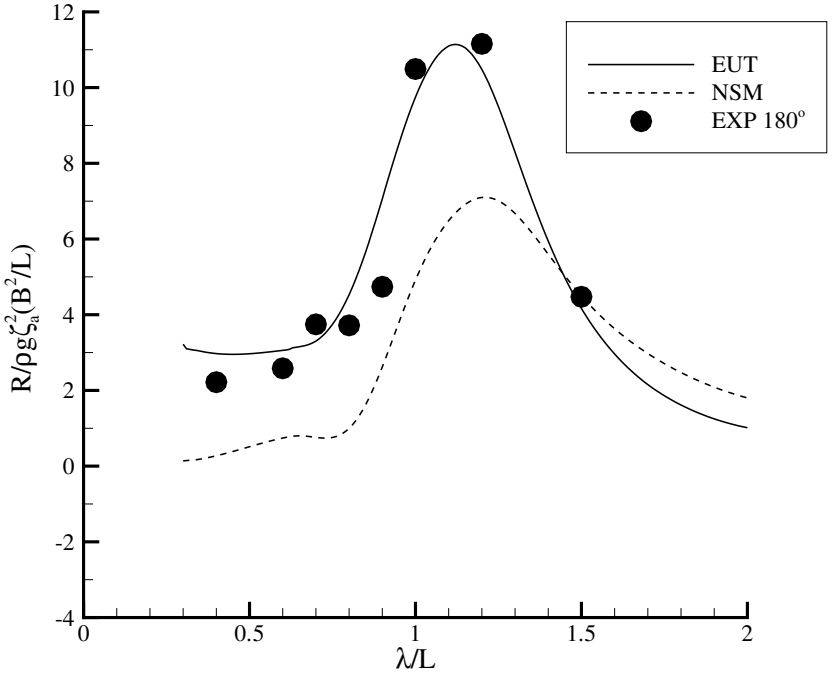

FIGURE 2.41: Added resistance of JASNAOE-BC084 (χ = 180°, Fn = 0.124)

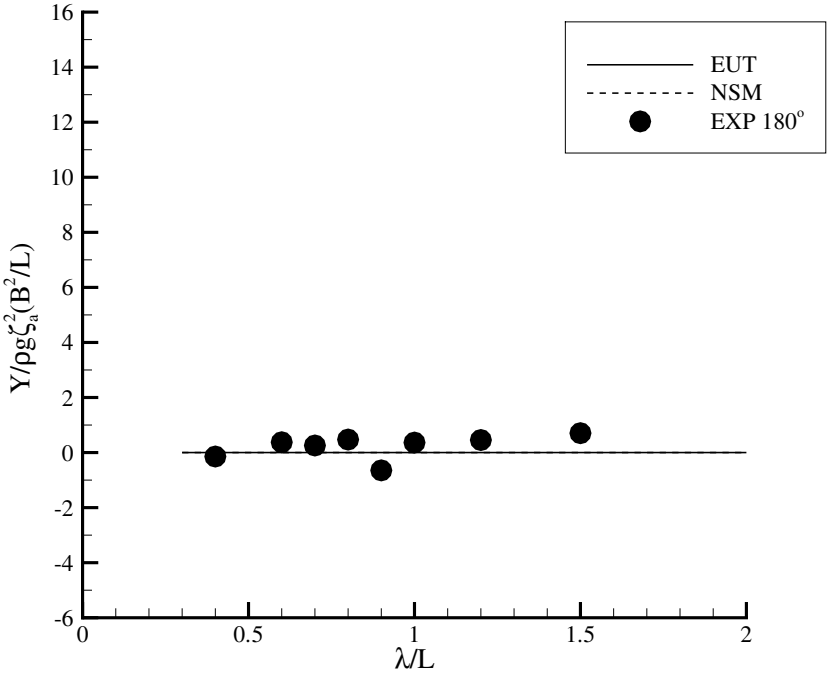

FIGURE 2.42: Steady sway force of JASNAOE-BC084 (χ = 180°, Fn = 0.124)

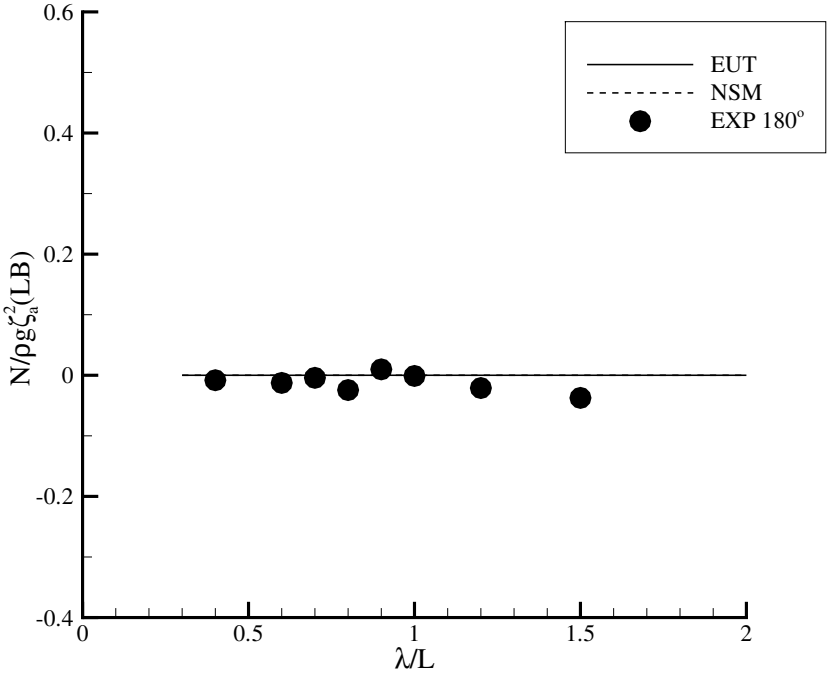

FIGURE 2.43: Steady yaw moment of JASNAOE-BC084 (χ = 180°, Fn = 0.124)

2.8.2 SR108 (Container Ship)

From Yasukawa [20], the measured steady forces and moment of SR108 container ship are available for $Fn = 0.15$ with $\chi = 90^\circ, 180^\circ$. Computations by EUT and NSM are presented in Figs. 2.44 ~ 2.47 together with the measured data in the experiment.

For the added resistance, we can observe good agreement between measured data and calculations. In Fig. 2.44, a slight issue in the shorter waves can be seen, in which the calculations underestimated the added resistance contributed mainly from reflected waves around the ship bow. The same issue is also evident for the beam-wave case shown in Fig. 2.45, while the NSM predicted virtually zero value.

On the other hand, steady sway force estimation by EUT showed promising agreement, especially in $\lambda/L \approx 0.5$. However, the diffraction part in the steady sway force diminishes very quickly as the wavelength increases which causes relative discrepancy with the experiment, especially in the range of $\lambda/L = 0.6 \sim 1.0$.

In the case of steady yaw moment, EUT is able to estimate the trend in a decent way, despite its underestimation in terms of the magnitude. In general, this validation implies that our seakeeping tool is adequately credible to compute the wave-drift forces acting on a ship in oblique waves.

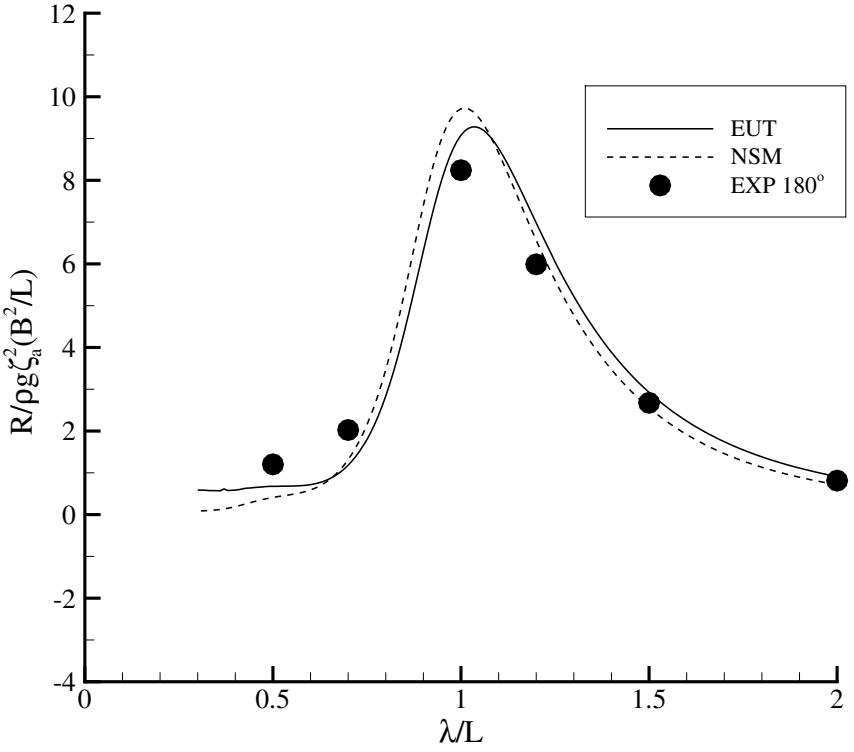

FIGURE 2.44: Added resistance of SR108 ($\chi = 180°$, $Fn = 0.15$)

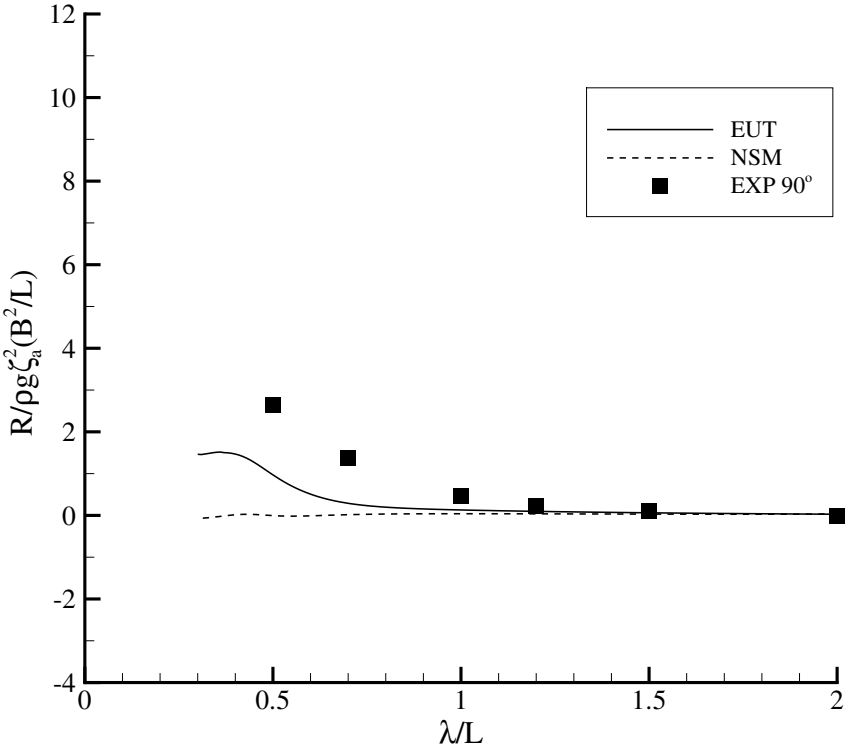

FIGURE 2.45: Added resistance of SR108 ($\chi = 90°$, $Fn = 0.15$)

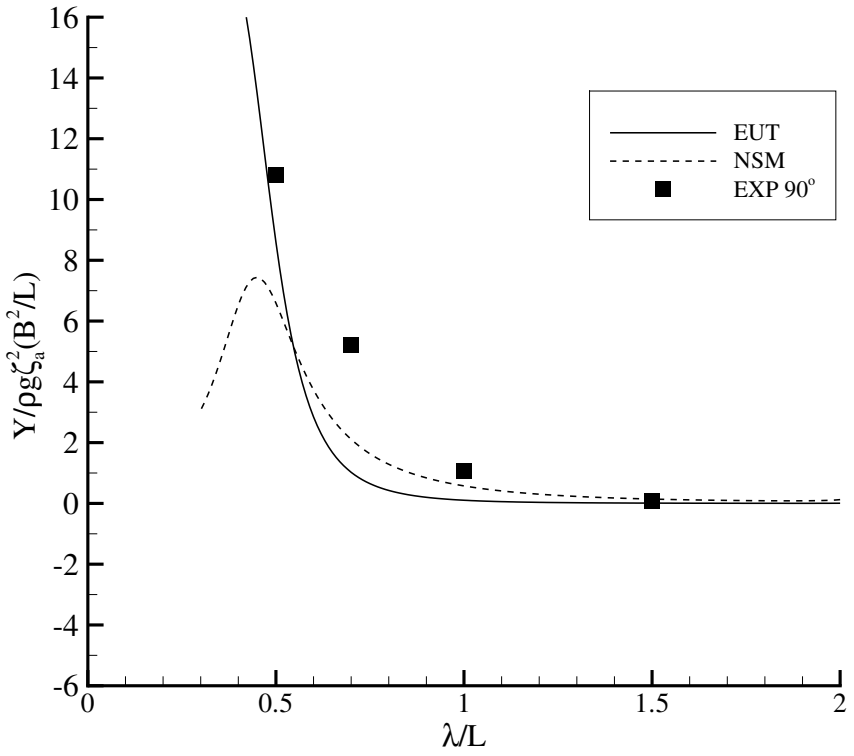

FIGURE 2.46: Steady sway force of SR108 ($\chi = 90°$, $Fn = 0.15$)

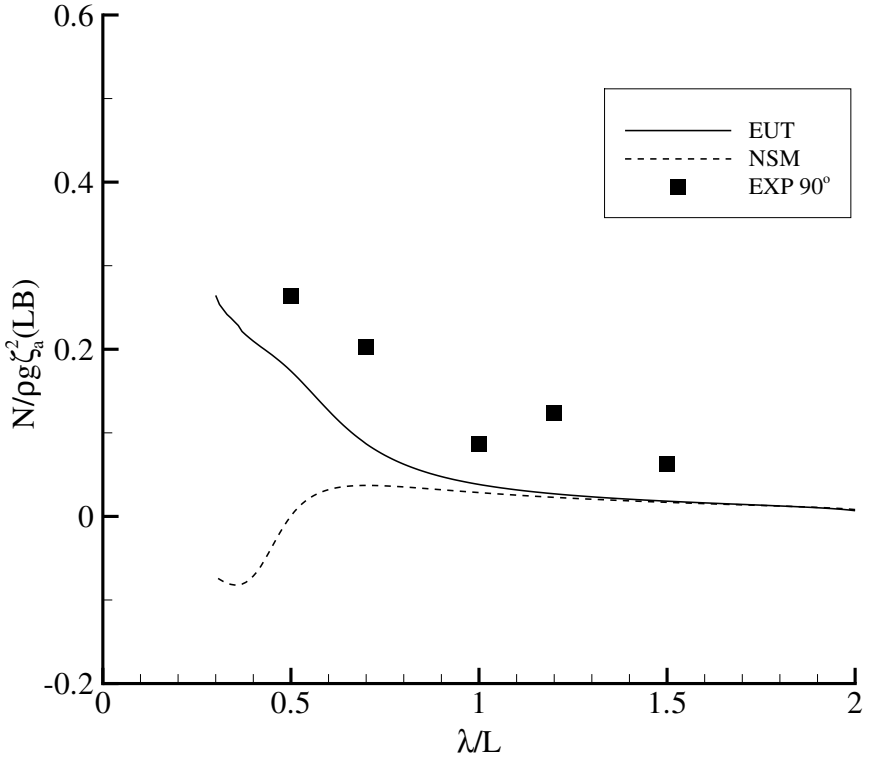

FIGURE 2.47: Steady yaw moment of SR108 ($\chi = 90°$, $Fn = 0.15$)

Chapter 3

Maneuvering in Calm Water by MMG Model

3.1 Introduction

As the foundation of MMG model, single-screw single-rudder ship is considered when explaining the maneuvering motion equations and the mathematical model of the fluid force acting on the ship. The very basic of MMG model was introduced comprehensively in MMG Reports I-V written collectively by Ogawa et al. [50], Hamamoto [51], Kasai and Yumuro [52], Kose and Kijima [53] and Ogawa et al. [54].

3.2 Basic Assumptions

As explained in MMG standard method [45], the following basic assumptions are made when setting up this model:

- Ship as a perfect rigid body.

- Hydrodynamic forces are simply composed of the velocity and acceleration components (quasi-steady assumption).
- Maneuvering motion is performed with low y-velocity compared to x-velocity. Does not apply for berthing and reversed propeller stopping motions.
- Adequately low ship speed to ensure negligible steady wave making. Does not apply for high-speed planing ships.
- Relatively large $\overline{GM}$ resulting negligible roll coupling (and heel) effect on maneuvering.
- Rudder angle and propeller revolutions are given. Does not consider about torque rich.

3.3 Equations of Motions

In horizontal plane, we may represent the maneuvering of a ship as surge, sway, and yaw motion equations of

$$m(\dot{u} - vr) = X \tag{3.1a}$$

$$m(\dot{v} + ur) = Y \tag{3.1b}$$

$$I_{zz}\dot{r} = N \tag{3.1c}$$

with u, v, r as the unknowns and right-hand side as the forcing functions. The derivation of (3.1) is explained to define the problem.

At first, let us consider a ship performing a certain maneuver in calm water by applying rudder angle, and observe this phenomenon from two different references. Figure 3.1 shows the co-ordinate systems consisting: space-fixed coordinate system O-x_0y_0 and the moving body-fixed coordinate system O-xy, in which the vertical z-axis here is independent from them. Now we

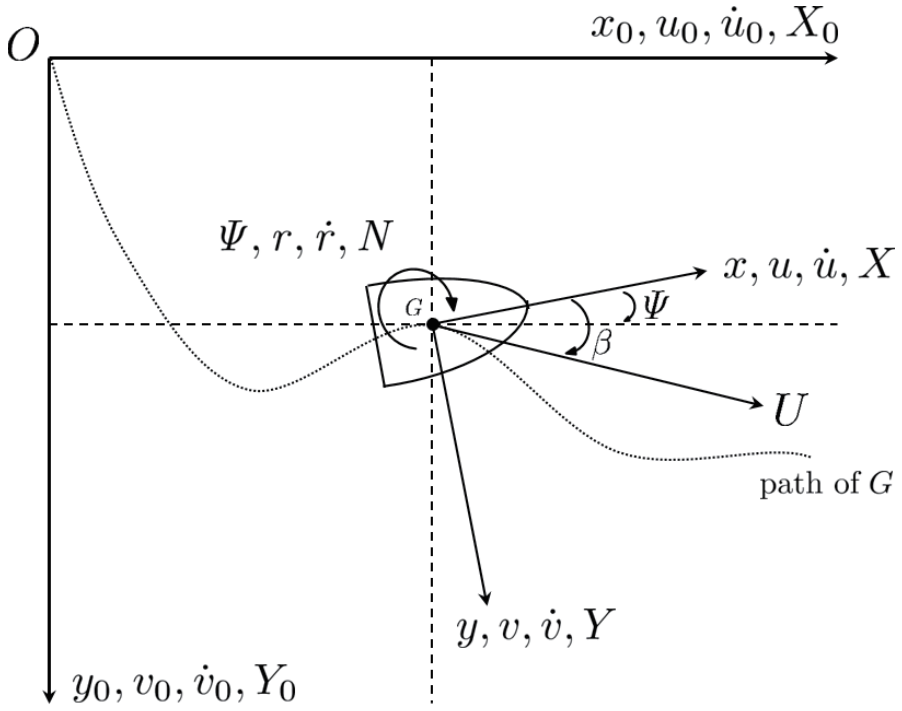

FIGURE 3.1: Coordinate systems

list all notations in the coordinate systems, as follows:

$$\{u_0, v_0, r, \dot{u}_0, \dot{v}_0, \dot{r}, X_0, Y_0, N\} = \text{space-referenced quantities} \tag{3.2a}$$

$$\{u, v, r, \dot{u}, \dot{v}, \dot{r}, X, Y, N\} = \text{body-referenced quantities} \tag{3.2b}$$

$$\{\Psi\} = \text{heading angle} \tag{3.2c}$$

$$\{\beta\} = \text{drift angle/angle of attack} \tag{3.2d}$$

If x_{OG} and y_{OG} are the distances from the O to the ship's center of gravity, we may, by Newton's Law, express the maneuvering forces and moment in space-fixed coordinate system as

$$X_0 = m\ddot{x}_{OG} = m\dot{u}_0 \tag{3.3a}$$

$$Y_0 = m\ddot{y}_{OG} = m\dot{v}_0 \tag{3.3b}$$

$$N = I_{zz}\ddot{\Psi} = I_{zz}\dot{r} \tag{3.3c}$$

Then as the ship maneuvers, the ship geometry in the space-fixed coordinate system changes with time, which dictates the necessity to translate the problem into the body-fixed coordinate

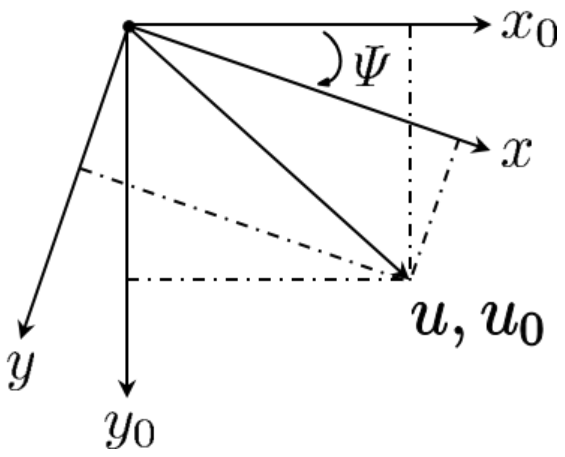

FIGURE 3.2: Transformation of coordinate systems

system for the sake of efficiency. For two axes connected at a point (z) rotated by angle Ψ as illustrated in Fig. 3.2, their vectorial relation to each other can be written as:

$$\{V\} = [R]\{V_0\} \tag{3.4a}$$

$$\{V_0\} = [R]^T\{V\} \tag{3.4b}$$

with the rotation matrix of

$$[R] = \begin{bmatrix} \cos\Psi & \sin\Psi \\ -\sin\Psi & \cos\Psi \end{bmatrix} \tag{3.5}$$

According to this identity, we can apply its transpose to transform space-fixed force vectors to body-fixed force vectors as

$$X = X_0 \cos\Psi + Y_0 \sin\Psi \tag{3.6a}$$

$$Y = Y_0 \cos\Psi - X_0 \sin\Psi \tag{3.6b}$$

likewise

$$\dot{x}_{OG} = u_0 = u\cos\Psi - v\sin\Psi \tag{3.7a}$$

$$\dot{y}_{OG} = v_0 = u\sin\Psi + v\cos\Psi \tag{3.7b}$$

Then, by taking these definitions, we may write the $\dot{u}_0$ and $\dot{v}_0$ in (3.3) as

$$\dot{u}_0 = \frac{d}{dt}u_0 = \frac{d}{dt}(u\cos\Psi) - \frac{d}{dt}(v\sin\Psi) \tag{3.8a}$$

$$\dot{v}_0 = \frac{d}{dt}u_0 = \frac{d}{dt}(u\sin\Psi) + \frac{d}{dt}(v\cos\Psi) \tag{3.8b}$$

where each term in the right-hand side has two parts because Ψ is changing with time:

$$\dot{u}_0 = \cos\Psi\frac{du}{dt} + u\frac{d}{dt}\cos\Psi - \sin\Psi\frac{dv}{dt} - v\frac{d}{dt}\sin\Psi \tag{3.9a}$$

$$\dot{v}_0 = \sin\Psi\frac{du}{dt} + u\frac{d}{dt}\sin\Psi + \cos\Psi\frac{dv}{dt} + v\frac{d}{dt}\cos\Psi \tag{3.9b}$$

and by the chain rule, we get

$$\begin{aligned}\ddot{x}_{OG} = \dot{u}_0 &= \cos\Psi\frac{du}{dt} + u\frac{d}{d\Psi}\cos\Psi\frac{d\Psi}{dt} - \sin\Psi\frac{dv}{dt} - v\frac{d}{d\Psi}\sin\Psi\frac{d\Psi}{dt}\\ &= \dot{u}\cos\Psi - ur\sin\Psi - \dot{v}\sin\Psi - vr\cos\Psi\end{aligned} \tag{3.10}$$

$$\begin{aligned}\ddot{y}_{OG} = \dot{v}_0 &= \sin\Psi\frac{du}{dt} + u\frac{d}{d\Psi}\sin\Psi\frac{d\Psi}{dt} + \cos\Psi\frac{dv}{dt} + v\frac{d}{d\Psi}\cos\Psi\frac{d\Psi}{dt}\\ &= \dot{u}\sin\Psi + ur\cos\Psi + \dot{v}\cos\Psi - vr\sin\Psi\end{aligned} \tag{3.11}$$

Therefore, by substituting (3.11) in (3.3) and inserting the resulting values of X_0 and Y_0 in (3.6), we recover the followings:

$$X = m(\dot{u} - vr) \tag{3.12a}$$

$$Y = m(\dot{v} + ur) \tag{3.12b}$$

of (3.1) by trigonometric identities. One should note that (3.1) is applicable when the origin O coincides with the center of gravity ($\mathbf{r}_G = [0, 0, 0]$).

With the forcing functions being defined as the contributions from hull ($_H$), rudder ($_R$) and propeller ($_P$), the final maneuvering motion equations can be formulated as:

$$(m + m_x)\dot{u} - (m + m_y)vr = X_H + X_R + X_P \tag{3.13a}$$

$$(m + m_y)\dot{v} + (m + m_x)ur = Y_H + Y_R \tag{3.13b}$$

$$(I_{zz} + J_z)\dot{r} = N_H + N_R \tag{3.13c}$$

when the horizontal added masses and moment of inertia (m_x, m_y, J_z) are included.

3.4 Hull Force

X_H, Y_H, and N_H are formulated as

$$X_H = (1/2)\rho L_{pp} d U^2 X'_H(v', r') \tag{3.14a}$$

$$Y_H = (1/2)\rho L_{pp} d U^2 Y'_H(v', r') \tag{3.14b}$$

$$N_H = (1/2)\rho L_{pp} d U^2 N'_H(v', r') \tag{3.14c}$$

where $v' = v/U$ and $r' = rL_{pp}/U$. X'_H, Y'_H and N'_H are expressed as the 1st to 4th order polynomial function of v' and r':

$$X'_H(v', r') = -R'_0 + X'_{vv}v'^2 + X'_{vr}v'r' + X'_{rr}r'^2 + X'_{vvvv}v'^4 \tag{3.15a}$$

$$Y'_H(v', r') = Y'_v v' + Y'_r r' + Y'_{vvv}v'^3 + Y'_{vvr}v'^2 r' + Y'_{vrr}v'r'^2 + Y'_{rrr}r'^3 \tag{3.15b}$$

$$N'_H(v', r') = N'_v v' + N'_r r' + N'_{vvv}v'^3 + N'_{vvr}v'^2 r' + N'_{vrr}v'r'^2 + N'_{rrr}r'^3 \tag{3.15c}$$

which are called the hydrodynamic derivatives on maneuvering, complemented by the resistance coefficient (R'_0) for X'_H. Evaluation of these derivatives can be made in several ways: model tests, cross-flow viscous drag analysis and experiment-based empirical formulas. Varieties of the empirical formulas can be found in many references, for instance in Fossen [55], Söding

[56] and Yoshimura and Masumoto [57]. On the other hand, the added masses (m_x and m_y) and added moment of inertia (J_z) can also be obtained through at least three ways: model test, strip theory, and Motora chart [58–61].

3.4.1 Model tests

Experiment in the tank is known to be the most reliable approach to estimate the viscous forces acting on a ship executing a maneuver. In order to correctly obtain the hull coefficients, control surfaces and propeller should be included in the measurements. There are several method of measurements: oblique towing test, circular motion test and planar motion mechanism.

In the oblique towing test, the model ship is fixed at different angles of attack, then we can measure sway force and yaw moment by towing the model. Rudder coefficients can also be approximated by applying various rudder angles.

On the other hand, the circular motion test needs a rotating arm device, or a set of main carriage and sub carriage that can work freely. This method was introduced by Koyama [62]. We measure the cross-body force and yaw moment as a function of yaw rate r that gives Y_r and N_r, or to fix the angle of attack that gives Y_v and N_v. One measurement is made over one rotation to avoid the model re-entering its own wake.

At last, the planar motion mechanism (PMM) procedure is to tow the vessel at constant speed U which is held by two posts located forward and aft, which can impose independent sway, therefore producing yaw. The comprehensive explanation of this procedure is available in [63], in order to figure out the linear hull derivatives for a given speed. One may obtain the nonlinear derivatives by varying the yaw rate and drift angle.

3.4.2 Strip Theory

By taking only the linear components of (3.15) into consideration and temporarily discarding the propeller and rudder forces in (3.13), the motion equations can be reduced into

$$m(\dot{u} - vr) = -m_x\dot{u} + m_y vr \tag{3.16a}$$

$$m(\dot{v} + ur) = -m_y\dot{v} - m_x ur + Y_v v + Y_r r \tag{3.16b}$$

$$I_{zz}\dot{r} = -J_z\dot{r} + N_v v + N_r r \tag{3.16c}$$

with remaining added masses $[m_x, m_y, J_z]$ and potential dampings $[Y_v, Y_r, N_v, N_r]$ to be determined, after considering y-symmetry. These expressions are consistent with the definitions in Imlay [64]. Then, neglecting the vertical motions (heave, roll and pitch), linearized added mass and potential damping matrices can be expressed as

$$M_A = \begin{bmatrix} A_{11} & 0 & 0 \\ 0 & A_{22} & A_{26} \\ 0 & A_{62} & A_{66} \end{bmatrix} \equiv -\begin{bmatrix} m_x & 0 & 0 \\ 0 & m_y & 0 \\ 0 & 0 & J_z \end{bmatrix} \tag{3.17}$$

$$D_M = \begin{bmatrix} B_{11} & 0 & 0 \\ 0 & B_{22} & B_{26} \\ 0 & B_{62} & B_{66} \end{bmatrix} \equiv -\begin{bmatrix} X_u & 0 & 0 \\ 0 & Y_v & Y_r \\ 0 & N_v & N_r \end{bmatrix} \tag{3.18}$$

with notice that $Y_r \neq N_v$ for damping matrix. By this definition, we can readily obtain all derivatives required in (3.16), for instance, as

$$A_{11} = -X_{\dot{u}} = \int_{-L/2}^{L/2} A_{11}^{(2D)}(y, z)dx \tag{3.19}$$

$$B_{66} = -N_r = \int_{-L/2}^{L/2} x^2 B_{22}^{(2D)}(y, z)dx \tag{3.20}$$

Our numerical survey shows that the slender-ship theory can be adequately accurate to approximate the added masses. However, it is not reliable when calculating the damping coefficients by the integration of hydrodynamic coefficients at $\omega_e = 0$. This is due to the strong lift and viscous effect on a drifting ship in maneuvering motion. Therefore, MMG model is presented with the derivatives obtained purely from model tests in order to maintain the level of prediction accuracy.

3.5 Propeller Thrust

Surge force due to propeller action X_p is defined as

$$X_P = (1 - t_P)T \tag{3.21}$$

with constant thrust deduction factor t_P at a designated propeller load. Thrust T is calculated as

$$T = \rho n_P^2 D_P^4 K_T(J_P) \tag{3.22}$$

with propeller revolution per second n_P, propeller diameter D_P and thrust coefficient K_T. K_T is approximated as the 2nd polynomial function of propeller advance ratio J_P, as follows:

$$K_T(J_P) = k_2 J_P^2 + k_1 J_P + k_0 \tag{3.23}$$

$$J_P = \frac{u(1 - w_P)}{n_P D_P} \tag{3.24}$$

where k_0, k_1 and k_2 are the open-water test constants. The $u(1 - w_P)$ term stands for the real fluid velocity considering the effective wake fraction w_P. In this propeller force expression, the rudder influence on the thrust T is omitted. However, this component is brought into play at the rudder force expression X_R.

3.6 Rudder Force

Fluid forces induced by rudder action are expressed as

$$X_R = -(1 - t_R)F_N \sin\delta \tag{3.25a}$$

$$Y_R = -(1 + a_H)F_N \cos\delta \tag{3.25b}$$

$$N_R = -(x_R + a_H x_H)F_N \cos\delta \tag{3.25c}$$

with factors t_R, a_H and x_H representing: the steering resistance deduction, the force on the bare hull induced by the rudder action (due to hydrodynamic interaction) and the position of additional lateral force component, respectively. These coefficients can be obtained by experiment or by empirical formula. Then, the rudder normal force F_N is defined as

$$F_N = \frac{1}{2}\rho A_R U_R^2 \frac{6.13\Lambda}{\Lambda + 2.25}\sin\alpha_R \tag{3.26}$$

with rudder area A_R and rudder aspect ratio Λ. U_R and α_R denote effective inflow velocity and its angle into the rudder, respectively, which are vital in rudder force estimation.

U_R is defined as the resultant of longitudinal and lateral components of inflow velocity:

$$U_R = \sqrt{u_R^2 + v_R^2} \tag{3.27}$$

The x-component u_R is taken as

$$u_R = \varepsilon(1 - w_p)u\sqrt{\eta\{1 + \kappa(\sqrt{1 + 8K_T/\pi J^2} - 1)\}^2 + 1 - \eta} \tag{3.28}$$

The derivation of this expression is explained in Appendix D based on Kashiwagi [65].

Then, the effective rudder inflow angle α_R is formulated as

$$\alpha_R = \delta + \frac{v_R}{u_R} \simeq \delta + \frac{\gamma_R\{-(v + x_R r)\}}{u_R} \tag{3.29}$$

with the longitudinal position of rudder x_R. From this equation, we may comprehend that γ_R acts as a correction factor to the lateral inflow velocity $-(v+x_R r)$ due to the existence of the hull. Hence, the expression of $\gamma_R\{-(v+x_R r)\}$ is used in this study to approximate the y-component of rudder inflow velocity v_R.

Further explanation on coefficients and terms used in MMG model can be found in the MMG standard method [43], MMG Reports I-V [50–54] and other related articles.

3.7 Experiment

The principal particulars and body plan of SR108 container ship model have been presented in Table 2.2 and Fig. 2.4, respectively. For the maneuvering simulation, the propulsion particulars and hull derivatives are shown in Table 3.1 and 3.2. Other necessary coefficients and parameters are also taken from the measurements [20].

TABLE 3.1: Propulsion particulars of SR108 container ship model

Item	**Real**	**Model**	**Unit**
Propeller diameter (D_P)	6.507	0.1301	m
Propeller pitch ratio (p)	0.7348	0.7348	-
Propeller rotational speed (n_P)	1.42	10.05	rps
Rudder height (H_R)	7.70	0.154	m
Rudder chord (B_R)	4.215	0.0843	m
Rudder area (A_R)	32.46	0.0130	m^2

TABLE 3.2: SR108 hull derivatives [20]

m'_x	0.0044	Y'_{vvr}	0.3942
m'_y	0.1299	Y'_{vrr}	0.7461
J'_z	0.0077	Y'_{rrr}	0.0326
X'_{vv}	-0.0711	N'_v	0.0710
X'_{vr}	0.0573	N'_r	-0.0409
X'_{rr}	0.0037	N'_{vvv}	-0.0275
X'_{vvvv}	-	N'_{vvr}	-0.7811
Y'_v	0.2137	N'_{vrr}	-0.0287
Y'_r	0.0446	N'_{rrr}	-0.0422
Y'_{vvv}	2.008		

3.7.1 Experimental Settings

The experiment was done in the maneuvering basin of Mitsubishi Heavy Industries, Nagasaki Laboratory. The turning test was performed in still water condition with approach speed of $Fn = 0.15$ (0.879 m/s in model scale). In accordance with the experiment of Yasukawa [20], the propeller revolution speed n_P and the rudder turning rate are set equal to 10.05 rps and 12.0 deg/s, respectively, for both turning and zig-zag tests.

3.8 Computation Results and Discussion

3.8.1 Turning Circle

The turning test was performed in still water condition with rudder angle $\delta = -35^\circ$ (to port-side). Comparison between the simulated and measured turning trajectories are shown in Fig. 3.3. The result confirms the reliability of our mathematical model for calm water maneuvering simulation. For additional information, the calculated ship forward speed (U), yaw rate (r), drift angle (β) and rudder angle (δ) are shown in Figs. 3.4 and 3.5 in function of completed turning angle (Ψ).

3.8.2 Zig-Zag

The zig-zag test was executed in still water condition with $10^\circ/10^\circ$ maneuver to the starboard. Once again, comparison between simulated and measured results shown in Fig. 3.6 shows the accuracy of our mathematical model. The calculated time series of ship forward speed (U) and yaw rate (r) are also shown in Fig. 3.7.

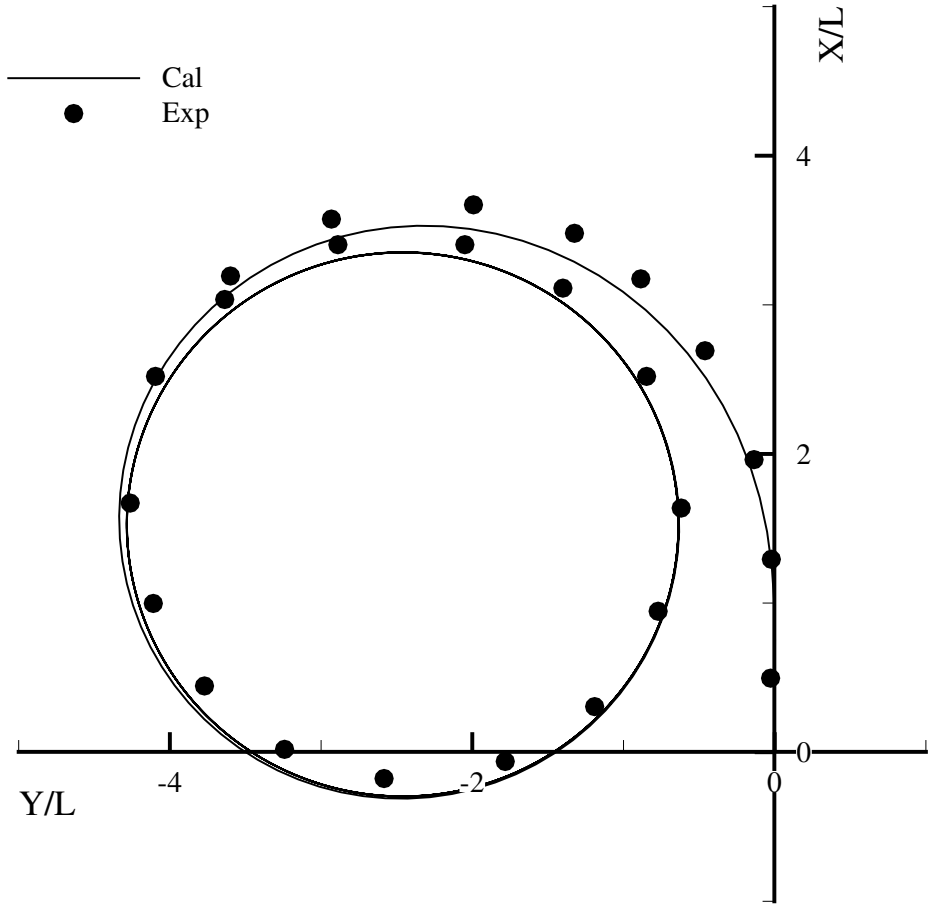

FIGURE 3.3: Comparsion between simulated and measured turning trajectories

3.8.3 Maneuverability Rating

Turning maneuver criteria Tactical diameter and advance are to be determined from the turning test defined in Fig. 3.8. IMO requires that the tactical diameter (TD) is to be less than 5 ship lengths and the advance (Ad) is to be less than 4.5 ship lengths [66]:

$$Ad \leq 4.5L \tag{3.30}$$

Provided that (3.30) is satisfied, the rating of turning ability is found from the following formulae

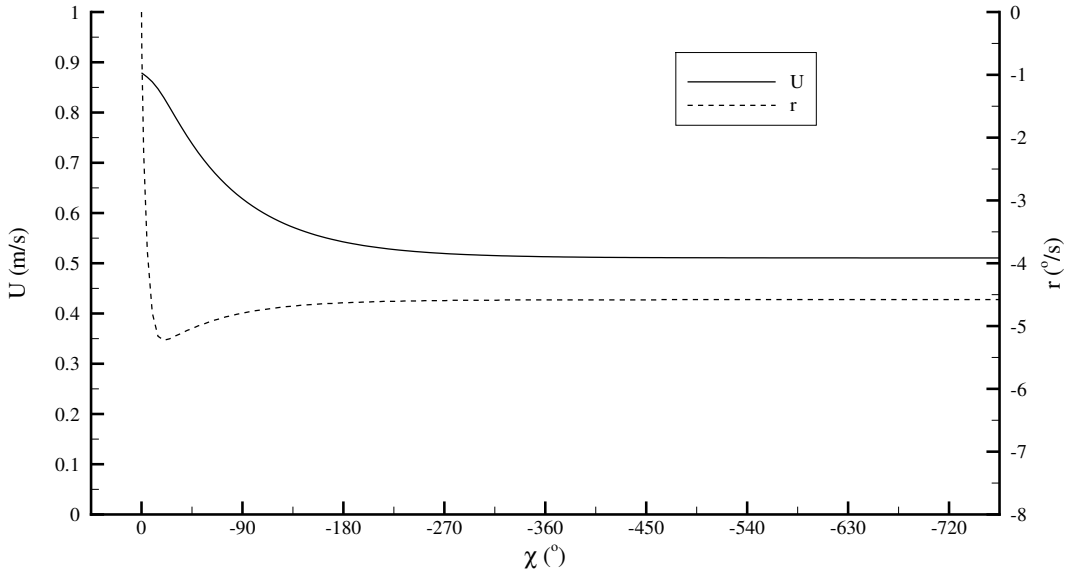

FIGURE 3.4: Calculated forward speed (U) and yaw rate (r) in function of turning angle (Ψ)

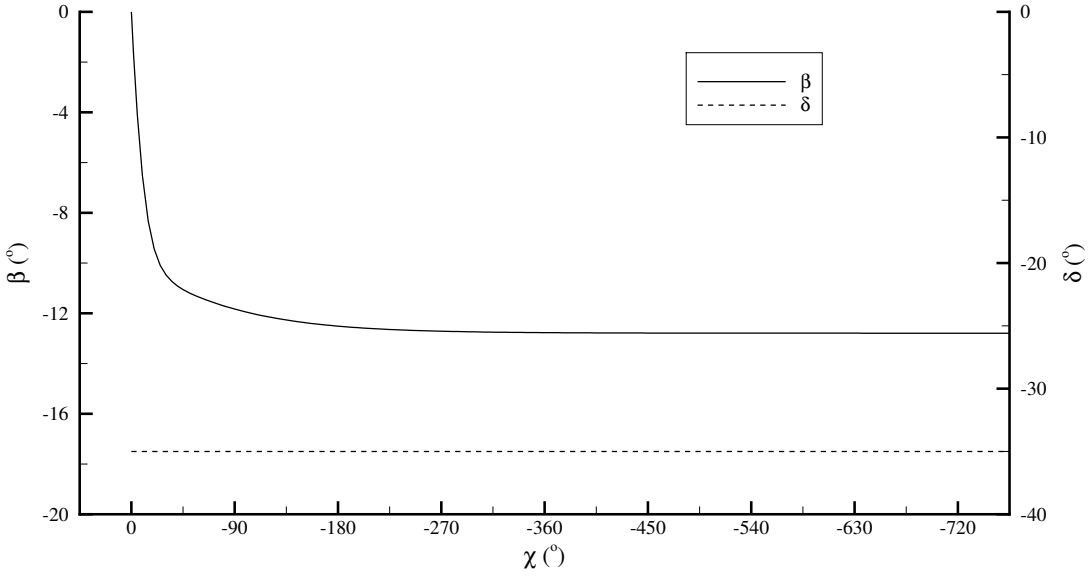

FIGURE 3.5: Calculated drift angle (β) and rudder angle (δ) in function of turning angle (Ψ)

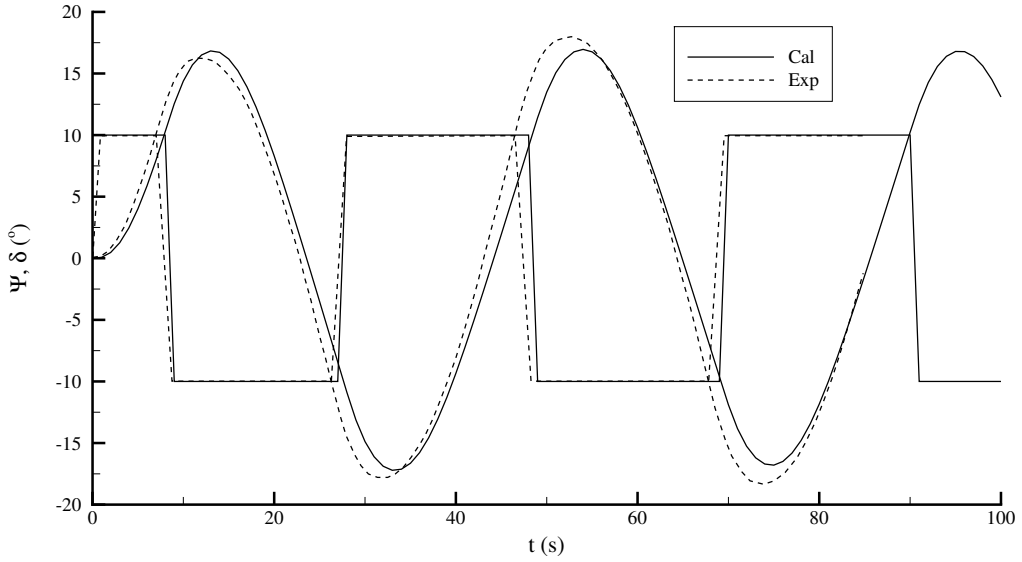

FIGURE 3.6: Calculated and measured heading angle (Ψ) and rudder angle (δ)

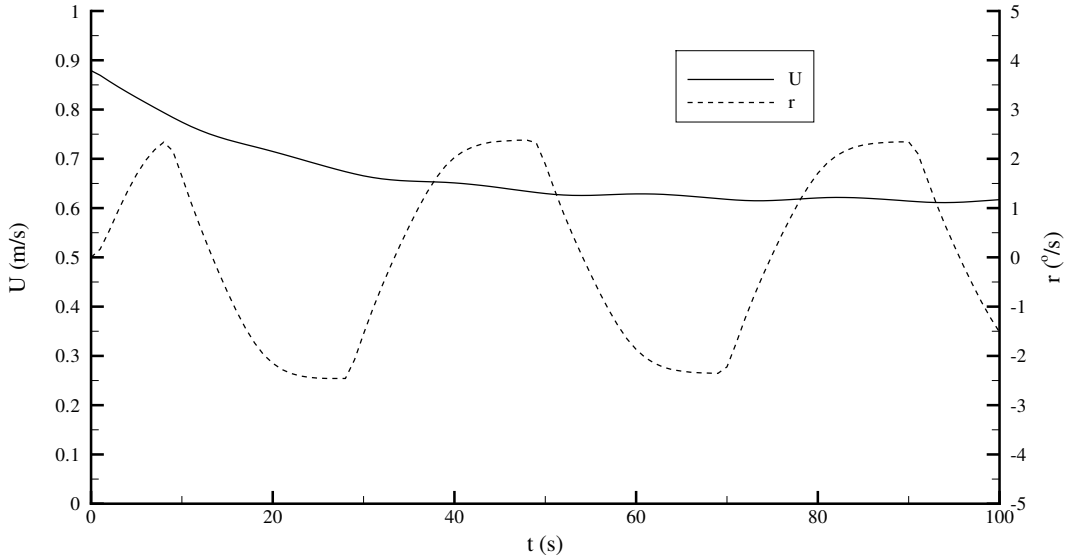

FIGURE 3.7: Calculated time series of ship forward speed (U) and yaw rate (r)

$$
\begin{aligned}
&\text{if } (4.26 - 1.62 \cdot 10^{-6}\Delta)L < TD \leq 5L && \text{then } Rtd = 1 \\
&\text{if } (3.63 - 1.62 \cdot 10^{-6}\Delta)L < TD \leq (4.26 - 1.62 \cdot 10^{-6}\Delta)L && \text{then } Rtd = 2 \\
&\text{if } (2.79 - 1.62 \cdot 10^{-6}\Delta)L < TD \leq (3.63 - 1.62 \cdot 10^{-6}\Delta)L && \text{then } Rtd = 3 \\
&\text{if } (2.16 - 1.62 \cdot 10^{-6}\Delta)L < TD \leq (2.79 - 1.62 \cdot 10^{-6}\Delta)L && \text{then } Rtd = 4 \\
&\text{if } (2.16 - 1.62 \cdot 10^{-6}\Delta)L > TD && \text{then } Rtd = 5
\end{aligned}
\tag{3.31}
$$

with ship length (L) in meters and displacement (Δ) in metric tons. Rtd indicates the rating of turning ability which is based on statistics of sea trials [68]. Accordingly, the turning indices derived from Fig. 3.3 are shown in Table 3.3. It is noted that the measured and simulated tactical

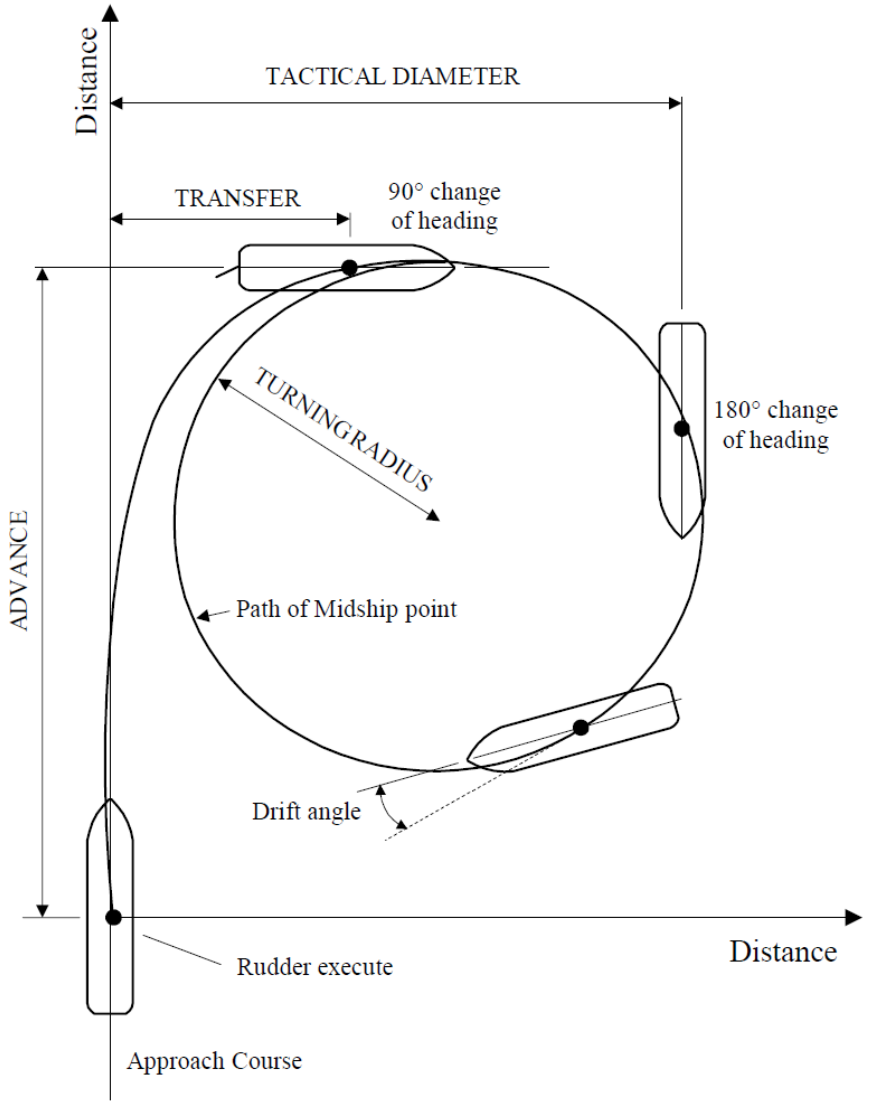

FIGURE 3.8: Notations and criteria in turning test [67]

diameters are close to the lower limit of $Rtd = 2$ at $TD \leq 4.22L$.

TABLE 3.3: SR108 turning indices

Index	Experiment	Simulation	IMO
Advance	$3.6L$	$3.47L$	$\leq 4.5L$
Tactical diameter	$4.23L$	$4.28L$	$\leq 5L$
Rating of turning ability	1	1	-

10°/10° zig-zag maneuver criteria The first overshoot angle (OSA) in the zig-zag test is a measure of the vessel's course checking ability which is defined in Fig. 3.9. The requirements are also according to IMO [66] based on statistics of sea trials [68]. As measured in the 10°/10° zig-zag test, the first OSA, $\alpha 10_1$, is to be evaluated with the following function:

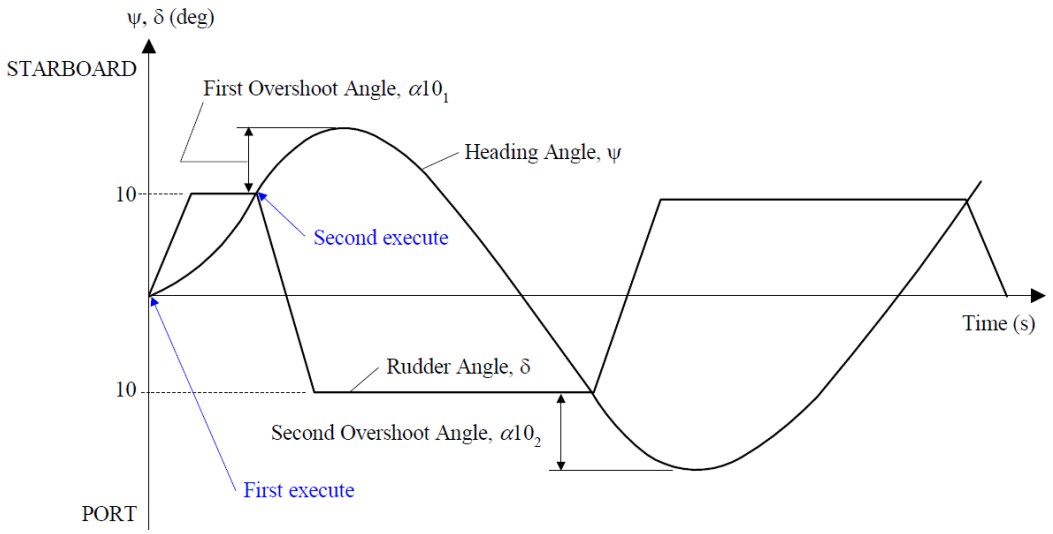

FIGURE 3.9: Notations and criteria in zig-zag test [67]

$$f_{101}(L/V) = \begin{cases} 10.0 & \text{if} \quad L/V \leq 10s \\ 5 + 0.5(L/V) & \text{if} \quad 10s < L/V < 30s \\ 20.0 & \text{if} \quad L/V \geq 30s \end{cases} \tag{3.32}$$

with V the vessel speed in m/s. The rating for the first OSA in the 10°/10° zig-zag test, $Rt\alpha_{10} = 1$, can be assigned only if:

$$10.04 + 2.22C_B < f_{101}(L/V) \tag{3.33}$$

Provided that (3.33) is satisfied:

$$\begin{aligned} &\text{if } \ 10.04 + 2.22C_B < \alpha 10_1 \leq f_{101}(L/V) && \text{then } \ Rt\alpha_{10} = 1 \\ &\text{if } \ 7.42 + 2.22C_B < \alpha 10_1 \leq 10.04 + 2.22C_B && \text{then } \ Rt\alpha_{10} = 2 \end{aligned} \tag{3.34}$$

If (3.33) is not satisfied:

$$\begin{aligned} &\text{if } \ 7.42 + 2.22C_B < \alpha 10_1 \leq f_{101}(L/V) && \text{then } \ Rt\alpha_{10} = 2 \\ &\text{if } \ 3.92 + 2.22C_B < \alpha 10_1 \leq 7.42 + 2.22C_B && \text{then } \ Rt\alpha_{10} = 3 \\ &\text{if } \ 1.29 + 2.22C_B < \alpha 10_1 \leq 3.92 + 2.22C_B && \text{then } \ Rt\alpha_{10} = 4 \\ &\text{if } \ \alpha 10_1 \leq 1.29 + 2.22C_B && \text{then } \ Rt\alpha_{10} = 5 \end{aligned} \tag{3.35}$$

with $Rt\alpha_{10}$ expresses the rating for the first OSA.

From our simulation (Fig. 3.6), SR108 does not satisfy the (3.33). Therefore, the evaluation is done through (3.35) to get Table 3.4. Based on the ratings of turning circle and zig-zag tests, we understand that the SR108 possesses higher course checking ability (Table 3.4) than its hard-over turning ability (Table 3.3).

TABLE 3.4: SR108 zig-zag criteria

Index	**Experiment**	**Simulation**
$\alpha 10_1$	6.257°	6.831°
Rating of OSA	3	3

Chapter 4

Seakeeping and Maneuvering in Waves by Two-Time Scale Method

4.1 Introduction

In order to solve the seakeeping and maneuvering problem in a weak-coupling framework, the two-time scale method is described here. The outline follows what has been presented in Skejic and Faltinsen [25], Seo and Kim [32] and Zhang et al. [37]. The main difference highlighted in our present study is the application of the developed form of slender-ship theory, the enhanced unified theory (EUT) [8], as well as the usage of far-field formulation of Wicaksono and Kashiwagi [69] in the estimation of second-order horizontal forces and moment.

By the employment of the slender ship theory in the two-time scale coupling method, an efficient and reasonably accurate mathematical model to address the maneuvering problem in waves is developed. Supplementary discussions on the results explained in this chapter are also presented in Wicaksono and Kashiwagi [70].

4.2 Two-Time Scale Method

By appending the second-order steady forces and moment as the added external forces, the maneuvering motion equations in waves can be rewritten from the MMG motion equations in calm water (3.13) to

$$\left.\begin{aligned}(m+m_x)\dot{u}-(m+m_y)vr &= X_H+X_R+X_P+X_W(\zeta_a,\omega_0,\chi_0-\Psi,U)\\ (m+m_y)\dot{v}+(m+m_x)ur &= Y_H+Y_R+Y_W(\zeta_a,\omega_0,\chi_0-\Psi,U)\\ (I_{zz}+J_z)\dot{r} &= N_H+N_R+N_W(\zeta_a,\omega_0,\chi_0-\Psi,U)\end{aligned}\right\} \tag{4.1}$$

in which the last terms on the right-hand side (X_W, Y_W and N_W) directly alter the initial ship steering motions in calm water. These added quantities are the functions of the incident wave amplitude ζ_a, frequency ω_0, ship-waves encountering angle $\chi_0 - \Psi$ and ship forward speed U. Notice that the symbol of second-order drift forces are changed from R, Y and N (in **Chapter 3**) into X_W, Y_W and N_W, correspondingly, in order to be consistent with the standard notations of MMG model.

In accordance with previous works employing the two-time scale method, the seakeeping and maneuvering problems are designed to be coupled in a functional space. The concept is to separate high-frequency wave-induced motions and low-frequency steering motions of a ship, with exchange of variables between them. In fact, there is variation with higher frequency in various forces acting on ship hull, rudder, and propeller due to wave motion. However, once the time average is taken over several periods which are the time scale in the maneuvering motion of a ship, the effect of that high-frequency variation can be regarded as almost zero and hence the influence on the maneuvering motion is little.

As shown in Fig. 4.1, the steps of simulation in this two-time scale method are as follows:

- The MMG model solves the maneuvering motion equations (4.1)
- u and $\chi_0 - \Psi$ are provided to the seakeeping code as the input data

- EUT and NSM determine the Kochin functions to calculate the steady drift forces as in (2.102), (2.114) and (2.131)
- Added resistance X_W, steady sway force Y_W and steady yaw moment N_W are supplied back to (4.1) as the additional force modules in the MMG model
- MMG model solves the maneuvering motion equations (4.1) for the next time step with the updated X_W, Y_W and N_W

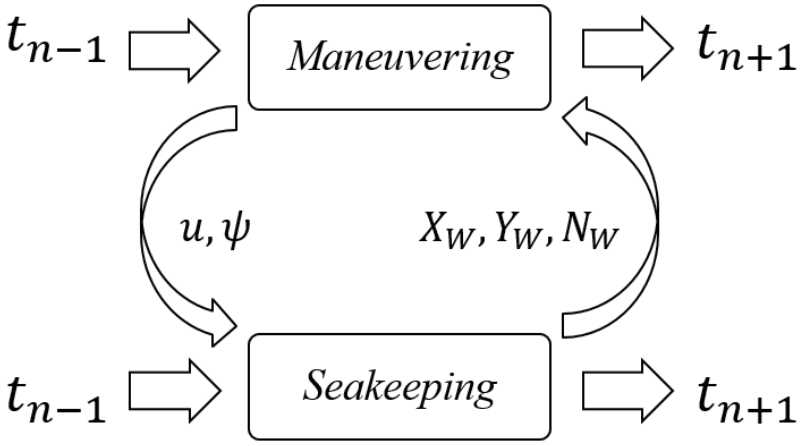

FIGURE 4.1: Feedback system in two-time scale method

The step of seakeeping computation in the time marching is also essential to ensure the accurate estimation of the slowly varying second-order drift forces. This step will be approximated later in a convergence test.

4.3 Experiment

In the experiment of Yasukawa [20], turning experiment in regular waves were performed with maximum rudder angle $\delta = -35°$, space-fixed incident wave direction $\chi_0 = 180°$ (initial head waves) and $\zeta_a/L_{PP} = 1/100$. The incident wave has various length of $\lambda/L = 0.5, 0.7, 1.0, 1.2$. Alike the calm water experiment, the propeller revolution speed n_P and the rudder turning rate are set equal to 10.05 rps and 12.0 deg/s. The converged forward speed and drift angle before the execution of turning maneuver were measured as well, as shown in Fig. 4.2.

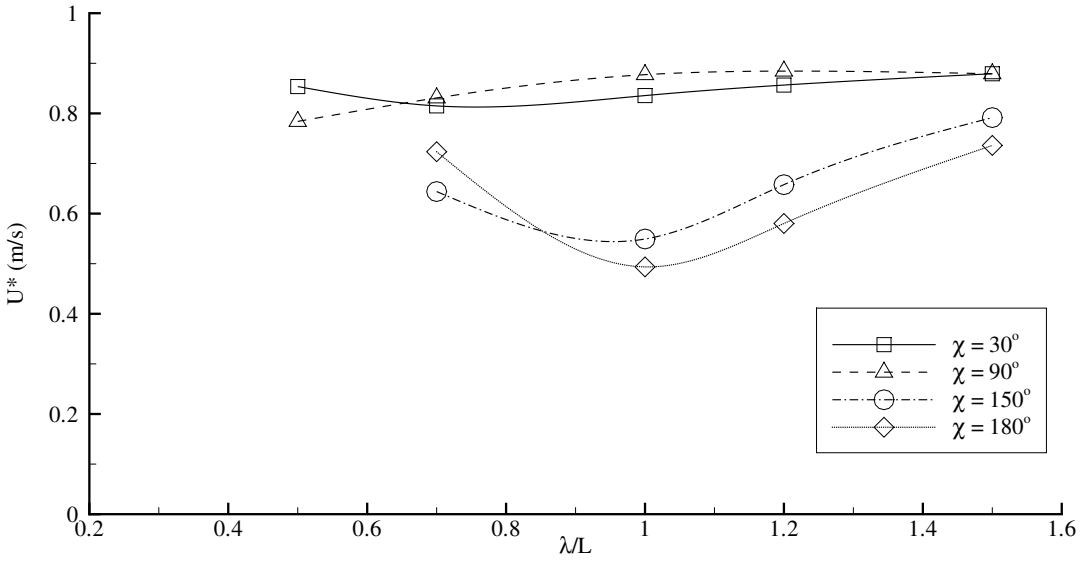

FIGURE 4.2: Measured converged forward speed in a straight moving in regular waves [20]

The ship in concern is SR108 container ship. Its body plan, principal particulars, propulsion particulars and hull derivatives have been described in previous chapters.

4.4 Computation Results and Discussion

4.4.1 Convergence Test of Heading Angle Step

Skejic and Faltinsen [25] recommended the step of seakeeping computation to follow the time-varying ship heading angle change of $\Delta\Psi \approx 2 \sim 3°$. However, due to the difference of utilized seakeeping tool and steady forces formulation, the convergence test in function of heading angle has to be performed. Without considering the converged forward speed in Yasukawa [20], convergence test is done with $\delta = -35°$, initial heading angle $\chi_0 = 180°$ (head waves), $\lambda/L = 1.0$ and $\zeta/L_{PP} = 1/100$.

As can be seen in Figs. 4.3 and 4.4, the turning test is converged when $\Delta\Psi \leq 0.5°$. The convergence stops beyond this point for all test cases, therefore it is unnecessary to use smaller heading angle step.

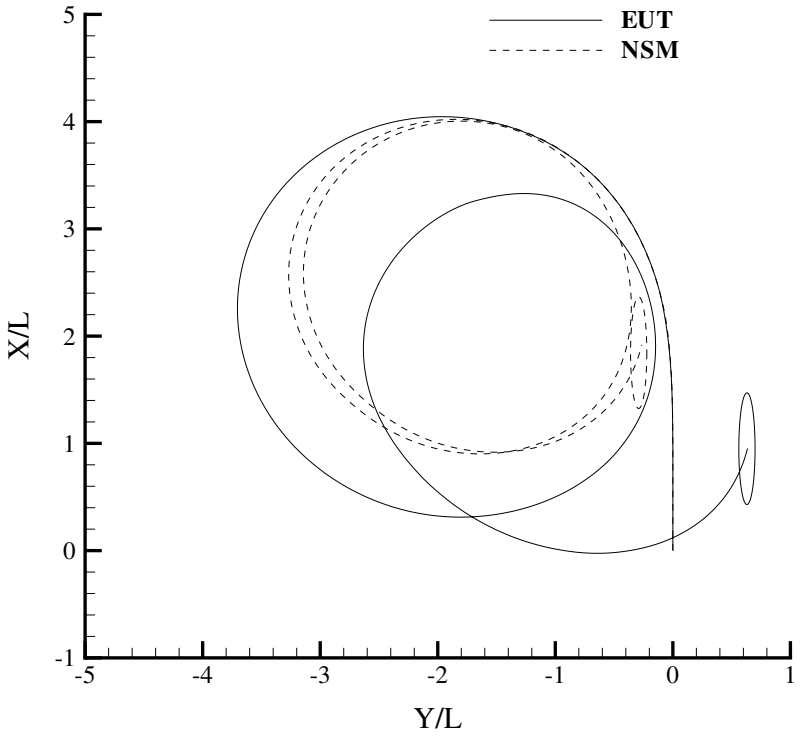

FIGURE 4.3: Time-step convergence test with $\Delta\psi \approx 1^\circ$

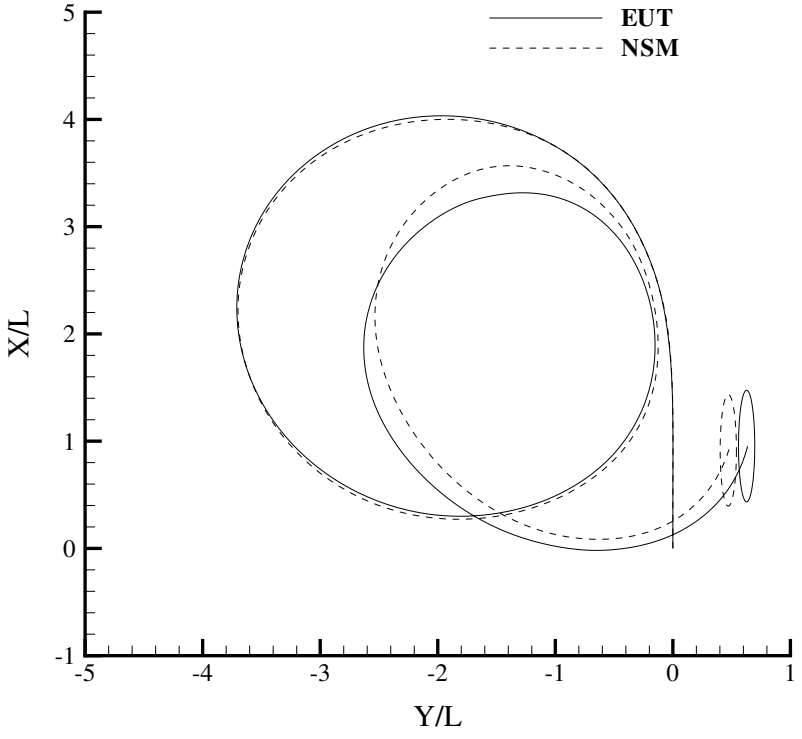

FIGURE 4.4: Time-step convergence test with $\Delta\psi \approx 0.5^\circ$

4.4.2 Comparison with Experiment

The simulations are performed in order to validate the results against the experimental data. Two representative cases of turning test in short and intermediate incident waves are selected: $\lambda/L = 0.5$ and 1.0. Both cases have similar test conditions: $\delta = -35^{\circ}$, space-fixed incident wave direction $\chi_0 = 180^{\circ}$ (initial head waves) and $\zeta_a/L_{PP} = 1/100$. The converged forward speed in these cases are directly taken from Fig. 4.2.

In short-wave case of $\lambda/L = 0.5$, the simulation was performed with $U_0 = 0.8259$ m/s ($Fn = 0.141$). The result is depicted in Fig. 4.5 along with the measured trajectory. Computed maneuvering trajectories when coupled with EUT and NSM are presented in solid line and dashed line, respectively. In addition, the time series of the wave-induced added resistance X_W, sway force Y_W, and yaw moment N_W are shown in Fig. 4.9. From Fig. 4.5, we can see qualitatively that NSM gives better agreement in terms of the lateral transfer, especially on the second circle, whereas the EUT gives better result in the advance distance, as well as the diameter of the second circle.

In a case of longer wave ($\lambda/L = 1.0$), the simulation was performed with $U_0 = 0.4929$ m/s ($Fn = 0.0841$). The comparison with the experimental trajectory is shown on Fig. 4.6. Due to underestimation of Y_W in longer wavelength region, the EUT-coupled model estimated smaller drift than NSM and the experiment. This finding justifies the observation in Fig. 2.46.

Nevertheless, we can say that the developed model is able to represent the maneuvering in waves when the λ is relatively long. This finding is understandable due to the significantly smaller wave drift effect in this wave condition. In addition, the time series of surge velocity (u), sway velocity (v), drift angle (β), resultant velocity (U) and yaw rate (r) for the EUT-coupled model in two test conditions are presented in Figs. 4.7 and 4.8 showing the influence of the incident waves to the ship maneuvering motion.

These two simulations in two different cases of λ/L indicate that the effect of steady drift forces and moment to the maneuvering motion is especially large when the incident wavelength is short

compared to the ship length. Therefore we extend our survey to the second-order forces acting on the ship in the short waves condition of $\lambda/L = 0.5$.

From the time series of drift forces and moment shown in Fig. 4.9, we can discover some facts. In beam-wave condition (e.g. $|\Psi|$ =90°, 270°), EUT estimated larger magnitude of X_W, Y_W and N_W than NSM. The effect can be seen from the advance of Cal (EUT) which is less than that of Cal (NSM), therefore the result of EUT complies with the experiment. In contrast, NSM predicted significantly larger value (2-3 times) than EUT for Y_W in stern quartering-wave condition (e.g. $|\Psi| = 135° \sim 230°$). The discrepancy between the experiment and the calculations apparently starts when the ship enters $|\Psi| = 270°$ of turning angle. EUT and NSM clearly estimated very small values of X_W, while the measurements in the seakeeping test suggests larger values. This deficit can be clearly observed in Fig. 2.45 thus understandable. In this reduced speed condition, the difference between the computed and real values of Y_W and N_W may exist, therefore contributes to the variation. As the result, the ship forward speed was too high in the simulation that yields overestimated circle diameter and excessive transfer to the positive Y/L domain.

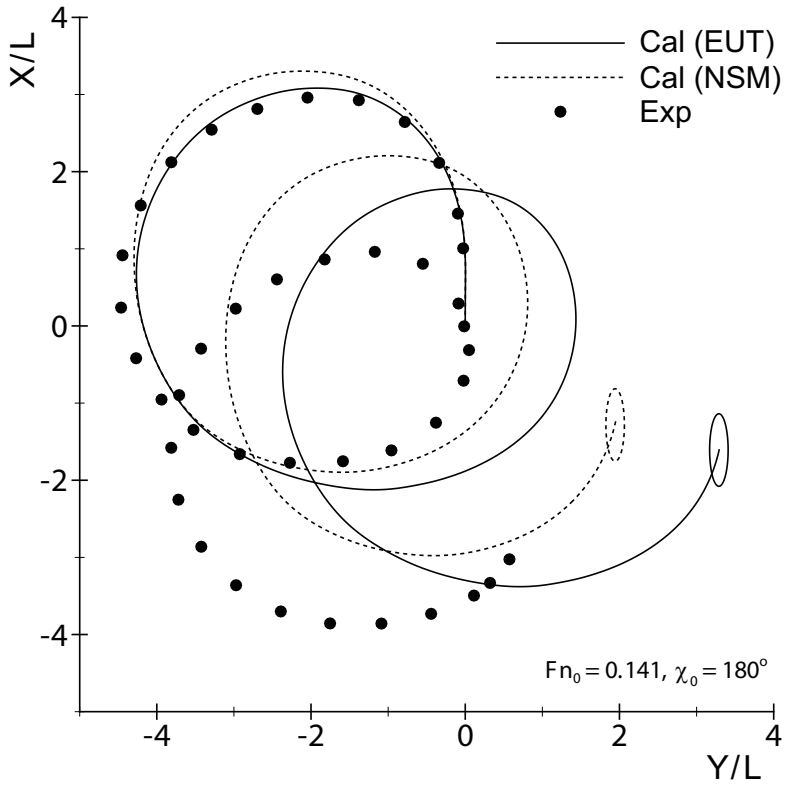

FIGURE 4.5: Comparison of turning trajectory in $\lambda/L = 0.5$ ($Fn_0 = 0.141, \chi_0 = 180°$)

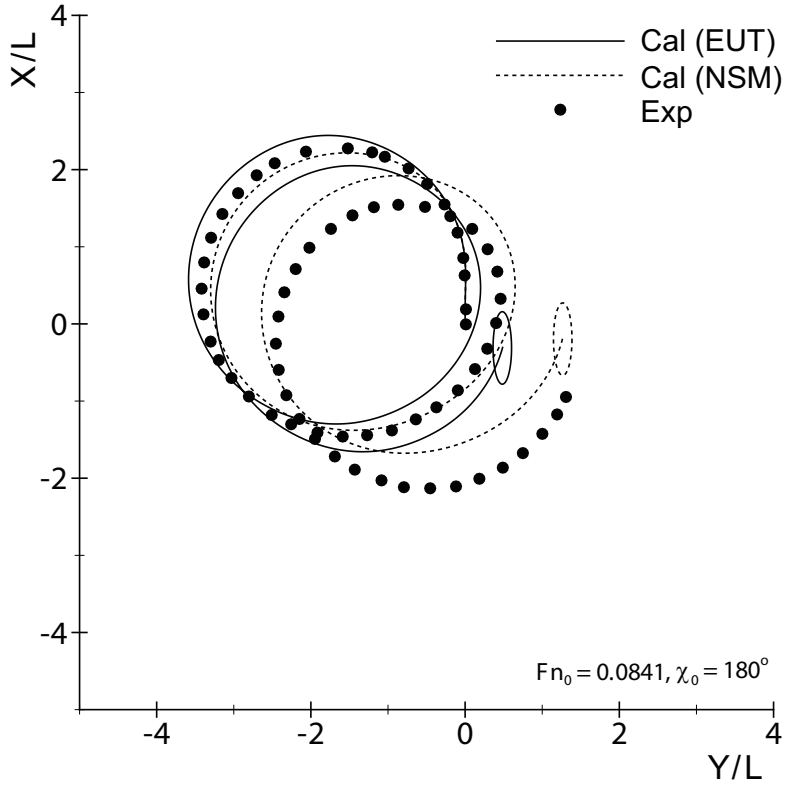

FIGURE 4.6: Comparison of turning trajectory in $\lambda/L = 1.0$ ($Fn_0 = 0.141, \chi_0 = 180^\circ$)

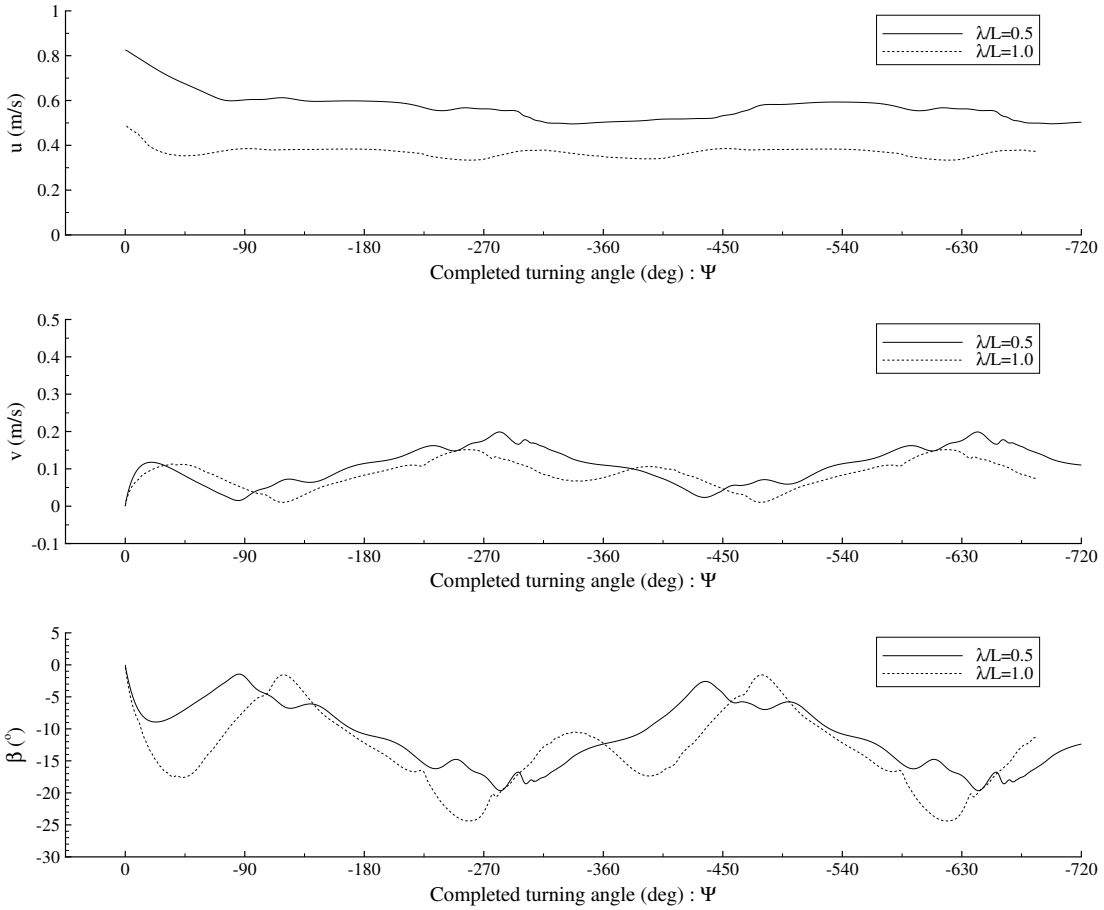

FIGURE 4.7: u, v and β as functions of completed turning angle at $\lambda/L = 0.5, 1.0$ ($\chi_0 = 180^\circ$)

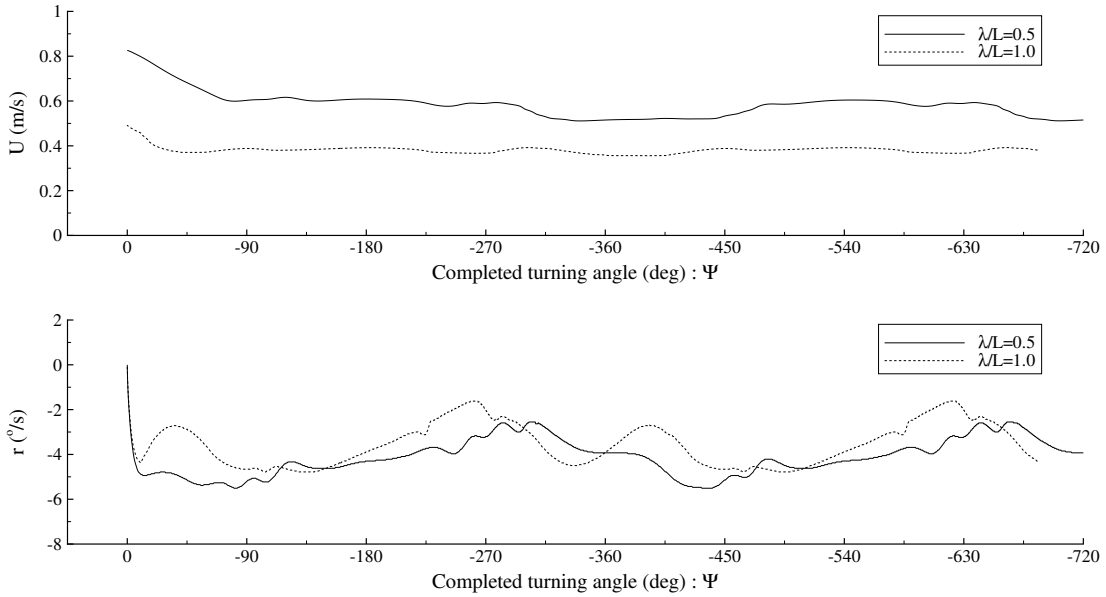

FIGURE 4.8: U and r as functions of completed turning angle at $\lambda/L = 0.5, 1.0$ ($\chi_0 = 180^\circ$)

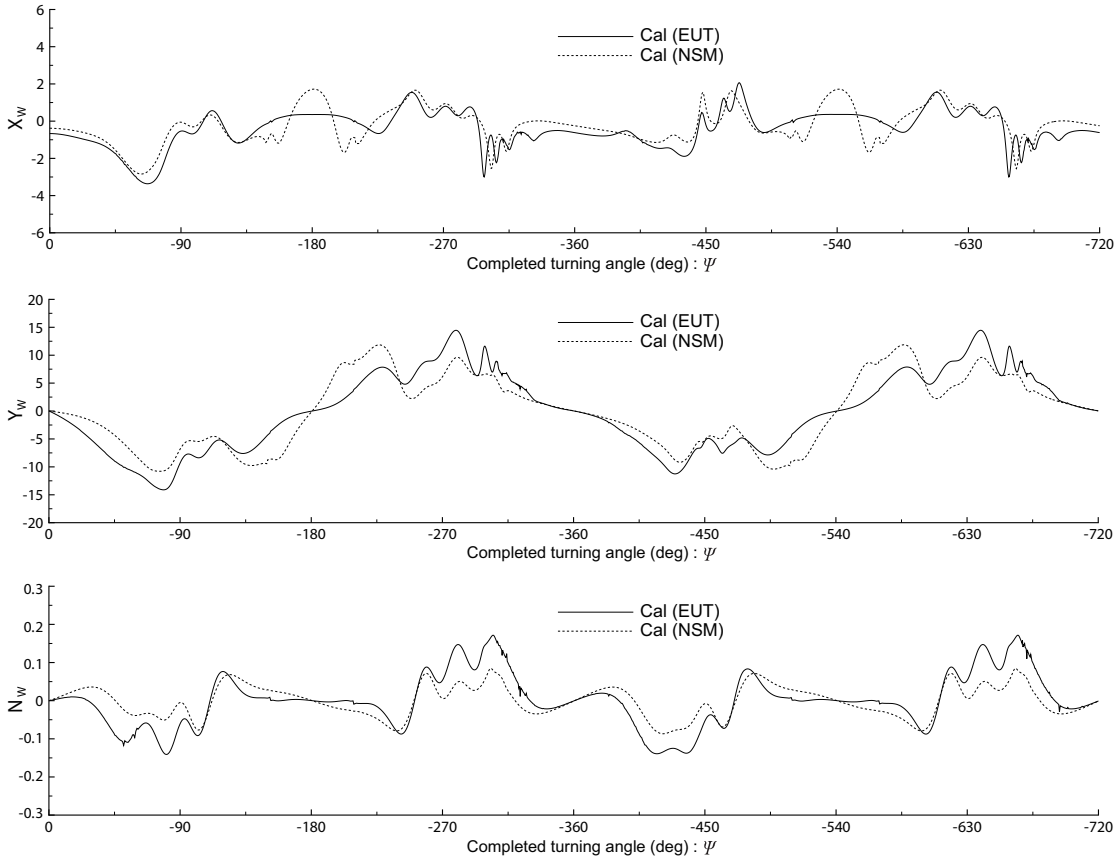

FIGURE 4.9: Steady forces and moment as functions of completed turning angle at $\lambda/L = 0.5$ ($Fn_0 = 0.141, \chi_0 = 180^\circ$)

4.4.3 Sensitivity Study

From the investigation in previous subsection, it became clear that the effect of wave drift to the low-frequency steering motion is more prominent in short waves. In this condition, relative discrepancy between computation and measurement could be seen. Therefore, in order to understand which force contributes the most to the drifting motion of a ship, a sensitivity study is performed by taking advantage of the modular nature of MMG model. The contribution of each of X_W, Y_W, and N_W to the deviation of turning-motion trajectory is evaluated simply by alternative inclusion and exclusion of these terms in the motion equations (4.1).

When $\lambda/L = 0.5$, the simulation results with the exclusion of X_W, Y_W and N_W are shown in Figs. 4.10 ~ 4.12 along with the original computed trajectory by EUT and measured data. The result implies that omission of added resistance X_W or steady yaw moment N_W alters the turning trajectory in short waves, yet the deviation from the original result is relatively small that the general properties/shape of the turning circle is basically preserved.

On the other hand, as shown in Fig. 4.11, exclusion of steady sway force Y_W caused the maneuvering trajectory to almost recover the trajectory in calm water simulation, except some drift to the space-fixed y-direction. The drift to the direction of the incident wave diminishes to virtually zero value, and thus the effect of Y_W is of critical importance in the investigation of drift phenomenon in waves.

The maneuvering velocities of the simulations shown in Figs. 4.10 ~ 4.12 are presented in Fig. 4.13. When the steady sway force is neglected, we can see the reduction of sway velocity to almost constant value, as well as the significant changes in surge velocity and yaw rate. This further shows the importance of the steady sway force in this problem.

Next, in order to verify this finding, the numerical simulation is performed for a turning test considering only Y_W as the wave effect by the following equations:

$$\left.\begin{aligned} (m+m_x)\dot{u} - (m+m_y)vr &= X_H + X_R + X_P \\ (m+m_y)\dot{v} + (m+m_x)ur &= Y_H + Y_R + Y_W(\zeta_a, \omega_0, \chi_0 - \Psi, U) \\ (I_{zz}+J_z)\dot{r} &= N_H + N_R \end{aligned}\right\} \tag{4.2}$$

where we entirely omit the added resistance X_W and steady yaw moment N_W in the equations.

The computed trajectory is shown in Fig. 4.14. Judging from improved agreement between the simulated trajectory and the experiment, it can be confirmed that the steady sway force Y_W dictates mostly the maneuvering of a ship in this wave condition ($\lambda/L = 0.5$). It is also obvious that this second-order lateral force component takes substantial portion of the total wave drift, where the diffraction wave provides immense contribution.

Even though the steady sway force Y_W plays the most important role in this case, improvement in the estimation of X_W and N_W is not less vital to improve the prediction accuracy and to represent the problem in physically rational manner.

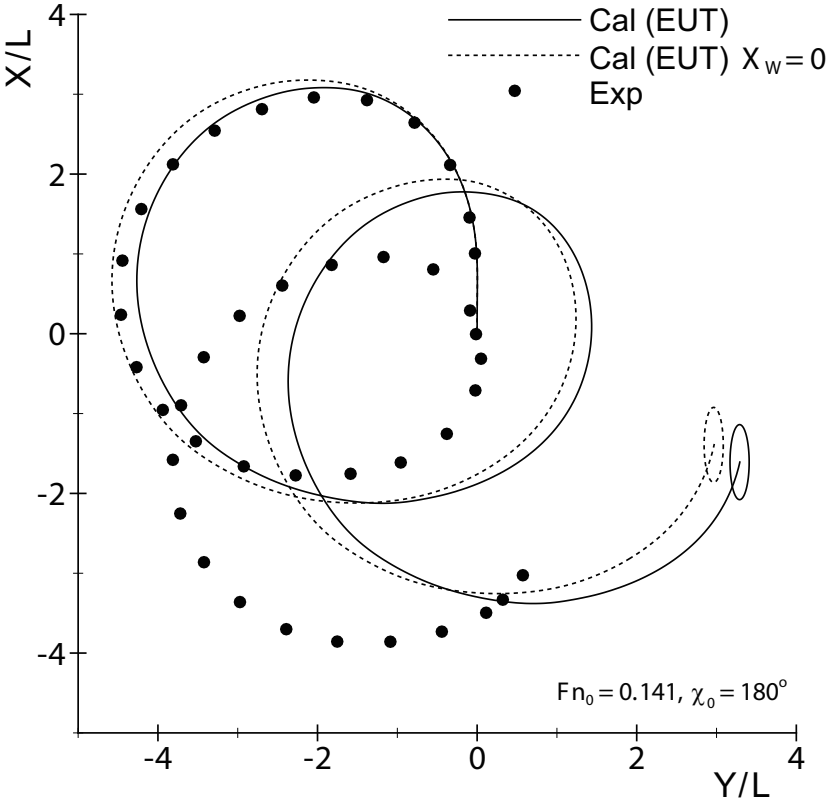

FIGURE 4.10: Turning test with $X_W = 0$ in $\lambda/L = 0.5$ ($Fn_0 = 0.141, \chi_0 = 180°$)

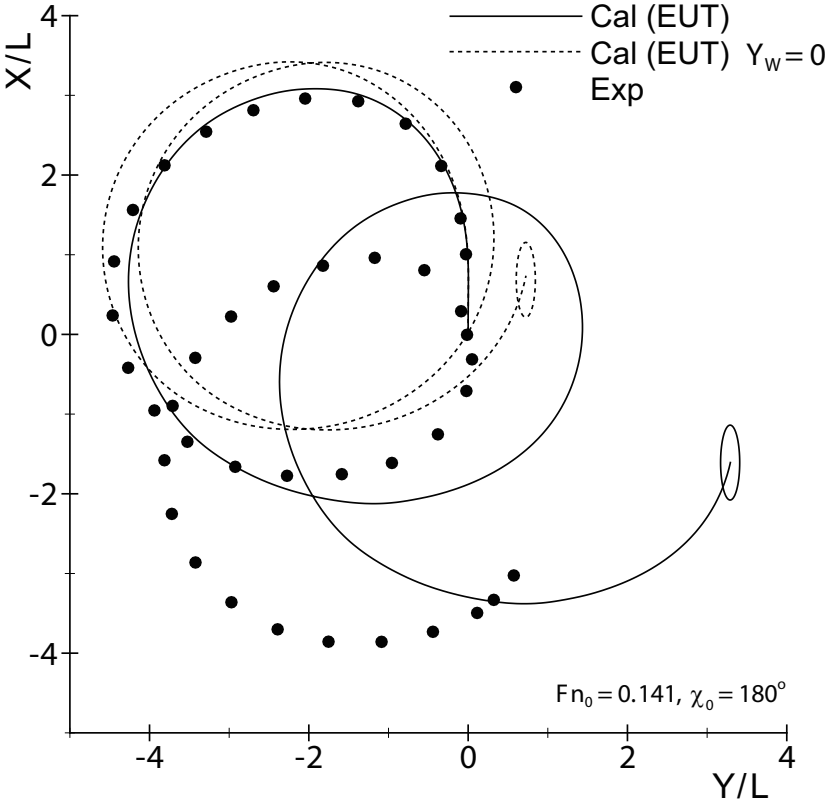

FIGURE 4.11: Turning test with $Y_W = 0$ in $\lambda/L = 0.5$ ($Fn_0 = 0.141, \chi_0 = 180°$)

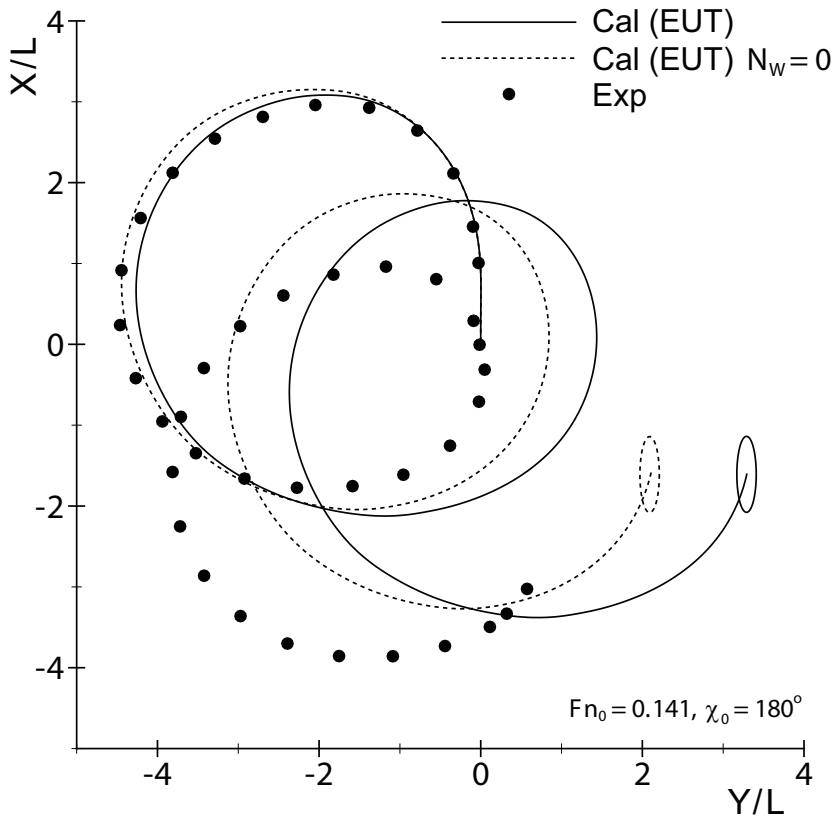

FIGURE 4.12: Turning test with $N_W = 0$ in $\lambda/L = 0.5$ ($Fn_0 = 0.141, \chi_0 = 180^\circ$)

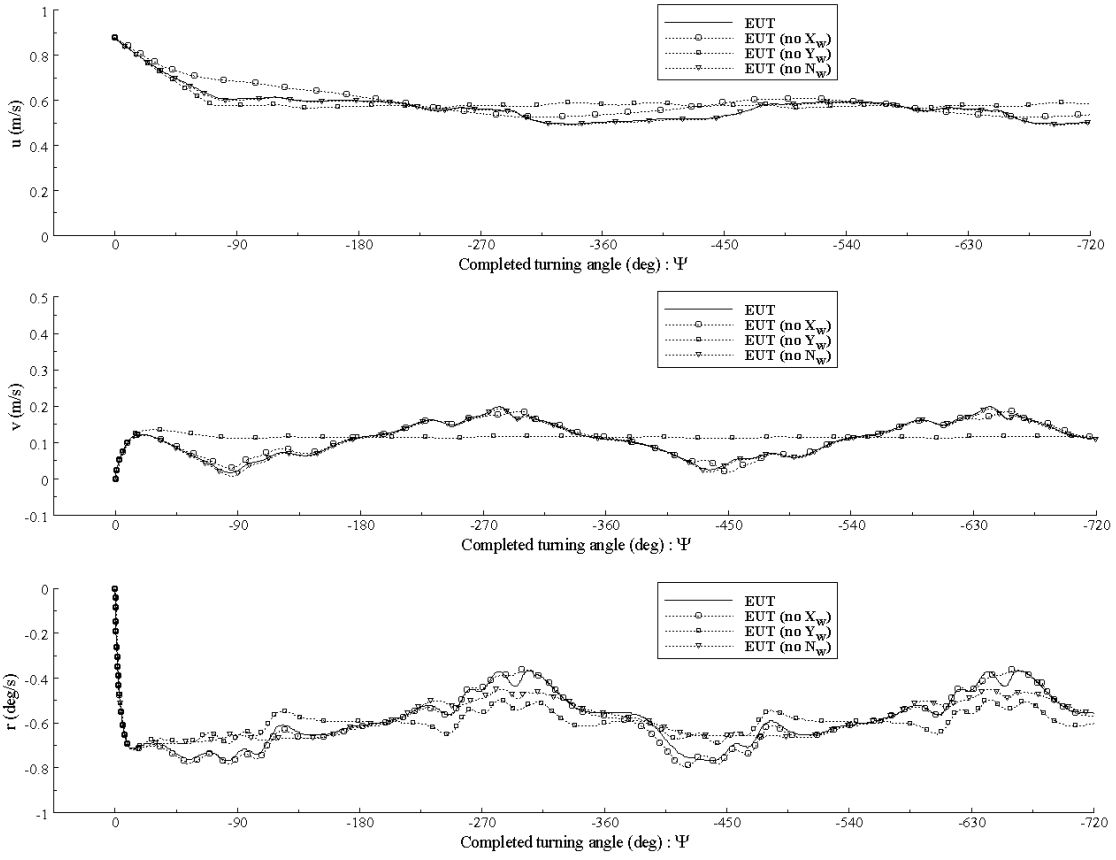

FIGURE 4.13: Time series of sensitivity study in $\lambda/L = 0.5$ ($Fn_0 = 0.141, \chi_0 = 180^\circ$)

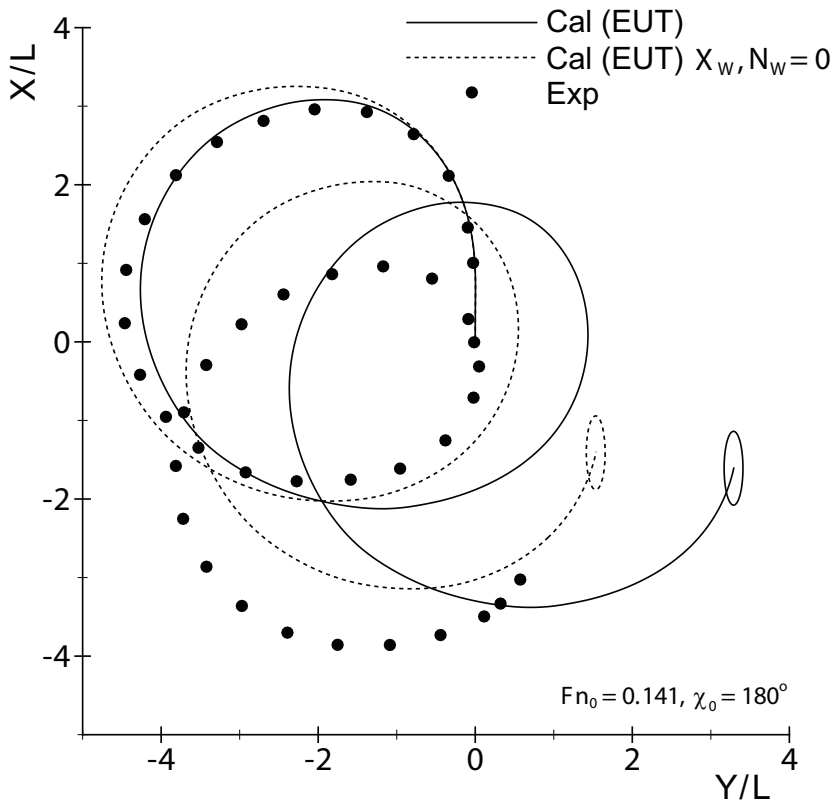

FIGURE 4.14: Turning test with only Y_W ($X_W, N_W = 0$) in $\lambda/L = 0.5$ ($Fn_0 = 0.141, \chi_0 = 180^\circ$)

Chapter 5

Conclusions

In this dissertation, wave-induced motions and steering motions of a ship are formulated as a unified problem of seakeeping and maneuvering in waves. A study is performed systematically through three main topics: seakeeping based on slender-ship theory and far-field concept, maneuvering in calm water by the modular mathematical model and their coupling by the two-time scale method. In each step, basic theories are derived, simulations are performed and validations with tank experiments are conducted.

In **Chapter 2**, investigation on the wave-induced steady forces and moment acting on an advancing ship in oblique waves has been made. We employed enhanced unified theory (EUT) and new strip method (NSM) for solving the radiation and diffraction problems, computing the ship motions in waves and the Kochin function equivalent to the complex amplitude of ship-generated disturbance waves at a distance from the ship. For validation of the computation method, we used the experimental data conducted by Yasukawa et al. [44] We observed that EUT can predict the steady horizontal forces and yaw moment better than NSM. When the wavelength is short, the wave diffraction near the ship ends becomes dominant. The EUT is superior in accounting for the effect of bow wave diffraction, due to the retained n_1-component in the body boundary condition. For wavelengths longer than $\lambda/L \approx 1.0$, contribution of the radiation Kochin function

becomes important and it was found to be rather sensitive to the ship's forward speed. Therefore, forward-speed effects must be taken into account in a reasonable way for the wave-induced steady horizontal forces and yaw moment.

In **Chapter 3**, the mathematical model of a ship maneuvering in calm water is developed. Basic principles of MMG model are adopted due to its simplicity, robustness and practical accuracy. The problem is formulated mainly based on MMG standard method [43]. The viscous hull derivatives are purely taken from the captive model tests in order to keep the reliability of the simulation. Validation of the model was peformed through the standard hard-turning test and $10^{\circ}/10^{\circ}$ zig-zag test of SR108 container ship. The model demonstrated high accuracy and excellent efficiency which is an important base for the seakeeping-maneuvering in waves.

In **Chapter 4**, study on the importance of the wave drift forces and moment to the steering motions in waves has been made through the turning tests in regular waves. The EUT and NSM were coupled with the MMG model using the weak-coupling approach of two-time scale method. The slender-ship theory is used to define the boundary conditions in the seakeeping problem so that the Kochin functions can be determined to estimate the steady forces and moment. These quantities are then supplied to the low-frequency MMG motion equations as the additional force modules. By this scheme, the coupling between the high-frequency wave-induced motions and the low-frequency maneuvering motions can be realized in a practically reasonable manner. Based on the comparison with the measured turning motion in waves [20], we observed that the influence of the slowly-varying drift forces to the maneuvering motion is especially large in short-wave condition. The steady sway force contributes largely to the total drift, as well as governs the ship drifting motion to the direction of incident waves. When the λ is comparable to the L_{PP}, the model is able to represent the experiment better than in shorter waves.

Through the use of present concept, one may simulate the maneuvering motion of a ship in regular waves, with robustness of the MMG model, practical accuracy of the far-field drift forces

formulae, and computational efficiency in the linear slender-ship theory. Nevertheless, fundamental improvement is necessary to refine the physics of the model, such as the consideration of drift angle into the basis flow, the wave effect on the propeller and rudder forces, and so on.

Appendix A

Removal of Singularity at Integration Limits

Once the Kochin function has been obtained as a function of k, the accuracy in computed values of the wave-induced steady forces ($\overline{R}$ and $\overline{Y}$) and yaw moment ($\overline{N}$) depends on the numerical integration with respect to k. One of the issues to be considered for correct numerical integration is the removal of square-root singularity at the limit of integration range k_j ($j = 1 \sim 4$).

In this process, we will have to consider two types of integral:

$$\mathcal{J}_{23} \equiv \int_{k_2}^{k_3} \frac{F(k)}{\sqrt{\kappa^2 - k^2}}\, dk,\ \mathcal{J}_4 \equiv \int_{k_4}^{\infty} \frac{F(k)}{\sqrt{\kappa^2 - k^2}}\, dk. \tag{A.1}$$

The square-root singularity exists in these integrals because of $\sqrt{\kappa^2 - k^2} = 0$ at k_j ($j = 2, 3, 4$). To explain the variable transformation method for this issue, let us consider the following two integrals in general:

$$\left.\begin{aligned} \mathcal{A} &= \int_a^b \frac{f(x)}{\sqrt{(x-a)(b-x)}}\, dx \\ \mathcal{B} &= \int_b^{\infty} \frac{f(x)}{\sqrt{(x-a)(x-b)}}\, dx \end{aligned}\right\}. \tag{A.2}$$

For integral $\mathcal{A}$, we will use the following transformation of variable:

$$x = \frac{b+a}{2} + \frac{b-a}{2}\,\xi, \quad \xi = \sin\theta. \tag{A.3}$$

Then $\mathcal{A}$ can be transformed into the following form:

$$\mathcal{A} = \int_{-1}^{1} \frac{f(x)}{\sqrt{1-\xi^2}}\,d\xi = \int_{-\pi/2}^{\pi/2} f(x)\,d\theta, \tag{A.4}$$

where x is given by (A.3) with θ. We can see no singularity in the last integral with respect to θ, hence the numerical integration can be done in a straightforward manner.

Next, for integral $\mathcal{B}$, similar idea can be applied and the following variable transformation is used

$$x = \frac{b+a}{2} + \frac{b-a}{2}\,\xi, \quad \xi = \sqrt{u^2+1}. \tag{A.5}$$

Then we can obtain the result as follows:

$$\mathcal{B} = \int_{1}^{\infty} \frac{f(x)}{\sqrt{\xi^2-1}}\,d\xi = \int_{0}^{\infty} \frac{f(x)}{\sqrt{u^2+1}}\,du, \tag{A.6}$$

which contains again no singularity at the integration limit ($u = 0$) so that the numerical integration can be performed with conventional schemes. In the present study, the Gauss quadrature has been used to successive integrals with finite integration range.

Appendix B

Semi-Infinite Integral

Many studies using the strip theory have been made so far for computing the Kochin function and then the added resistance based on (2.102). Most of those studies usually multiply the integrand by an artificial convergence factor, like $\exp(-\kappa z_s)$, to ensure the convergence as $k \to \infty$, and the value of z_s is tuned to see reasonably fast convergence and relatively good agreement with experiments. However, this treatment implies that the depthwise position of the line distribution of singularities in the outer solution is not on $z = 0$ and hence inconsistent in the context of slender-ship theory. Kashiwagi [5, 6] settled this problem by showing no difficulty in convergence of the integral in (2.102) for the added resistance, even if the sources are placed exactly on $z = 0$. In this paper, the calculation method in Kashiwagi [5, 6] is extended to the integrals for $\overline{Y}$ and $\overline{N}$, and an analytical mistake in Kashiwagi [5, 6] is corrected.

As an example for explaining the calculation method, let us consider the following semi-infinite integral:

$$\begin{aligned}
&\int_{k_4}^{\infty} \left|C(k)\right|^2 \frac{\kappa\,(k - k_0 \cos\chi)}{\sqrt{\kappa^2 - k^2}}\, dk \\
&= \int_{k_4}^{\infty} \left|C(k)\right|^2 \frac{(1 - \sqrt{1 - k^2/\kappa^2})(k - k_0 \cos\chi)}{\sqrt{\kappa^2 - k^2}}\, dk \\
&\quad + \mathcal{R}_4 - \mathcal{T}_4\, k_0 \cos\chi,
\end{aligned} \tag{B.1}$$

where

$$\mathcal{R}_4 \equiv \int_{k_4}^{\infty} \left|C(k)\right|^2 k\, dk,\ \mathcal{T}_4 \equiv \int_{k_4}^{\infty} \left|C(k)\right|^2 dk. \tag{B.2}$$

Note that the first term on the right-hand side of (B.1) arises no problem in convergence, because $1 - \sqrt{1 - k^2/\kappa^2}$ in the numerator becomes rapidly zero as k increases. Therefore, our attention will be focused on how to evaluate the integrals denoted as $\mathcal{R}_4$ and $\mathcal{T}_4$.

At first, with the assumption that k and x are non-dimensionalized with half the ship length $L/2$, the Kochin function $C(k)$ is written in the form

$$C(k) = \int_{-1}^{1} Q(x) e^{ikx}\, dx. \tag{B.3}$$

After partial integration, it follows that

$$C(k) = \frac{i}{k} \int_{-1}^{1} Q(x) e^{ikx}\, dx, \tag{B.4}$$

where we have used the assumption of $Q(\pm 1) = 0$, that is, both ship ends are closed, which is plausible in the potential-flow problem. Substituting these into (B.2), we have

$$\left.\begin{aligned} \mathcal{R}_4 &= i \int_{-1}^{1} Q(x)\, dx \int_{-1}^{1} Q^*(\xi)\, I_4(\xi - x)\, d\xi \\ \mathcal{T}_4 &= \int_{-1}^{1} Q(x)\, dx \int_{-1}^{1} Q^*(\xi)\, I_4(\xi - x)\, d\xi \end{aligned}\right\}, \tag{B.5}$$

where

$$I_4(\xi - x) \equiv \int_{k_4}^{\infty} e^{ik(x-\xi)}\, dk = \pi\delta(\xi - x) - i\frac{e^{-ik_4(\xi - x)}}{\xi - x}, \tag{B.6}$$

and $\delta(\xi - x)$ denotes Dirac's delta function, which is obtained from the following relations:

$$\left.\begin{aligned} \lim_{k\to\infty} \frac{\cos k(\xi - x)}{\xi - x} &= 0 \\ \lim_{k\to\infty} \frac{\sin k(\xi - x)}{\xi - x} &= \pi\,\delta(\xi - x) \end{aligned}\right\}. \tag{B.7}$$

Substituting (B.6) in (B.5) gives the following results:

$$\begin{aligned}\mathcal{R}_4 = \quad & i\pi \int_{-1}^{1} Q(x)Q^*(x)\,dx \\ & + \int_{-1}^{1} Q(x)e^{ik_4 x}\,dx \int_{-1}^{1} \frac{Q^*(\xi)e^{-ik_4\xi}}{\xi - x}\,d\xi,\end{aligned} \tag{B.8}$$

$$\begin{aligned}\mathcal{T}_4 = \quad & \pi \int_{-1}^{1} \left|Q(x)\right|^2 dx \\ & -i \int_{-1}^{1} Q(x)e^{ik_4 x}\,dx \int_{-1}^{1} \frac{Q^*(\xi)e^{-ik_4\xi}}{\xi - x}\,d\xi.\end{aligned} \tag{B.9}$$

The first terms on the right-hand side of (B.8) and (B.9) are missing in the analysis of Kashiwagi [5, 6]. However, we note that these terms have nothing to do with k_4, and they will cancel out with corresponding terms to be obtained from the integral for $-\infty < k < k_1$. In order to show this, let us consider the integral for $-\infty < k < k_1$ in the same way. Namely

$$\begin{aligned}& -\int_{-\infty}^{k_1} \left|C(k)\right|^2 \frac{\kappa\,(k - k_0\cos\chi)}{\sqrt{\kappa^2 - k^2}}\,dk \\ & = \int_{k_1}^{-\infty} \left|C(k)\right|^2 \frac{(1 - \sqrt{1 - k^2/\kappa^2})(k - k_0\cos\chi)}{\sqrt{\kappa^2 - k^2}}\,dk \\ & \quad + \mathcal{R}_1 - \mathcal{T}_1\,k_0\cos\chi,\end{aligned} \tag{B.10}$$

where

$$\mathcal{R}_1 \equiv \int_{k_1}^{-\infty} \left|C(k)\right|^2 k\,dk,\ \mathcal{T}_1 \equiv \int_{k_1}^{-\infty} \left|C(k)\right|^2 dk. \tag{B.11}$$

Following the same procedure as that for $\mathcal{R}_4$ and $\mathcal{T}_4$, we come across an integral corresponding to (B.6), which can be written by use of (B.7) in the form

$$\begin{aligned}I_1(\xi - x) \quad & \equiv \quad \int_{k_1}^{-\infty} e^{ik(x-\xi)}\,dk \\ & = \quad -\pi\delta(\xi - x) - i\frac{e^{-ik_1(\xi - x)}}{\xi - x}.\end{aligned} \tag{B.12}$$

It can be seen that the first term on the right-hand side of (B.12) is opposite in sign to that of

(B.6). Thus, in the end after summing up, there is no contribution from the first terms in (B.8) and (B.9).

Regarding the singular integral with respect to ξ in (B.8) and (B.9), the analytical integration method shown in Kashiwagi [5, 6] can be applied, using the Fourier-series representation for the line distribution of sources. The resulting singular integral is the same in form as Glauert's integral popular in the wing theory and thus can be evaluated analytically. Specifically, introducing the variable transformation of $x = \cos\theta$ and $\xi = \cos\varphi$, we have the following:

$$\begin{aligned} \int_{-1}^{1} \frac{Q^*(\xi)e^{-iv\xi}}{\xi - x}\, d\xi &= \sum_{n=1}^{\infty} c_n^* \int_0^{\pi} \frac{\sin n\varphi \sin\varphi}{\cos\varphi - \cos\theta}\, d\varphi \\ &= -\pi \sum_{n=1}^{\infty} c_n^* \cos n\theta, \end{aligned} \tag{B.13}$$

where

$$\left.\begin{aligned} Q(x)e^{ivx} &= \sum_{n=1}^{\infty} c_n \sin n\theta \\ c_n &= \frac{2}{\pi}\int_0^{\pi} Q(\cos\theta)e^{iv\cos\theta} \sin n\theta\, d\theta \end{aligned}\right\} \tag{B.14}$$

and ν must be understood as k_4 or k_1.

By using these results and performing resultant integrals with respect to θ, $\mathcal{R}_j$ and $\mathcal{T}_j$ ($j = 4$ or 1) defined in (B.2) and (B.11) can be expressed as

$$\begin{aligned} \mathcal{R}_j &= (-1)^j i\pi \int_{-1}^{1} Q(x)Q^*(x)\, dx \\ &\quad + \frac{\pi^2}{2} \sum_{n=1}^{\infty} \Big[k_j\, \Im(c_n\, c_{n+1}^*) + n\, |c_n|^2 \Big], \end{aligned} \tag{B.15}$$

$$\mathcal{T}_j = (-1)^j \pi \int_{-1}^{1} \big|Q(x)\big|^2\, dx + \frac{\pi^2}{2} \sum_{n=1}^{\infty} \Im(c_n\, c_{n+1}^*). \tag{B.16}$$

As already mentioned, the first terms on the right-hand side of (B.15) and (B.16) do not contribute to the final result because of cancellation after summing up the terms of $j = 1$ and $j = 4$. Needless to say, the same calculation method will be used to the integrals related to the antisymmetric component of the Kochin function $S(k)$ in (2.132).

The same technique can be applied to the integrals for the steady sway force $\overline{Y}$ in (2.114) and for the steady yaw moment $\overline{N}$ in (2.131). Let us start with the steady sway force. We will have to consider the following integral:

$$\begin{aligned}
&\int_{\nu}^{\infty} \kappa\, \Im\Big\{C(k)S^*(k)\Big\}\, dk \\
&= \int_{\nu}^{\infty} \kappa\Big(\sqrt{1-k^2/\kappa^2}-1\Big)\, \Im\Big\{C(k)\widehat{S}^*(k)\Big\}\, dk \\
&\quad + \int_{\nu}^{\infty} \kappa\, \Im\Big\{C(k)\widehat{S}^*(k)\Big\}\, dk,
\end{aligned} \tag{B.17}$$

where $\widehat{S}(k)$ is defined in (2.133).

It should be noted again that no problem exists in convergence for the first term on the right-hand side of (B.17), because $\sqrt{1-k^2/\kappa^2} \to 1$ rapidly as $k \to \infty$. Thus we consider the last integral.

Since $\kappa = K + 2k\tau + k^2/K_0$, we should evaluate analytically the following integrals:

$$\mathcal{Y}_n \equiv \int_{\nu}^{\infty} k^n\, \Im\Big\{C(k)\widehat{S}^*(k)\Big\}\, dk, \quad n = 0, 1, 2. \tag{B.18}$$

With these results, the last term in (B.17) can be computed from

$$\int_{\nu}^{\infty} \kappa\, \Im\Big\{C(k)\widehat{S}^*(k)\Big\}\, dk = K\,\mathcal{Y}_0 + 2\tau\,\mathcal{Y}_1 + \frac{1}{K_0}\mathcal{Y}_2. \tag{B.19}$$

The analysis for (B.18), using the Fourier-series representation for the line distribution of sources and doublets, are shown in Appendix C.

Likewise, the semi-infinite integral in the steady yaw moment can be written as follows:

$$\begin{aligned}
&\int_{\nu}^{\infty} \kappa\, \Re\Big\{C(k)S^*(k) - S(k)C^*(k)\Big\}\, dk \\
&= \int_{\nu}^{\infty} \kappa\Big(\sqrt{1-k^2/\kappa^2}-1\Big) \\
&\qquad \times \Re\Big\{C(k)\widehat{S}^*(k) - \widehat{S}(k)C^*(k)\Big\}\, dk \\
&\quad + \int_{\nu}^{\infty} \kappa\, \Re\Big\{C(k)\widehat{S}^*(k) - \widehat{S}(k)C^*(k)\Big\}\, dk.
\end{aligned} \tag{B.20}$$

The first term on the right-hand side of (B.20) can be numerically integrated without any difficulty. For evaluating the last term in (B.20), we consider analytically the following integrals:

$$\mathcal{N}_n \equiv \int_\nu^\infty k^n \,\Re\left\{C(k)\widehat{S}^*(k)\right\} dk, \quad n = 0, 1, 2, \tag{B.21}$$

$$\widetilde{\mathcal{N}}_n \equiv \int_\nu^\infty k^n \,\Re\left\{\widehat{S}(k)C^*(k)\right\} dk, \quad n = 0, 1, 2. \tag{B.22}$$

With the results of these integrals, we can readily evaluate the last integral in (B.20) from

$$\begin{aligned}&\int_\nu^\infty \kappa \,\Re\left\{C(k)\widehat{S}^*(k) - \widehat{S}(k)C^*(k)\right\} dk \\ &= K(\mathcal{N}_0 - \widetilde{\mathcal{N}}_0) + 2\tau\,(\mathcal{N}_1 - \widetilde{\mathcal{N}}_1) + \frac{1}{K_0}(\mathcal{N}_2 - \widetilde{\mathcal{N}}_2).\end{aligned} \tag{B.23}$$

The analytical procedure for computing (B.21) and (B.22) is essentially the same as that for $\mathcal{Y}_n$ ($n = 0, 1, 2$), and we note that the calculation of $\widetilde{\mathcal{N}}_n$ can be done easily from the result of $\mathcal{N}_n$ simply by exchanging $C(k)$ and $\widehat{S}(k)$. The final expressions for $\mathcal{N}_n$ and $\widetilde{\mathcal{N}}_n$ ($n = 0, 1, 2$) are also summarized in Appendix of this paper.

Appendix C

Analytical integration for $\mathcal{Y}_n$, $\mathcal{N}_n$, and $\widetilde{\mathcal{N}}_n$

For computing the wave-induced steady sway force and yaw moment, the following integrals should be integrated analytically:

$$\mathcal{Y}_n \equiv \int_{\nu}^{\infty} k^n \ \Im\left\{C(k)\widehat{S}^*(k)\right\} dk, \quad n = 0, 1, 2, \tag{C.1}$$

$$\mathcal{N}_n \equiv \int_{\nu}^{\infty} k^n \ \Re\left\{C(k)\widehat{S}^*(k)\right\} dk, \quad n = 0, 1, 2, \tag{C.2}$$

$$\widetilde{\mathcal{N}}_n \equiv \int_{\nu}^{\infty} k^n \ \Re\left\{\widehat{S}(k)C^*(k)\right\} dk, \quad n = 0, 1, 2, \tag{C.3}$$

where ν must be understood as a value equal to or larger than k_4 or $|k_1|$.

We consider $\mathcal{Y}_n$ first. By substituting the definition of the Kochin functions $C(k)$ and $\widehat{S}(k)$ shown in (2.133) and performing partial integration with assumption of $Q(\pm 1) = 0$ and $D(\pm 1) = 0$, we

have

$$\mathcal{Y}_0 = \Im\Big[\int_{-1}^{1} Q(x)\,dx \int_{-1}^{1} D^*(\xi)\,d\xi \int_{\nu}^{\infty} e^{ik(x-\xi)}\,dk\Big], \tag{C.4}$$

$$\mathcal{Y}_1 = \Im\Big[i\int_{-1}^{1} Q(x)\,dx \int_{-1}^{1} D^*(\xi)\,d\xi \int_{\nu}^{\infty} e^{ik(x-\xi)}\,dk\Big], \tag{C.5}$$

$$\mathcal{Y}_2 = \Im\Big[\int_{-1}^{1} Q(x)\,dx \int_{-1}^{1} D^*(\xi)\,d\xi \int_{\nu}^{\infty} e^{ik(x-\xi)}\,dk\Big]. \tag{C.6}$$

The semi-infinite integral with respect to k can be given by the formula of (B.6), but as explained in the analysis for the added resistance, there is no need to consider the contribution from Dirac's delta function in the final result for the steady sway force as well. To evaluate singular integrals with respect to ξ to be obtained from the last term in (B.6), we prepare the following Fourier series:

$$\left.\begin{aligned} D^*(\xi)e^{-i\nu\xi} &= \sum_{n=1}^{\infty} s_n^* \sin n\varphi \\ D^*(\xi)e^{-i\nu\xi} &= -\frac{1}{\sin\varphi}\sum_{n=1}^{\infty} s_n^* \\ &\quad \times\{-i\nu\sin\varphi\sin n\varphi + n\cos n\varphi\} \\ s_n^* &= \frac{2}{\pi}\int_0^{\pi} D^*(\cos\varphi)e^{-i\nu\cos\varphi}\sin n\varphi\,d\varphi \end{aligned}\right\}. \tag{C.7}$$

Then the singular integrals with respect to ξ can be analytically integrated like (B.13), and the results are written as

$$\int_{-1}^{1} \frac{D^*(\xi)e^{-i\nu\xi}}{\xi - x}\,d\xi = -\pi\sum_{n=1}^{\infty} s_n^* \cos n\theta, \tag{C.8}$$

$$\int_{-1}^{1} \frac{D^*(\xi)e^{-i\nu\xi}}{\xi - x}\,d\xi = -\pi\sum_{n=1}^{\infty} s_n^* \times\Big\{i\nu\cos n\theta + n\frac{\sin n\theta}{\sin\theta}\Big\}, \tag{C.9}$$

where $x = \cos\theta$ has been used. Then after substituting (B.14), resulting integrals with respect to x can be evaluated as the integrals with respect to θ, for which the following formulae will be

used:

$$\int_0^\pi \cos m\theta \sin n\theta \sin\theta \, d\theta = \frac{\pi}{4}\{\, \delta_{m+1,n} - \delta_{m,n+1} \,\} \tag{C.10}$$

$$\int_0^\pi \cos m\theta \cos n\theta \, d\theta = \int_0^\pi \sin m\theta \sin n\theta \, d\theta = \frac{\pi}{2}\, \delta_{m,n} \tag{C.11}$$

$$\int_0^\pi \frac{\sin m\theta \cos n\theta}{\sin\theta} \, d\theta = \begin{cases} \pi & \text{for } m > n \\ 0 & \text{otherwise} \end{cases} \tag{C.12}$$

where $\delta_{m,n}$ denotes Kroenecker's delta symbol, equal to 1 when $m = n$ and zero otherwise.

Performing integration by using these formulae, we can obtain the following results:

$$\begin{aligned} \mathcal{Y}_0 &= \Im\Big[-i \int_{-1}^{1} Q(x) e^{i\nu x} \, dx \int_{-1}^{1} \frac{D^*(\xi) e^{-i\nu\xi}}{\xi - x} \, d\xi \Big] \\ &= \frac{\pi^2}{4} \Re \sum_{n=1}^{\infty} \{\, c_{n+1}\, s_n^* - c_n\, s_{n+1}^* \,\}, \end{aligned} \tag{C.13}$$

$$\begin{aligned} \mathcal{Y}_1 &= \Im\Big[\int_{-1}^{1} Q(x) e^{i\nu x} \, dx \int_{-1}^{1} \frac{D^*(\xi) e^{-i\nu\xi}}{\xi - x} \, d\xi \Big] \\ &= \frac{\pi^2}{4} \Re \sum_{n=1}^{\infty} \Big[\nu \{\, c_{n+1}\, s_n^* - c_n\, s_{n+1}^* \,\} - i(2n\, c_n\, s_n^*) \Big], \end{aligned} \tag{C.14}$$

$$\begin{aligned} \mathcal{Y}_2 &= \Im\Big[-i \int_{-1}^{1} Q(x) e^{i\nu x} \, dx \int_{-1}^{1} \frac{D^*(\xi) e^{-i\nu\xi}}{\xi - x} \, d\xi \Big] \\ &= \frac{\pi^2}{4} \Re \sum_{n=1}^{\infty} \Big[\nu^2 \{ c_{n+1}\, s_n^* - c_n\, s_{n+1}^* \,\} - i\nu(4n\, c_n\, s_n^*) \\ &\quad + 2n \sum_{\ell=1}^{\infty} (n + 2\ell - 1) \{\, c_{n+2\ell-1}\, s_n^* - s_{n+2\ell-1}\, c_n^* \} \Big] \end{aligned} \tag{C.15}$$

where the Fourier-series coefficient c_n is given in (B.14).

Next we consider $\mathcal{N}_n$ and $\widetilde{\mathcal{N}}_n$. We note that $\widetilde{\mathcal{N}}_n$ can be computed from the results of $\mathcal{N}_n$, simply by replacing c_n and s_n^* with s_n and c_n^*, respectively, in the Fourier-series coefficients.

In the calculation for $\mathcal{N}_n$ and $\widetilde{\mathcal{N}}_n$, the derivatives of the Kochin functions with respect to k are needed, which can be given simply as

$$\left.\begin{aligned} C(k) &= \int_{-1}^{1} ix\, Q(x) e^{ikx}\, dx \\ \widehat{S}(k) &= \int_{-1}^{1} ix\, D(x) e^{ikx}\, dx \end{aligned}\right\}. \tag{C.16}$$

Since the analytical procedure is almost the same as that for $\mathcal{Y}_n$ ($n = 0, 1, 2$), only the final results for $\mathcal{N}_n$ ($n = 0, 1, 2$) are written below.

$$\mathcal{N}_0 = -\frac{\pi^2}{8} \Re \sum_{n=1}^{\infty} (c_{n+2}\, s_n^* - c_n\, s_{n+2}^*), \tag{C.17}$$

$$\begin{aligned} \mathcal{N}_1 = -\frac{\pi^2}{8} \Re \sum_{n-1}^{\infty} \Big[& \nu(c_{n+2}\, s_n^* - c_n\, s_{n+2}^*) \\ & -i\, 2\{n\, c_{n+1}\, s_n^* + (n+1)\, c_n\, s_{n+1}^*\} \Big], \end{aligned} \tag{C.18}$$

$$\begin{aligned} \mathcal{N}_2 = -\frac{\pi^2}{8} \Re \sum_{n=1}^{\infty} \Big[& \nu^2(c_{n+2}\, s_n^* - c_n\, s_{n+2}^*) \\ & -i\, \nu 4\{n\, c_{n+1}\, s_n^* + (n+1)\, c_n\, s_{n+1}^*\} \\ & -4\, n\, c_n \sum_{\ell-1}^{\infty} \Big\{ (n+2\ell)\, s_{n+2\ell}^* \\ & +(n+2\ell-2)\, s_{n+2\ell-2}^* \Big\} \Big]. \end{aligned} \tag{C.19}$$

Appendix D

Derivation of longitudinal rudder inflow velocity u_R

As can be seen from (3.26), it is clear that the averaged inflow velocity dictates the rudder normal force. In order to understand the nature of this problem, we firstly assume that the ship advances straightly. In the general theory on propeller wake flow, we will first describe the simple momentum theory as a foundation.

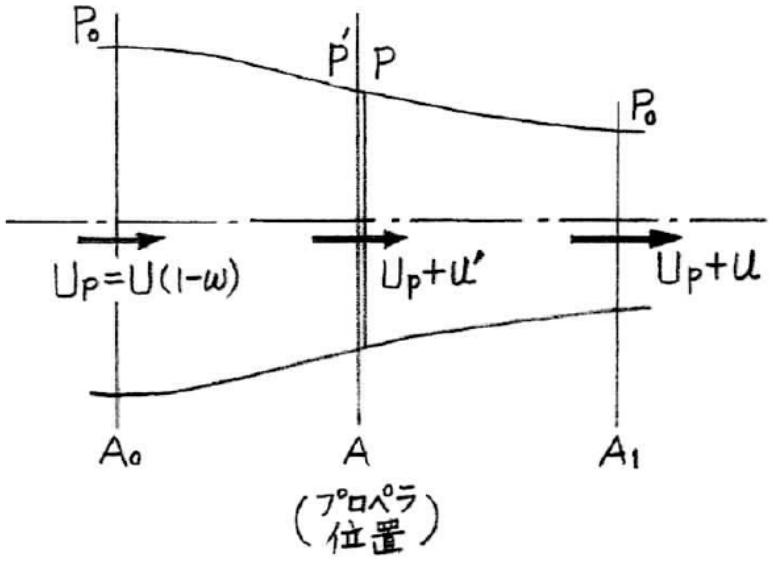

FIGURE D.1: Momentum theory (actuator disk) [65]

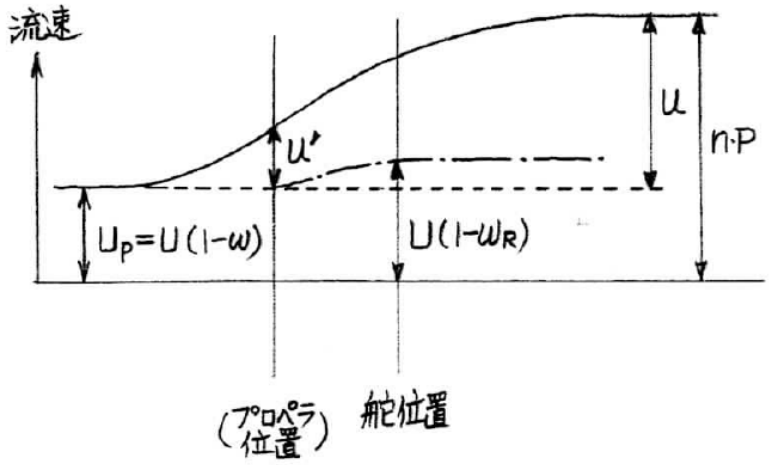

FIGURE D.2: Change in flow velocity [65]

By applying the Bernoulli's theorem independently in the upstream and downstream of the propeller disk shown in Fig. D.1,

$$\begin{aligned} P_0 + \frac{1}{2}\rho u_P^2 &= P' + \frac{1}{2}\rho(u_P + u')^2 \\ P + \frac{1}{2}\rho(u_P + u')^2 &= P_0 + \frac{1}{2}\rho(u_P + u)^2, \end{aligned} \tag{D.1}$$

then by substraction of both sides,

$$P - P' = \frac{\rho}{2}[(u_P + u)^2 - u_P^2] = \rho u(u_P + \frac{u}{2}) \tag{D.2}$$

and considering the constant flow rate

$$m = \rho A(u_P + u') = \rho A_0 u_P = \rho A_1(u_P + u) \equiv \rho Q \tag{D.3}$$

as well as thrust,

$$T = (p - p')A = \rho Q u \tag{D.4}$$

substitution of (D.2) and (D.3) into (D.4) obtains

$$\begin{aligned} &\rho A u(u_P + \frac{u}{2}) = \rho A u(u_P + u') \\ &\text{therefore} \quad u' = \frac{1}{2}u \end{aligned} \tag{D.5}$$

In Fig. D.2, the flow velocity accelerated at infinity u is twice the flow velocity accelerated by the propeller disk u'. Next, by substituting (D.2) into (D.4):

$$T = \rho u(u_P + \frac{u}{2})A = K_T \rho n^2 D^4 \tag{D.6}$$

therefore

$$u = u_P\left[\sqrt{1 + \frac{8K_T}{\pi J^2}} - 1\right] \tag{D.7}$$

with n the propeller rotational speed, D the propeller diameter, and J the propeller advance ratio ($= \frac{u_P}{nD}$). Furthermore, from Fig. D.2, since the flow velocity at infinity is given by $u_P + u$, we may write (D.7) as:

$$u_P + u = u_P\sqrt{1 + \frac{8K_T}{\pi J^2}} \tag{D.8}$$

For convenience afterwards, it can be seen that when the flow rate Q is obtained from the equation (D.3), the following equation is obtained,

$$Q = \frac{1}{2}Au_P\left[1 + \sqrt{1 + \frac{8K_T}{\pi J^2}}\right] \tag{D.9}$$

Notice that the $8K_T/\pi J^2$ that appeared in (D.7) through (D.9) is the thrust loading coefficient (C_T). This can be verified as follows:

$$\tau \equiv \frac{T}{\frac{1}{2}\rho A u_P^2} = \frac{K_T \rho n^2 D^4}{\frac{1}{2}\rho\pi(\frac{D}{2})^2 u_P^2} = \frac{8K_T}{\pi J^2} \tag{D.10}$$

Now, the above formula cannot be used unless we understand the propeller characteristics (K_T). Then, let us consider its expression using a propeller slip ($S = 1 - u_P/nP$). Due to assumption of ideal fluid, it has the maximum velocity at infinity. Since this velocity should be the flow velocity when the propeller has zero slip, the (D.8) can be rewritten as follows:

$$u_P + u = nP = \frac{u_P}{1 - S} = u_P\sqrt{1 + \frac{S(2 - S)}{(1 - S)^2}} \tag{D.11}$$

therefore

$$u = \frac{S}{1-S} u_P \tag{D.12}$$

In the next step, if the rudder height differs from the propeller diameter, we have to describe a method to consider its influence to the rudder normal force formula.

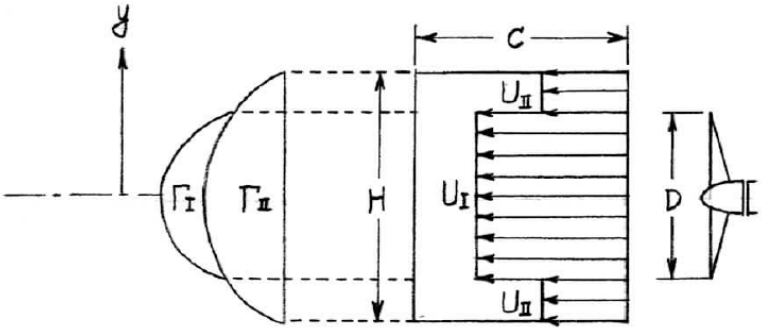

FIGURE D.3: Flow velocity at the rudder position [65]

As shown in the Fig. D.3, u_{I} denotes the propeller wake velocity at rudder position, u_{II} the velocity on the upper- and bottom-end of rudder unaffected by propeller wake, D the propeller diameter, H the rudder height and Λ the aspect ratio ($= H/C$).

The simplest method is to independently apply the (3.26) to the segment of u_{I} and of u_{II} and subsequently add them, that can be written as:

$$\begin{aligned} F_N &= \frac{1}{2}\rho\left(A_R \frac{D}{H}\right) u_{\mathrm{I}}^2 f_\alpha \sin\delta + \frac{1}{2}\rho\left(A_R \frac{H-D}{H}\right) u_{\mathrm{II}}^2 f_\alpha \sin\delta \\ &= \frac{1}{2}\rho A_R [(1-\eta) u_{\mathrm{II}}^2 + \eta u_{\mathrm{I}}^2] f_\alpha \sin\delta \end{aligned} \tag{D.13}$$

However, since the (3.26) is originally obtained from elliptical field force distribution, it is better to consider the Fig. D.3 with the same concept. Therefore, if the circulation strengths due to $u_{\mathrm{I}} - u_{\mathrm{II}}$ and u_{II} are to be written as Γ_{I} and Γ_{II}, the force-field strength is given as follows:

$$\begin{aligned} L &= \int_{-\frac{H}{2}}^{-\frac{D}{2}} \rho u_{\mathrm{II}} \Gamma_{\mathrm{II}} dy + \int_{-\frac{D}{2}}^{\frac{D}{2}} \rho u_{\mathrm{I}} (\Gamma_{\mathrm{I}} + \Gamma_{\mathrm{II}}) dy + \int_{\frac{D}{2}}^{\frac{H}{2}} \rho u_{\mathrm{II}} \Gamma_{\mathrm{II}} dy \\ &= \rho u_{\mathrm{II}} \int_{-\frac{H}{2}}^{\frac{H}{2}} \Gamma_{\mathrm{II}} dy + \rho (u_{\mathrm{I}} - u_{\mathrm{II}}) \int_{-\frac{D}{2}}^{\frac{D}{2}} \Gamma_{\mathrm{II}} dy + \rho u_{\mathrm{I}} \int_{-\frac{D}{2}}^{\frac{D}{2}} \Gamma_{\mathrm{I}} dy \end{aligned} \tag{D.14}$$

$$\text{with} \quad y = \frac{D}{2}\cos\psi \ , \ y = \frac{H}{2}\cos\theta \tag{D.15}$$

According to the wing theory, the elliptical circulation distribution is given as follows:

$$\begin{aligned}
&\Gamma_{\mathrm{I}} = 2D(u_{\mathrm{I}} - u_{\mathrm{II}})a_1 \sin\psi \\
&\text{with } a_1 = \frac{2}{\Lambda' + 2}\sin\delta \quad \Lambda' = \frac{D}{C} = \Lambda\frac{D}{H} \\
&\Gamma_{\mathrm{II}} = 2Hu_{\mathrm{II}}a_2 \sin\theta \\
&\text{with } a_2 = \frac{2}{\Lambda + 2}\sin\delta
\end{aligned} \tag{D.16}$$

Then, by substituting (D.15) and (D.16) into (D.14),

$$J_1 \equiv \int_{-\frac{H}{2}}^{\frac{H}{2}} \Gamma_{\mathrm{II}} dy = H^2 u_{\mathrm{II}} a_2 \int_0^{\pi} \sin^2\theta d\theta = \frac{1}{2}u_{\mathrm{II}}A_R\frac{2\pi\Lambda}{\Lambda + 2}\sin\delta \tag{D.17}$$

Next, since $\frac{D}{2} = \frac{H}{2}\cos\theta_P$ from (D.15) can be written as $\theta_P = \cos^{-1}(\frac{D}{H})$,

$$\begin{aligned}
J_2 \equiv \int_{-\frac{D}{2}}^{\frac{D}{2}} \Gamma_{\mathrm{II}} dy &= H^2 u_{\mathrm{II}} a_2 \int_{\theta_P}^{\pi-\theta_P} \sin^2\theta d\theta = u_{\mathrm{II}}A_R\Lambda a_2\left[\frac{\pi}{2} - \theta_P + \sin\theta_P\cos\theta_P\right] \\
&= \frac{1}{2}u_{\mathrm{II}}A_R\frac{2\pi\Lambda}{\Lambda + 2}\xi\sin\delta \\
\text{with} \quad \xi &= \frac{1}{\pi}\left[\pi - 2\cos^{-1}\frac{D}{H} + 2\frac{D}{H}\sqrt{1 - \left(\frac{D}{H}\right)^2}\right]
\end{aligned} \tag{D.18}$$

$$\begin{aligned}
J_3 \equiv \int_{-\frac{D}{2}}^{\frac{D}{2}} \Gamma_{\mathrm{I}} dy &= D^2(u_{\mathrm{I}} - u_{\mathrm{II}})a_1 \int_0^{\pi} \sin^2\psi d\psi \\
&= \frac{1}{2}(u_{\mathrm{I}} - u_{\mathrm{II}})A_R\frac{2\pi\Lambda}{\Lambda + 2}C_0\sin\delta \\
\text{with} \quad C_0 &= \left(\frac{D}{H}\right)\frac{\Lambda + 2}{\Lambda + \frac{2}{(D/H)}}
\end{aligned} \tag{D.19}$$

Then, substitution of (D.17) through (D.19) into (D.14) yields the following equation:

$$L = \frac{1}{2}\rho A_R\frac{2\pi\Lambda}{\Lambda + 2}[u_{\mathrm{II}}^2 + (u_{\mathrm{I}} - u_{\mathrm{II}})u_{\mathrm{II}}\xi + u_{\mathrm{I}}(u_{\mathrm{I}} - u_{\mathrm{II}})C_0]\sin\delta \tag{D.20}$$

Here, when the $f_\alpha(\Lambda)$ is used as the correction term in the (3.26) ($=\frac{6.13\Lambda}{\Lambda+2.25}$), following expression is obtained,

$$\begin{aligned} F_N &= \frac{1}{2}\rho A_R[(1-\xi)u_{\mathrm{II}}^2 + (\xi - C)u_{\mathrm{I}}u_{\mathrm{II}} + Cu_{\mathrm{I}}^2]f_\alpha(\Lambda)\sin\delta \\ \text{with} \quad C &= \left(\frac{D}{H}\right)\frac{\Lambda+2.25}{\Lambda+\frac{2.25}{(D/H)}} \end{aligned} \tag{D.21}$$

Nevertheless, when we compare (D.13) and (D.21), we see that they can be matched if subsequent approximation is taken.

$$\xi \simeq C \simeq \frac{D}{H} = \eta \tag{D.22}$$

Since there will be no significant difference between the two, this approximation seems proper, therefore (D.13) is considered to be sufficient in order to avoid the complication.

Then, it is important to calculate the u_{I} and u_{II} in Fig. D.3. First, the flow velocity u_{II} which is not affected by the propeller wake flow is expressed using the w_R at the rudder position as

$$\begin{aligned} u_{\mathrm{II}} &= (1-w_R)U = \varepsilon u_P \\ \text{with} \quad \varepsilon &= \frac{1-w_R}{1-w} \end{aligned} \tag{D.23}$$

The value of w_R is experimentally obtained by the matching with the rudder normal force when the propeller is non existent (or when the propeller idles). Next, with respect to the propeller wake flow u_{I}, the increase in the flow velocity due to the rotation of the propeller is expressed as follows using the coefficient k. (See Fig. D.2)

$$\begin{aligned} \Delta U &= k(U_\infty - u_P) \\ \text{with} \quad U_\infty &= u_P + u \quad \text{or} \quad nP \end{aligned} \tag{D.24}$$

And at the time of idling propeller, $u_P = nP(= U_\infty)$ then $u_{\mathrm{I}} = u_{\mathrm{II}}$, so u_{I} can be defined as:

$$\begin{aligned} u_{\mathrm{I}} &= u_{\mathrm{II}} + \Delta U \\ u_P\left\{\varepsilon + k\left(\frac{U_\infty}{u_P} - 1\right)\right\} &= u_P\left\{\varepsilon + k\frac{u}{u_P}\right\} \end{aligned} \tag{D.25}$$

The coefficient k is experimentally obtained by the matching with the rudder normal force when the ship is stopped. In this case, since $S = 1, u_{\mathrm{II}} = 0, u_{\mathrm{I}} = knP$, the calculation is straightforward, with rough assumption of $k = 0.6$.

Finally, by substituting (D.23) and (D.25) into (D.13), and by taking the definition of u in (D.7) into (D.25), the rudder effective inflow velocity u_R is given as follows:

$$\begin{aligned} u_R &= \varepsilon u_P \sqrt{\eta\{1 + \kappa(\sqrt{1 + 8K_T/\pi J^2} - 1)\}^2 + 1 - \eta} \\ \text{with} \quad \kappa &= \frac{k}{\varepsilon} \simeq \frac{0.6}{\varepsilon} \end{aligned} \tag{D.26}$$

Bibliographies

[1] Maruo H (1960) Wave resistance of a ship in regular head seas. Bulletin of Faculty of Engineering 9:73-91, Yokohama National University

[2] Newman JN (1967) The drift force and moment on ships in waves. Journal of Ship Research 11(1):51-60

[3] Lin WC and Reed AM (1976) The second order steady force and moment on a ship moving in an oblique seaway. In: Proceedings of the 11th symposium on naval hydrodynamics, London, pp 333-345

[4] Kashiwagi M (1991) Calculation formulas for the wave-induced steady horizontal force and yaw moment on a ship with forward speed. Reports of Research Institute of Applied Mechanics 37(107):1-18, Kyushu University

[5] Kashiwagi M (1992) Added resistance, wave-induced steady sway force and yaw moment on an advancing ship. Schiffstechnik 39(1):3-16

[6] Kashiwagi M and Ohkusu M (1993) Study on the wave-induced steady force and moment. Journal of the Japan Society of Naval Architects and Ocean Engineers 173:185-194

[7] Sclavounos PD (1984) The diffraction of free-surface waves by a slender ship. Journal of Ship Research 28(1):29-47

[8] Kashiwagi M (1995) Prediction of surge and its effect on added resistance by means of the enhanced unified theory. Transactions of the West-Japan Society of Naval Architects 89:77-89

[9] Newman JN (1978) The theory of ship motions. Advances in Applied Mechanics 18:221-283

[10] Naito S, Mizoguchi S and Kagawa K (1991) Steady forces acting on ships with advance velocity in oblique waves. Journal of the Kansai Society of Naval Architects 213:45-50

[11] Iwashita H, Ito A, Okada T, Ohkusu M and Mizoguchi S (1992) Wave forces acting on a blunt ship with forward speed in oblique sea. Journal of the Japan Society of Naval Architects and Ocean Engineers 171:109-123

[12] Ueno M, Nimura T, Miyazaki H, Nonaka K and Haraguchi T (2001) Steady wave forces and moment acting on ships in manoeuvring motion in short waves. Journal of the Japan Society of Naval Architects and Ocean Engineers 188:163-172

[13] Joncquez SAG (2009) Second-order forces and moments acting on ships in waves. PhD thesis. Technical University of Denmark, Copenhagen

[14] Cummins WE (1962) The impulse response function and ship motions. Schiffstechnik 9:101-109

[15] Bailey PA, Price WG and Temarel P (1997) A unified mathematical model describing the maneuvering ofa ship travelling in a seaway. Transactions of the Royal Institution of Naval Architects 140:131-149

[16] Lee S (2000) The calculation of zig-zag maneuver in regular waves with use of the impulse response functions. Ocean Engineering 27:87-96

[17] Fossen TI (2005) A nonlinear unified state-space model for ship maneuvering and control in seaway. International Journal of Bifurcation and Chaos 15:2717-2746

[18] Subramanian R and Beck R (2015) A time-domain strip theory approach to maneuvering in a seaway. Ocean Engineering 104:107-118

[19] Kobayashi E and Wada Y (1993) Development of a simulation system to evaluate ship maneouvrability in waves. In: Proceedings of the international conference on marine simulation and ship manoeuvrability, Canada, pp 295-304

[20] Yasukawa H (2006) Simulations of ship maneuvering in waves (1st report: turning motion). Journal of Japan Society of Naval Architects and Ocean Engineers 4:127-136

[21] Yasukawa H (2008) Simulations of ship maneuvering in waves (2nd report: zig-zag and stopping motion). Journal of Japan Society of Naval Architects and Ocean Engineers 7:163-170

[22] Fujii H and Takahashi T (1975) Experimental study on the resistance increase of a large full ship in regular oblique waves. Journal of the Society of Naval Architects of Japan 137:132-137

[23] 日本造船学会 海洋工学委員会性能部会編 (2003) 実践 浮体の流体力学、前編ー動揺問題の数値解法. 成山堂書店

[24] Maruo H (1960) The drift of body floating in waves. Journal of Ship Research 4:1-10

[25] Skejic R and Faltinsen OM (2008) A unified seakeeping and maneuvering analysis of ships in regular waves. Journal of Marine Science and Technology 13:371-394

[26] Salvesen N, Tuck EO and Faltinsen OM (1970) Ship motions and sea loads. Transactions of the Society of Naval Architects and Marine Engineers 78:250-287

[27] Newman JN (1977) Marine hydrodynamics. MIT Press, Cambridge

[28] Faltinsen OM (1990) Sea loads on ships and offshore structures. Cambridge University Press, Cambridge

[29] Loukakis TA and Sclavounos PD (1978) Some extensions of the classical approach to strip theory of ship motions, including the calculation of mean added forces and moments. Journal of Ship Research 22:1-19

[30] Salvesen N (1974) Second-order steady state forces and moments on surface ships in oblique regular waves. In: Proceedings of the international symposium on dynamics of marine vehicles and structures in waves, London, pp 212–227

[31] Faltinsen OM, Minsaas K, Liapis N and Skjørdal SO (1980) Prediction of resistance and propulsion of a ship in a seaway. In: Proceedings of the 13th symposium on naval hydrodynamics, Tokyo, pp 505–529

[32] Seo M and Kim Y (2011) Numerical analysis on ship maneuvering coupled with ship motion in waves. Ocean Engineering 38:1934-1945

[33] Yasukawa H and Adnan FA (2006) Experimental study on wave induced motions and steady drift forces of an obliquely moving ship. Journal of Japan Society of Naval Architects and Ocean Engineers 3:133-138

[34] Lee JH and Kim Y (2018) Time-domain approach for speed loss of ship in waves. In: Proceedings of the 13th pacific-asia offshore mechanics symposium, Jeju, pp 16-23

[35] Zhang W and Zou Z (2016) Time domain simulations of the wave-induced motions of ships in maneuvering condition. Journal of Marine Science and Technology 21:154-166

[36] Morino L and Kuo CC (1974) Subsonic potential aerodynamics for complex configurations: a general theory. American Institute of Aeronautics and Astronautics Journal 12(2):191–197

[37] Zhang W, Zou Z and Deng D (2017) A study on prediction of ship maneuvering in regular waves. Ocean Engineering 137:367-381

[38] Sprenger F, Maron A, Delefortrie G, van Zwijnsvoorde T, Cura-Hochbaum A, Lengwinat A and Papanikolau A (2017) Experimental studies on seakeeping and maneuverability of ships in adverse weather conditions. Journal of Ship Research 61(3):131-152

[39] Shigunov V, el Moctar O, Papanikolau A, Potthoff R and Liu S (2018) International benchmark study on numerical simulation methods for prediction of maneouvrability of ships in waves. Ocean Engineering 165:365-385

[40] Sanada Y, Elsheikh H, Toda Y and Stern F (2018) ONR Tumblehome course keeping and maneuvering in calm water and waves. Journal of Marine Science and Technology

[41] Sanada Y, Tanimoto K, Takagi K, Gui L, Toda Y, Stern F (2013) Trajectories for ONR Tumblehome maneuvering in calm water and waves. Ocean Engineering 72:45-65

[42] Kim DJ, Yun K, Park JY, Yeo DJ and Kim YG (2019) Experimental investigation on turning characteristics of KVLCC2 tanker in regular waves. Ocean Engineering 175:197-206

[43] Yasukawa H, Hirata N, Yonemasu I, Terada D and Matsuda A (2015) Maneuvering simulation of a KVLCC2 tanker in irregular waves. In: Proceedings of the international conference on marine simulation and ship manoeuvrability, Newcastle.

[44] Yasukawa H, Hirata N, Matsumoto A, Kuroiwa R, Mizokami S (2018) Evaluations of wave-induced steady forces and turning motion of a full hull ship in waves. Journal of Marine Science and Technology 24(1):1-15 20:37-52

[45] Yasukawa H and Yoshimura Y (2015) Introduction of MMG standard method for ship maneuvering predictions. Journal of Marine Science and Technology 20:37-52

[46] Kashiwagi M (2017) Wave-Body Interaction Theory (Theory of Ship Waves) - Lecture Notes for Graduate Course. Osaka University

[47] Tasrief M (2014) Improvement of Ship Geometry for High Performance in Waves by a Practical Integrated Optimization Method. PhD Thesis, Osaka University

[48] Newman JN and Sclavounos P (1980) The unified theory of ship motions. In: Proceedings of 13th symposium on naval hydrodynamics, pp 373-394

[49] Himeno Y (1981) Prediction of ship roll damping - a state of the art. Report of Naval Architecture and Marine Engineering No 239, University of Michigan

[50] Ogawa A, Koyama T and Kijima K (1977) MMG Report-I, on the mathematical model of maneuvering mathematical model. Bulletin of the Society of Naval Architects of Japan 575:192-198

[51] Hamamoto M (1977) MMG Report-II, theoretical background of maneuvering mathematical model. Bulletin of the Society of Naval Architects of Japan 575:322-329

[52] Kasai H and Yumuro A (1977) MMG Report-III, force induced by the rudder and interaction between hull and propeller. Bulletin of the Society of Naval Architects of Japan 578:358-372

[53] Kose K and Kijima K (1977) MMG Report-IV, method and experimental apparatus for restrained maneuverability test. Bulletin of the Society of Naval Architects of Japan 579:404-413

[54] Ogawa A, Hasegawa K and Yoshimura Y (1980) MMG Report-V, experimental study and improvement of maneuvering motion mathematical model. Bulletin of the Society of Naval Architects of Japan 616:565-576

[55] Fossen TI (1994) Guidance and Control of Ocean Vehicles. John Wiley & Sons Ltd., Chichester, England

[56] Söding H (1982) Prediction of ship steering capabilities. Schiffstechnik 29:3-29

[57] Yoshimura Y and Masumoto Y (2012) Hydrodynamic database and maneouvring prediction method with medium high-speed merchant ships and fishing vessels. In: Proceedings of the international conference on marine simulation and ship manoeuvrability, Singapore

[58] Motora S (1959) On the measurement of added mass and added moment of inertia for ship motions. Journal of Japan Shipbuilding Association 105:83-92

[59] Motora S (1960) On the measurement of added mass and added moment of inertia for ship motions (part 2. added mass abstract for the longitudinal motions). Journal of Japan Shipbuilding Association 106:59-62

[60] Motora S (1960) On the measurement of added mass and added moment of inertia for ship motions (part 3. added mass for the transverse motions). Journal of Japan Shipbuilding Association 106:63-68

[61] Motora S (1960) On the measurement of added mass and added moment of inertia for ship motions (part 4. pitching motion) Journal of Japan Shipbuilding Association 107:83-89

[62] Koyama T, Motora S, Chyu JH and Koyanagi M (1975) On the circular motion test (CMT) for the maneuverability model test. Journal of the Society of Naval Architects of Japan 138:151-157

[63] Triantafyllou MS and Hover FS (2003) Maneuvering and Control of Marine Vehicles. Department of Ocean Engineering, MIT, USA

[64] Imlay FH (1961) The complete expressions for added mass of a rigid body moving in an ideal fluid. DTMB Report 1528, Washington, DC

[65] Kashiwagi M (1983) Summary on the theory of maneuvering motion: revised edition. Kobe University of Mercantile Marine

[66] International Maritime Organization (2002) Resolution: standards for ship maneuverability. MSC 137(36)

[67] American Bureau of Shipping (2006) Guide for vessel maneuverability. Houston, USA

[68] Barr RA, Miller ER, Ankudinov V and Lee FC (1981) Technical basis for maneuvering performance standards. Report CG-M-8-81 Hydronautics, Inc. Technical Report 8103-3, Maryland, USA

[69] Wicaksono A and Kashiwagi M (2018) Wave-induced steady forces and yaw moment of a ship advancing in oblique waves. Journal of Marine Science and Technology 23:767-781

[70] Wicaksono A and Kashiwagi M (2019) Efficient coupling of slender ship theory and modular maneuvering model to estimate the ship turning motion in waves. In: Proceedings of 29th international ocean and polar engineering conference, Honolulu

Publication List

International Journal

[i] A. Wicaksono and M. Kashiwagi, "Wave-induced steady forces and yaw moment of a ship advancing in oblique waves", *Journal of Marine Science and Technology*, Vol. 23, no. 04, pp. 767-781, 2018 (first online 2017).

Proceedings in International Conference

[i] A. Wicaksono and M. Kashiwagi, "Efficient Coupling of Slender Ship Theory and Modular Maneuvering Model to Estimate the Ship Turning Motion in Waves", *The 29th International Ocean and Polar Engineering Conference*, Honolulu, Hawaii, USA, 2019.

Oral Presentations in International Workshop

[i] A. Wicaksono, "Wave-Induced Steady Forces and Maneuvering of a Ship in Waves", *3rd Program of International Platform on Ocean Energy for Young Researcher 2017*, Saga, Japan, 1 March 2017.

Indonesian National Journal

[i] A. Trimulyono and A. Wicaksono, "Numerical simulation of large-deformation surface wave by smoothed particle hydrodynamics" (In Indonesian), *Kapal*, Vol. 15, no. 03, pp. 102-106, 2019.

Proceedings in Indonesian National Conference

[i] A. Wicaksono, E.B. Djatmiko and M. Murtedjo "Study on the motion characteristics and operability of semi-submersible drilling rig with rectangular section of vertical columns and pontoons" (In Indonesian), *National Seminar of Marine Technology (SENTA)*, Surabaya, Indonesia, 2013.